KINEMATICS, DESIGN, PROGRAMMING AND CONTROL OF A ROBOTIC PLATFORM FOR SATELLITE TRACKING AND OTHER APPLICATIONS

A thesis presented for the degree of Doctor of Philosophy in

Mechanical Engineering at the

University of Canterbury, Christchurch,

New Zealand.

N.V. Afzulpurkar B.E.

1990

There is one great and covetable gift which is distinctly ours at all times. This is our profound capacity to discover, develope and usefully employ the Infinite Essennce in us. The secret of our strength is our knowledge.

Swami Chinmayananda

To my Parents

CONTENTS

ABSTRACT

In order to avoid the keyhole problems associated with present antenna mounting systems and to meet the requirements of acquisition and tracking for high gain and narrow beamwidth antennas, a novel antenna mount system is developed. The antenna is mounted on a microprocessor controlled robotic platform with six degrees of freedom. The mechanism is based on the principles of Stewart platform, which employes six variable length actuators constrained between a fixed base and a movable platform. This antenna mount is especially suitable for high gain antennas using high frequency band widths for marine satellite communications.

The kinematics and geometry of the parallel link mechanism has been studied in detail. The kinematic analysis for the parallel manipulator consists of developing a set of kinematic equations for the six linear actuators in terms of the "world coordinates" (Φ,θ,α,x,y,z). These kinematic equations are then solved for the "machine coordinates" (L1,L2,L3,L4,L5,L6), which are the six actuator lengths. A computer simulation has been done to model the motion of the platform. The simulation has simplified the task of examining various mechanism configurations, the range of motion and the mechanism mechanical constraints.

A six motor controller board based on the motion controller microprocessors has been developed. Limited unipolar pulse width modulated servo drives are used to drive the permanent magnet DC motors of the linear actuators. A desktop computer is used as the host processor to generate the command data. The motion control microprocessors generate the velocity and acceleration profiles and drive the six axes simultaneously. The main control programme residing in the host processor schedules the overall operation. The orbital satellite bearings are calculated on a minicomputer and downloaded to the control desktop computer .

A prototype antenna mount based on the descriptions above was designed, constructed and tested for tracking a high pass and low pass of an orbiting weather satellite, (the NOAA-7). A microwave antenna mounted on the

platform was found to be capable of tracking an orbital satellite throughout the visible hemisphere, although the reception tracking has not been inplemented. This antenna mount offers a light weight, structurally strong and fast dynamic response tracking system for land and marine applications.

This parallel robotic mechanism has potential for further applications such as a prepackaged portable communications system which can be deployed rapidly at remote construction sites or during civil defence emergencies. In addition it may be employed as a stabilized platform which can be used for marine VTOL aircraft recovery during rough weather. The application of this antenna mount in a low cost marine satellite communications system is emphasized since the fast dynamic response of the system will eliminate the need for an expensive stabilized platform.

ACKNOWLEDGEMENTS

Completion of this thesis concludes an important phase in my life and I am grateful to all the people who have played an important part in it. I am especially indebted to my supervisor, Dr G.R. Dunlop for his guidance and motivation during the course of this work. Indeed, without his constant encouragement this project would never have been completed.

I also wish to thank Professor H. McCallion, Head of Mechanical Engineering Department, University of Canterbury, New Zealand for his active support and valuable guidance. I am also grateful to Dr P.J. Ellis, former Director of the Information Technology Division of the D.S.I.R., New Zealand for the information on the satellite earth station keyhole problems.

I am grateful to my colleague Ma Li for designing the motor interface and to Mr G.R.Johnson, Senior Technical Officer, Mechanical Engineering Department for the design of the manipulator joints. I also wish to thank Mr Scott Amies and Mr Otto Bolt of Mechanical Engineering Department for manufacturing and assistance in the assembly of the robotic platform.

The funding of this project by the New Zealand University Grants Committee and the University of Canterbury is gratefully acknowledged. I am grateful to Royal Society of New Zealand, Canterbury branch for providing me with a conference travel grant and to Mercer Memorial scholarship for the financial assistance during the year 1988-89. The assistance of Zenith Australia, Ltd. for providing the Zenith Z-286 computer and Telecom, New Zealand in lending the antenna is acknowledged.

Thanks to my parents for their ever present support and confidence in my ability to undertake research work.

Finally, I take the opportunity to thank, Mrs Beverley MacKenzie for typing the thesis and all the Post graduate students in the Mechanical Engineering Department and my flatmates Sankar, Suresh and Dr R Ratnaraj for the many helpful discussions.

LIST OF PUBLICATIONS

1. Dunlop G.R., Afzulpurkar, N.V., "Six degree of freedom parallel link manipulator: geometrical and design considerations", IMC conf. 1988, Christchurch.

2. Afzulpurkar, N.V., Dunlop, G.R., Ma Li, Johnson, G.R. "Design of a Parallel Robot", NELCON conf. 1988, Christchurch.

3. Afzulpurkar, N.V., Dunlop, G.R. "Application of parallel link mechanism for satellite tracking system", NELCON conf. 1989, Wellington, NZ.

4. Afzulpurkar, N.V., Dunlop, G.R. "A novel antenna mount for orbital satellite tracking and marine communications", Fifth National Space Engineering Symposium, 1989, Canberra, Australia.

LIST OF SYMBOLS

A	Zero, HCTL-1000
Az	Azimuth, $90^o - \Phi$
B	Pole, HCTL-1000
β	Angle between adjacent base vectors/2
C	Cosine
C/N	Carrier to noise ratio
CHA	Channel A
CHB	Channel B
D	Antenna directivity
DOF	Degree of Freedom
ΔT	Sample time, HCTL-1000
E	Motor back emf
EBS	Electronic beam squinting
El	Elevation, $90^o - \theta$
Φ,θ,α	Euler angles
FOV	Field of view
γ_i, i = 1..6	The angle between the actuators and the platform local elevation axes
I/O	Input/Output
K	Gain, HCTL-1000
k_p	Proportionality constant: motor winding
L	Distance between the platform and base centroids
P	Prismatic joint
PTP	Point to point motion control
R	Revolute joint
Rb	Base pitch circle radius
R_e	Linear actuator expansion ratio
Rp	Platform pitch circle radius
RSTP	Robotic satellite tracking platform
S	Sine
SNR	Signal to noise ratio
T	System noise temperature

G	Antenna gain
τ_m	Motor torque
V_{in}	PWM servo drive input voltage
V_m	Motor terminal voltage
ω	Motor angular velocity
Ψ_{jj}, i ,j = 1..6	The angle between the actuator pairs at the top joint assembly
μ_i, i = 1..6	The angle between the actuators and the base plane

LIST OF FIGURES

LIST OF TABLES

CHAPTER 1

SATELLITE TRACKING: AN OVERVIEW

1.1 INTRODUCTION

Satellite tracking systems are employed to track fast moving weather or earth resources satellites, space shuttles and unmanned deep space probes on interplanetary voyages. Over the years, various tracking system designs have been developed and employed to suit the application. The design of a satellite communication system is a complicated process. Considering the enormous expenses involved in putting a satellite into the orbit or in launching a space probe, a foolproof yet cost effective design must be adopted to extract maximum benefits from putting large spacecraft into the orbit.

An earth station which transmits or receives signals from a satellite, constitutes an important link in the global communication systems. A great deal of research has been carried out on design techniques for improving the efficiency of large antenna dishes. To characterize the performance of earth stations the gain to noise temperature (G/T) ratio is usually quoted (c.f. section 2.9.5). The received signals are weak, so the G/T ratio must be maximized within the constraints of antenna size and receiver cost. The specified G/T can be achieved by many combinations of G and T (c.f. equation 2.1 and section 2.9.5). There are practical limits on reducing the system noise temperature so, for a fixed satellite transmission system, the gain of the antenna is increased by using a larger aperture area. Large antennas produce narrower beams. For a narrow beamwidth antenna the required pointing accuracy is greatly increased so as to maintain the received and transmitted signal levels within the defined limits i.e. to keep the satellite within the beam (c.f. Eley, 1970, CCIR report, 1978).

To steer a large antenna dish with the required pointing accuracy, (a 25-m antenna operating at 4 GHz needs an accuracy of ± 1 min of arc to avoid pointing loss (c.f. Pratt et al., 1986))a sophisticated antenna mount system

must be employed. Present ground based satellite tracking stations use a two axis mounting of either Alt-Azimuth type or X-Y type (c.f. CCIR report, 1978, Miya, 1981). For a ship based tracking system the antenna is mounted on a stabilized platform which isolates the antenna from the dynamic motion of the ship (c.f. Brown et al., 1970, Johnson, 1978).

1.2 A NOVEL ANTENNA MOUNT DESIGN

Satellite communication using the conventional mounting systems suffers from the kinematic limitations of the mechanism employed in steering the antenna dish. This causes a break in the communication link when the satellite passes through some regions of the visible hemisphere. Each such region in the sky is called a "keyhole" of the mounting systems. The Alt-Azimuth (A-Z) type of mounting system has a "keyhole" around the zenith, which makes it difficult to track an overhead relay satellite (usually stationary) in the equatorial regions (c.f. section 2.5.1). The X-Y mount has "keyholes" near the horizon that makes it difficult to track satellites at low elevation angles (c.f. section 2.5.1). For a maritime communication system, the effect of these "keyhole" regions is greatly magnified because of the rolling, pitching and yawing of the ship.

The ideal antenna mounting mechanism is kinematically capable of moving the antenna dish through the visible hemisphere and is strong enough to withstand the wind and other loads. Such a mechanism was found in the form of a Stewart platform (c.f. Stewart, 1965) modified for a large angular range. It is essentially a closed link mechanism consisting of six parallel variable length actuators constrained between a fixed base and a movable platform. This mechanism offers six degrees of freedom. The closed link structure results in a very strong mechanism capable of fast and accurate movements. When equipped with a closed loop control system and controlled through a computer, an antenna mount based on this parallel link mechanism offers a novel tracking system design. This antenna mount with proper joint designs enables large antenna dishes to track a moving target through the zenith without target loss, even during heavy weather. For a maritime satellite communication system this antenna mount offers a low cost alternative to the existing antenna stabilizing methods (c.f. section 5.9).

1.3 DESIGN, CONSTRUCTION AND CONTROL OF THE MOUNT MECHANISM

The development of the prototype parallel linkage robotic platform requires a careful study of the kinematics and geometry of the mechanism. For a practical construction, the theoretical design needs simplification and the effect of these changes on the geometry and kinematics needs to be carefully considered. Of prime importance is the design of the joints connecting the base and the parallel actuators, and the platform and the actuators to achieve the required angular range. A mathematical model for the motion of the platform is developed to study the effects of varying the sizes of the various mechanism parameters (c.f. section 5.3.2.2).

The parallel link mechanism forms a separate category of robotic manipulators (c.f. Stewart, 1965, Hunt, 1978, Fitcher and McDowell, 1980). The six linear actuators constitute the six axes of the manipulator. The required end-effector coordinates (Φ, θ, α x, y, z) are transformed into the six joint coordinates (L_i, i =1..6) by using the inverse kinematic transformations (c.f. section 3.7). To position the platform at the desired points accurately and to achieve the required velocities and accelerations essentially require the application of multi-axis machinery numerical control principles. A control system based on closed loop feedback control and dedicated microprocessors for the control of each axis offers a solution to the problem of multi-axis real time control (c. f. Dunlop and Ma Li, 1988, Ma Li, 1989). A main control programe residing in the host processor schedules the execution of the required motion.

A prototype parallel linkage robotic platform has been designed, manufactured, and tested as a part of the research. Essentially the thrust was on the practical side of the electromechanical interface and the development of the necessary hardware and software. The successful testing of the platform for satellite tracking application demonstrated the capabilities of the novel antenna mount design and verified the theorotical derivations.

The following chapters discuss, in detail, the design, construction and control of the parallel linkage robot. Chapter 2 gives a review of conventional tracking system methods. Problems associated with the

conventional mounts are clearly identified. Chapter 3 discusses the geometrical and kinematic analysis of the parallel linkage manipulator along with the joint design details. In chapter 4 the actuating system, feedback control components and the multi-motor controller design are elaborated. Chapter 5 addresses the variable geometry configuration, the simulation programme to model the robot motion and the software implementation part of the project. Chapter 6 contains summary of the techniques and results along with suggestions for further research. In Appendix A, a general method for development of the stiffness matrix for the RSTP is given.

CHAPTER 2

REVIEW OF SATELLITE COMMUNICATION ANTENNA MOUNTING SYSTEMS FOR EARTH STATIONS

2.1 INTRODUCTION

The antennas developed in modern satellite communications systems have steadily increased in size, complexity and efficiency. The most visible part of a satellite communication station is the antenna. The antenna size varies from 70-m diameter, as in the NASA deep space communications network, to 0.7-m for direct broadcast satellite television (DBS-TV). The high cost of large antennas (several million dollars for a 30-m steerable dish) means highest possible gains and the lowest system noise temperatures are required to be achieved. Figures 2.1 and 2.2 show typical large earth station antenna installations. For the large antennas the total structure including the concrete pedestal weighs several thousand tons.

Large antennas produce narrow beams with the result that any satellite moving by a fraction of a degree must be tracked. Large antennas require high gain to noise (G/T) ratio and are capable of carrying large numbers of telephone, television and data channel simultaneously. In designing an antenna for a satellite communications earth station, the basic requirements are: maximum gain, low system noise temperature, and low side lobes to minimize the interference problems (c.f. section 2.9). The Cassegrain type antenna is popular with large earth stations because higher gains and lower noise temperatures can be achieved.

In the following discussion, present standard antenna mounting systems are evaluated. The "keyhole" problem associated with each system is described. Special attention is given to the maritime satellite communication requirements and problems. Also considered are various signal error detection techniques for the autotracking of the satellite once the acquisition has been made. Lastly the most important parameters involved in the antenna design are briefly examined.

Fig. 2.1 Examples of large earth station antennas. Foreground: 19-m 14/11 GHz Standard C Cassegrain antenna with wheel and track mount. Background: 32-m 6/4 GHz Standard A antenna. source: Pratt T (1986).

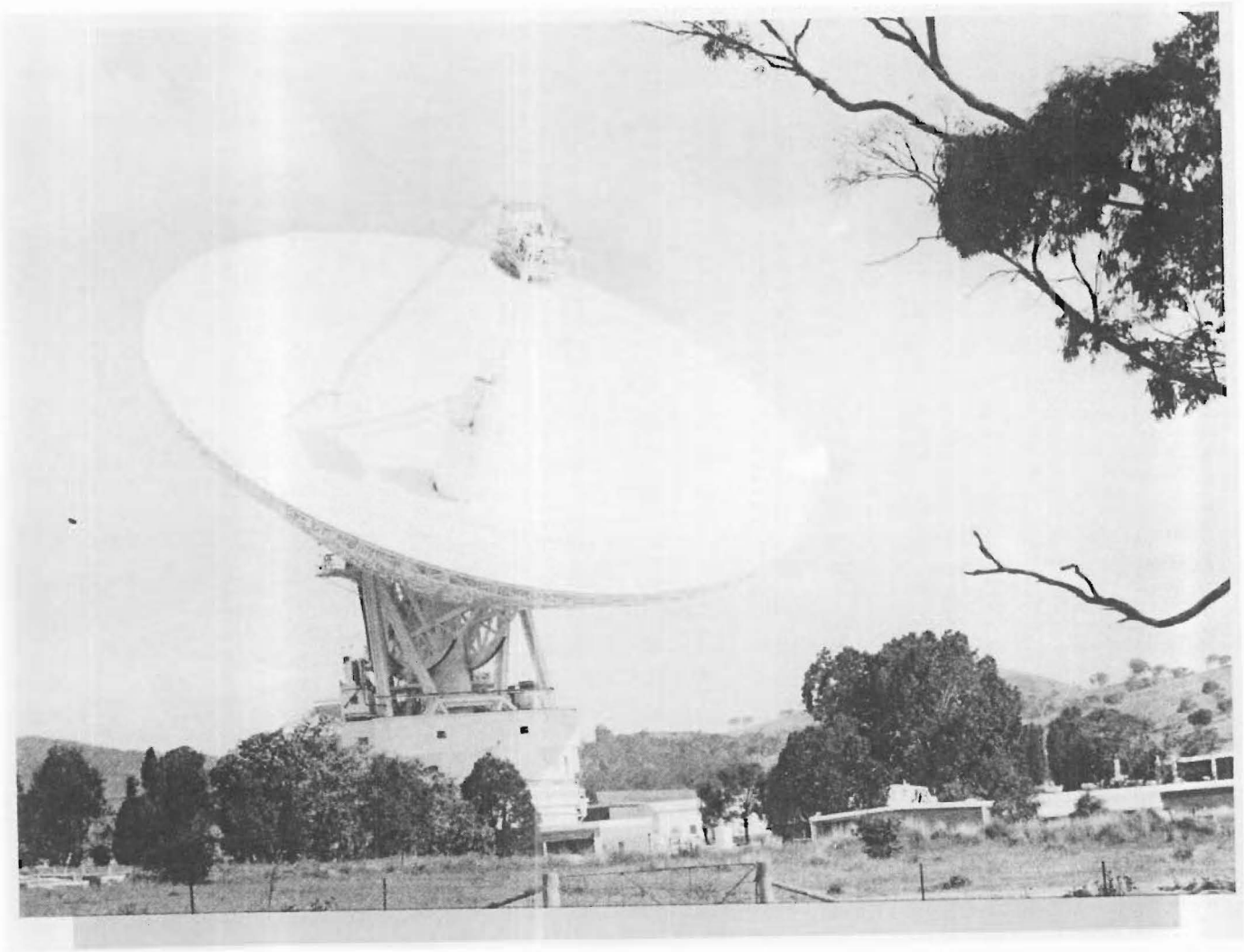

Fig. 2.2 A 60-m diameter antenna at the NASA deep space earth station, Tidbinbilla, Australia.

2.2 TRACKING REQUIREMENTS FOR SATELLITE COMMUNICATIONS

Satellite tracking has developed since 1965. This followed from the first artificial satellite launch of INTELSAT 1 on April 6, 1965. The satellite tracking station forms the link between ground control station and the earth orbiting scientific and communications satellites, manned orbiting shuttle flights and unmanned interplanetary shuttles. Four areas have been identified in which tracking techniques need to be applied to maintain a satisfactory communications link between a satellite and an earth station (c.f. Hawkins et al., 1988).

The first area is a ground station tracking a subsynchronous orbiting satellite. Subsynchronous satellites have periods much less than the period of rotation of the earth. They are low orbiting and fast moving satellites. Examples of such satellites are weather and earth resources satellites or space shuttles (c.f. Fig. 2.3). The area on earth which is visible from the satellite is called the FIELD OF VIEW (FOV). For a subsynchronous satellite the FOV is moving. A ground station within the FOV will have limited contact with the satellite unless a continuous tracking system is employed by the ground station.

The second case involves a geostationary satellite being tracked by a ground station. Such a satellite follows approximately an elliptical orbit in the space. Communication satellites in a geostationary orbit above the equator rotate at the same rate as the earth so that they appear stationary when viewed from earth's surface. Small perturbations occur due to the nonhomogeneous nature of the earth and due to the gravitational attraction of celestial bodies. Such a satellite undergoes a slow cyclic movement ($\pm 3^{o}$, c.f. Hawkins et al.,1988). Thus if the beamwidth of the antenna is less than $\pm 6^{o}$ then tracking is necessary to maintain the communication contact. Communication stations which are tolerant to the satellite orbit variations will result in increased life span of the satellite. Inou et al. (1981) have discussed the system design for a K-band earth station antenna using monopulse tracking technique to track geostationary satellites with an accuracy of $\pm 0.01^{o}$. They have employed both the Alt-Azimuth and X-Y type (c.f. section 2.5.1 and 2.5.2) antenna mounting systems with limited driving range.

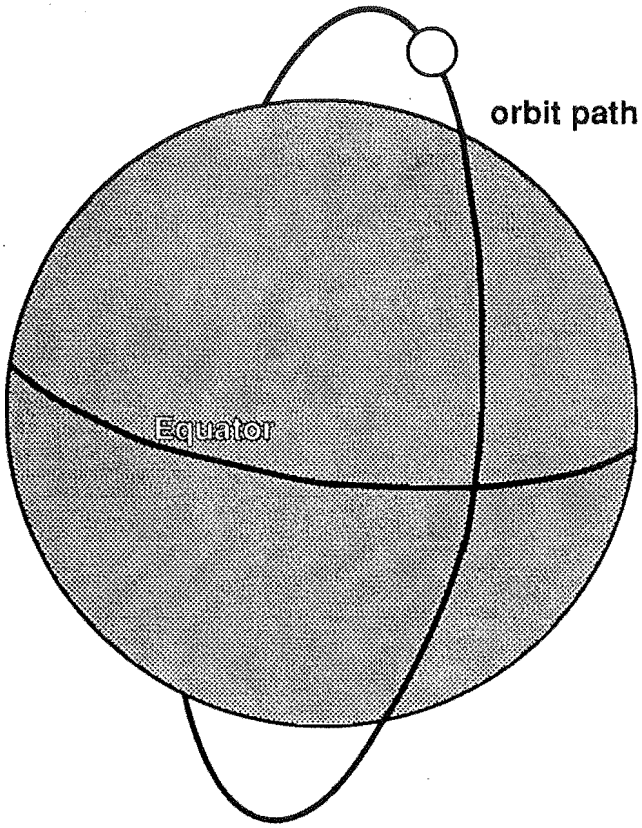

Fig. 2.3 Near-polar orbit of a weather satellite

The third area is satellite to satellite communication which is particularly important for military operations. The fourth area is a ship based satellite tracking system. The ship is subjected to roll, pitch and yaw motion. Also as the ship travels around the globe the direction to the satellite will vary. Thus an antenna positioning mechanism is necessary to acquire and maintain contact with the satellite.

2.3 GEOSTATIONARY SATELLITES

A satellite which is moving eastward in a circular orbit, coplanar with earth's equatorial plane, 35,786 km above the earth's surface with a velocity of 3.08 km/s will have the same period as earth's rotation. Hence the satellite is observed from the earth as if it is stationed at one point. Such a satellite is called a geostationary satellite and the circular orbit is called a geostationary satellite orbit (c.f. Fig. 2.4).

2.4 LOOK ANGLES

The path followed by any satellite moving around the earth is an ellipse in the orbital plane. The coordinates to which the antenna boresight axis must be pointed to communicate with the satellite are called the "look angles". These are most commonly specified as 'Azimuth' (Az) and 'Elevation' (El). Azimuth ($90^{o} - \Phi$) is measured eastward from geographic North to the projection of the satellite path on the horizontal plane at the earth station. Elevation ($90^{o} - \Theta$) is the angle measured above the horizontal plane to the path (c.f. Fig. 2.5).

2.5 STANDARD ANTENNA MOUNT SYSTEMS

An antenna mount system is employed to steer the antenna so that the orbital satellite or space shuttle path can be tracked continuously. Most early antenna mounting systems were patterned after radio astronomy antennas (polar-equatorial mounts). Present ground based satellite tracking stations use a two axis mounting of either Alt-Azimuth type or X-Y type with two degrees of freedom. For a ship based tracking system the antenna is mounted on a stabilized platform which isolates the antenna from the dynamic motion of the ship.

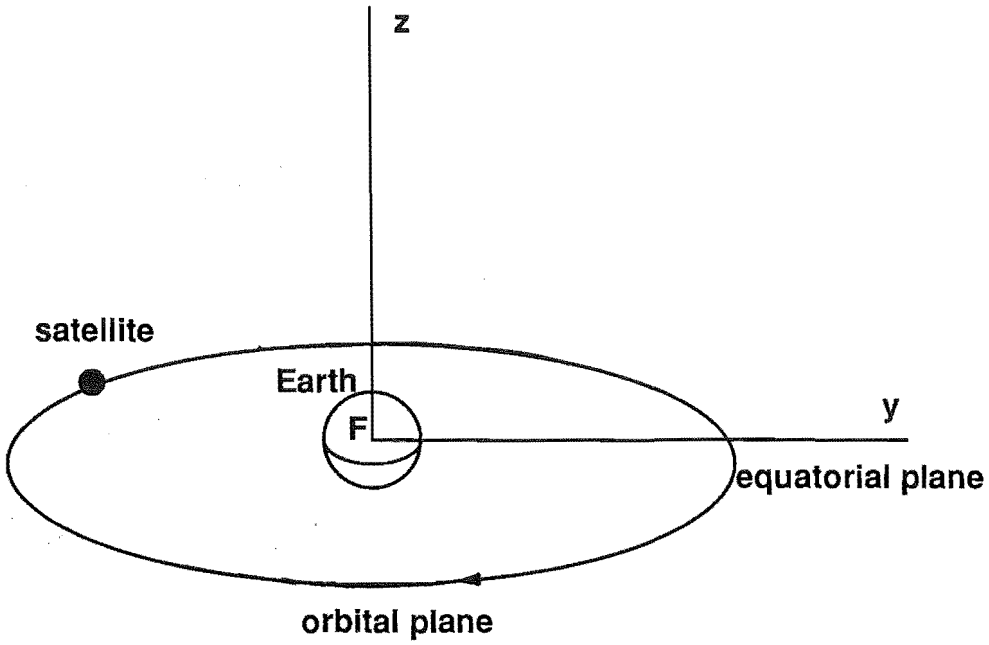

F : centre of the earth

Fig. 2.4 Geostationary satellite orbit

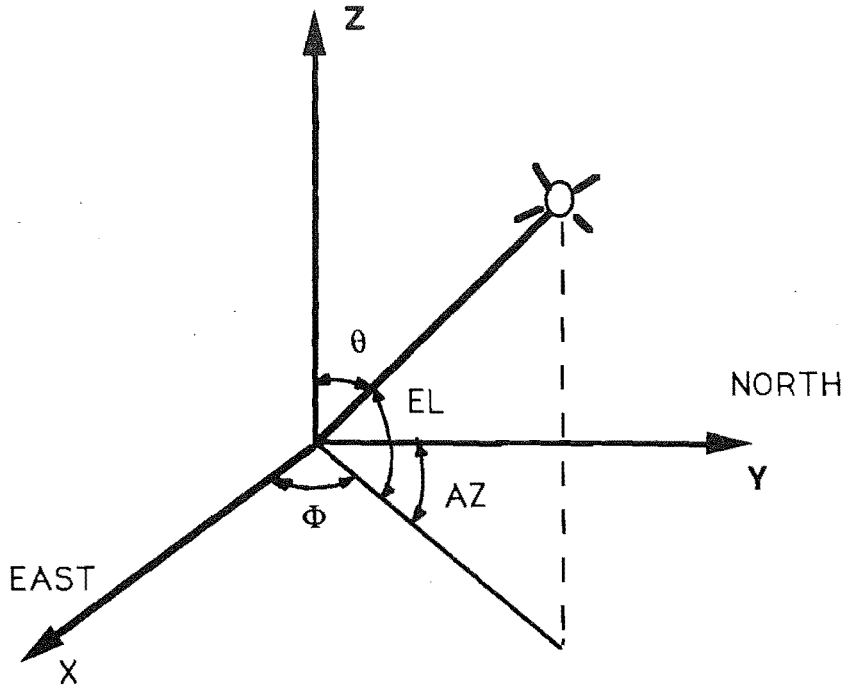

Fig. 2.5 Look angles

2.5.1 Alt-Azimuth Mount and Associated "Keyhole"

This is the most common type of mounting system and has independently controlled azimuth and elevation axes. It consists of a vertical axis revolute joint which carries a horizontal axis revolute joint. The antenna dish is mounted on the horizontal axis (c.f. Fig. 2.6). The antenna boresight axis is positioned by rotating the vertical joint through the azimuth angle from the North and then rotating the horizontal joint through the elevation angle from the horizon. Once the satellite is acquired, there is a direct 1:1 mapping of the tracking errors and a control computer is not required.

This mount has a singular position (keyhole) near the zenith. If a moving satellite is tracked through the zenith, or very close to it, then as the elevation angle reaches 90° the azimuth angle must rotate through 180°. The satellite can move on out of the antenna beam while this rotation takes place and the contact is lost. This region is called the "keyhole" of the Alt-Azimuth mount system.

When this mounting system is used on a ship and the antenna boresight axis is pointing at the zenith, the rolling motion of the ship will produce an azimuth change of 180° in a relatively short time. This results in an excessive speed requirement for the servo mechanism and effectively the ship looses contact with the satellite.

For a high gain, narrow beamwidth antenna, the rolling and pitching action of the ship will cause the singularity of the Alt-Azimuth mount to trace out a flattened conical region around the zenith. Communication with a satellite within this region will be unreliable. This region is the effective "keyhole" of the system (c.f. Fig. 2.8) and is greatly enlarged by the motion of the ship. For ground stations, prediction can be used to reduce the severity of the keyhole problem. As the elevation angle starts approaching 90°, the azimuth axis begins to rotate so that the 180° azimuth rotation can be completed within a larger time interval (c.f. Fig. 2.7). This type of mount is suitable for high latitudes operations. Ships in the equatorial region tracking a geostationary satellite will have communication problems for overhead relay satellites. An antenna positioning servo system developed at the Bell Laboratories, USA using Alt-Azimuth type mount is described by Lozier et al.(1963). This mounting system has the keyhole problem near the zenith.

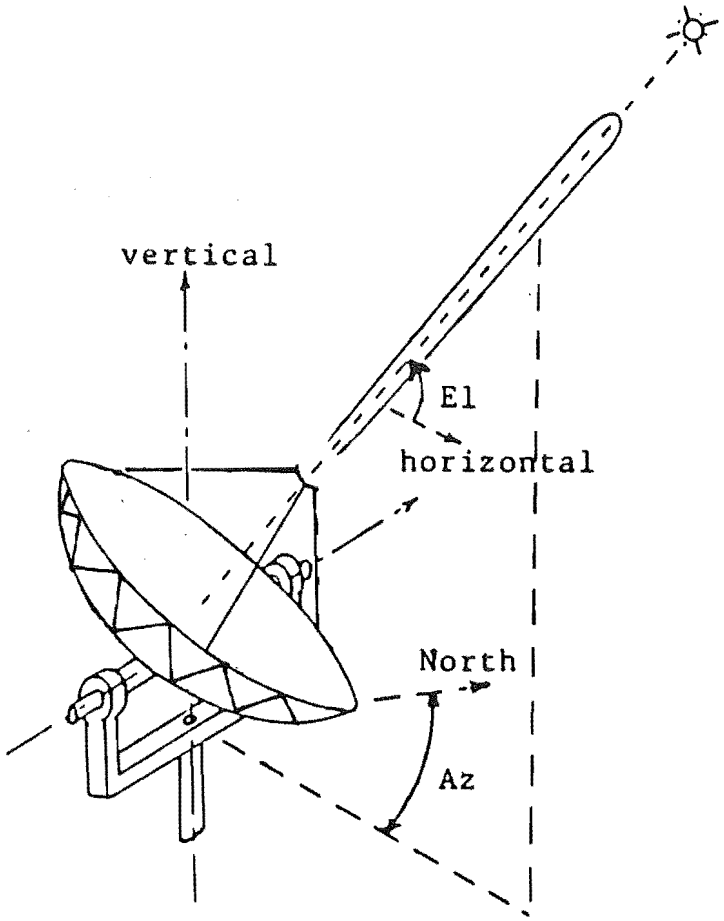

Fig. 2.6 The alt-azimuth mount

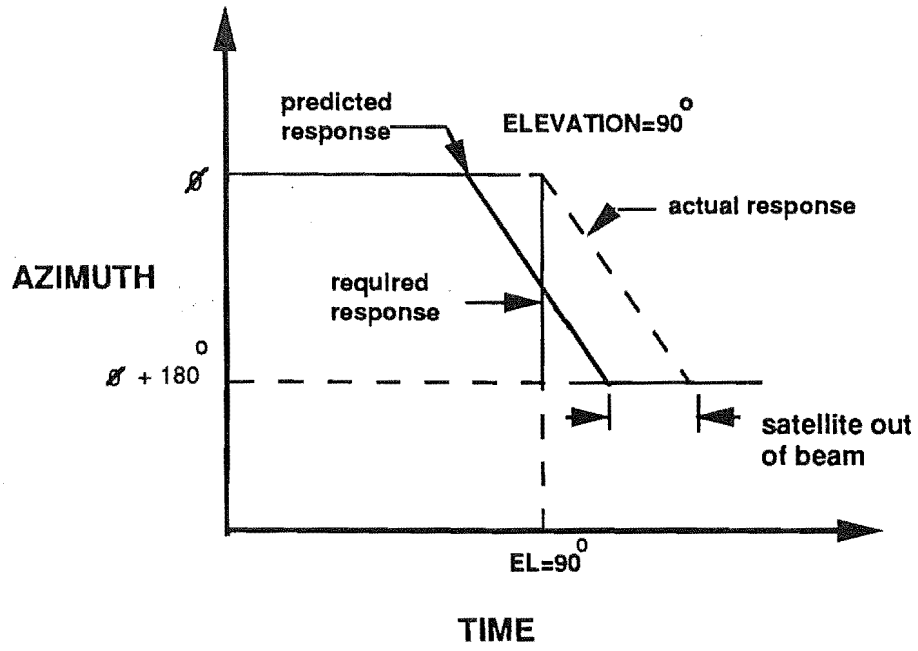

Fig. 2.7 Alt-Azimuth mount keyhole problem

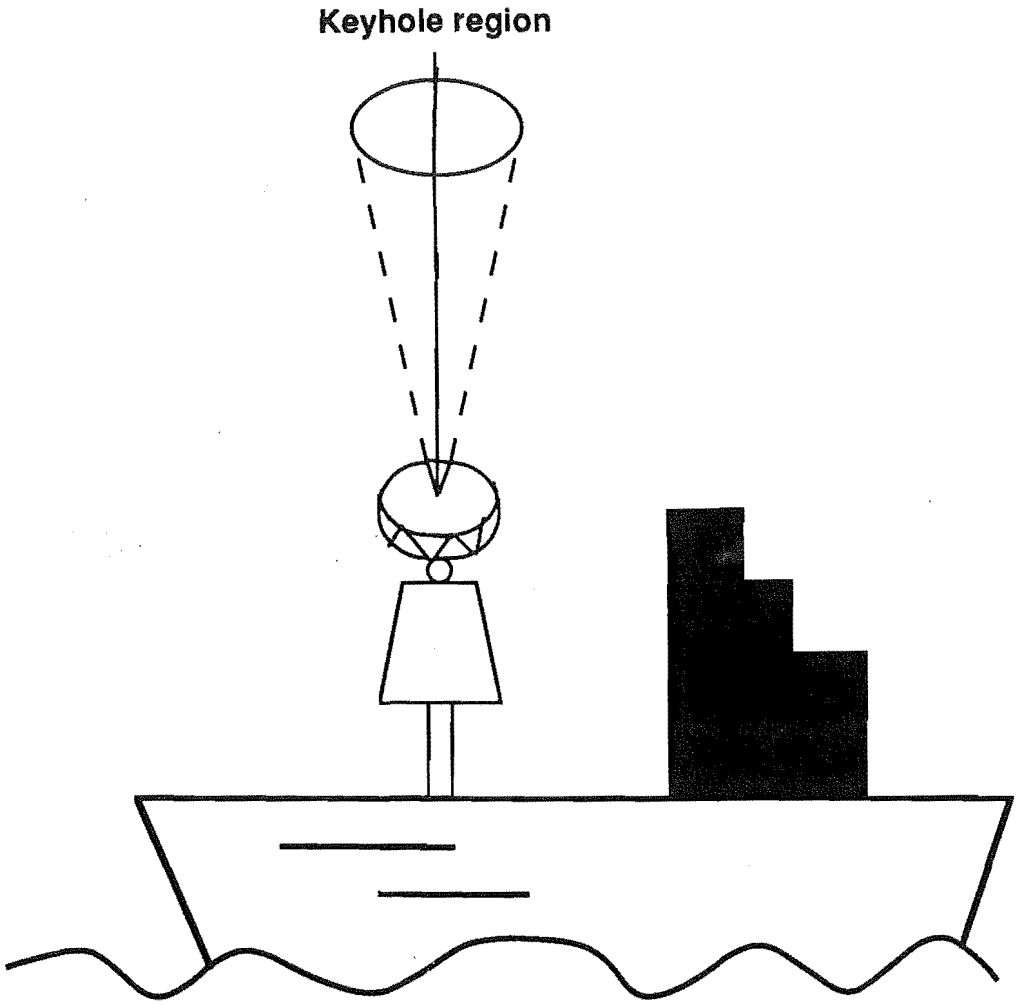

Fig. 2.8 Alt -Azimuth Mount "keyhole" region for the ship mounted antenna

2.5.2 X - Y Mount and Associated "Keyholes"

The X-Y mount consists of two controlled orthogonal axes. A horizontal axis revolute joint which carries another revolute joint at right angles, which in turn supports the antenna (c.f. Fig. 2.9). Each look angle is a function of both the controlled angles. Thus the two axes are not decoupled, as is the case with Alt-Azimuth mount and control is therefore more complex. The tracking errors do not map directly to each axis and computer control is necessary.

This mounting system does not have a keyhole problem about the vertical axis. However it does have keyhole problems. The keyholes are located at each end of the horizontal axis, so ships near the polar region could have difficulty in communicating with geostationary satellites. Also, contact with a subsynchronous satellite making a low pass (skimming pass) could be difficult (c.f. Fig. 2.10).

This keyhole problem can be overcome by installing two X-Y mount antennas perpendicular to each other. Each antenna covers the singularities of the other. This doubles the cost of the tracking system, but the extra reliability plus full hemispherical coverage is sometimes worthwhile. For example, in the case of NASA deep space exploration antennas, two X-Y mounted antennas are used at each of the three receiving sites. This is an effective but expensive solution to the keyhole problem. The cost of not collecting spacecraft data during a planetary fly past is even more expensive.

2.5.3 Multi-axis Antenna Mount Systems

To overcome the limitations of a two axis mount, extra axes are introduced in the multi-axis antenna mount systems. The operation of the multi-axis mounting systems are discussed in the following section.

2.5.3.1 Cross elevation over elevation over azimuth

To overcome the problem of keyholes near the zenith or near the horizon, addition of a cross elevation axis over the elevation axis is quite common in marine communication mounting systems and in the earth resource and weather satellite tracking systems (c.f. Fig. 2.11). The details of the marine

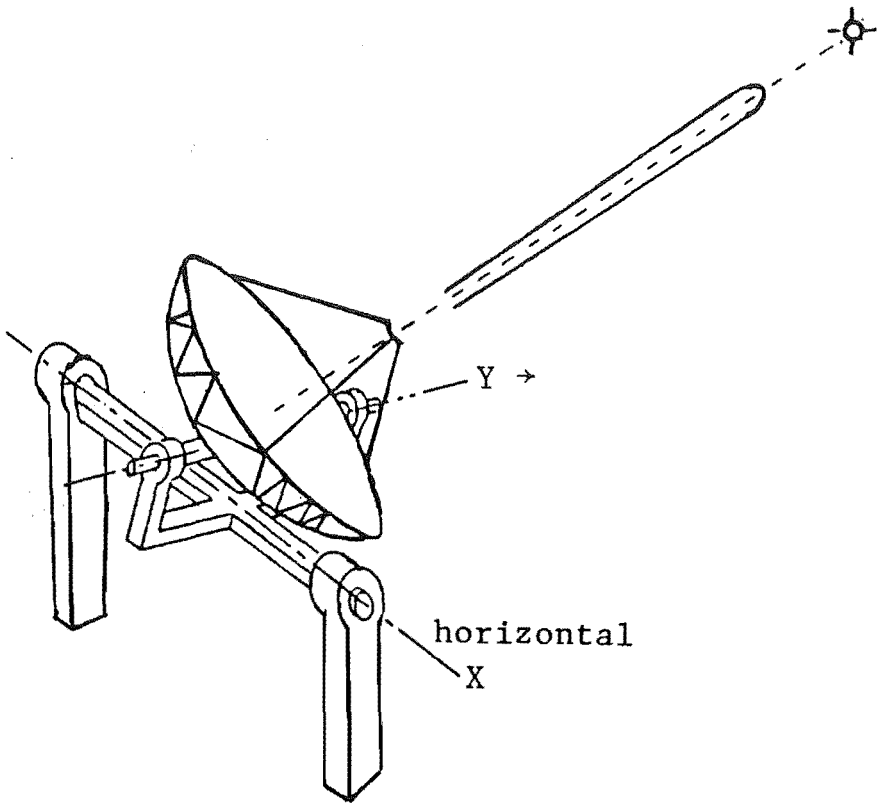

Fig. 2.9 The X-Y mount

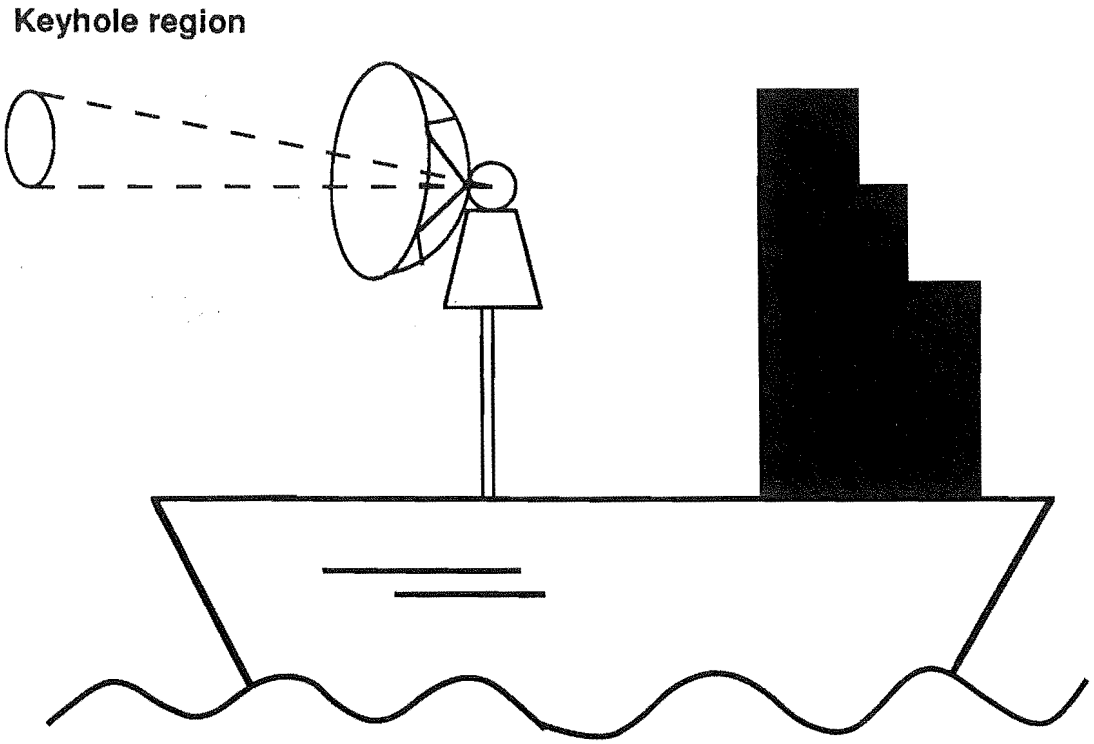

Fig. 2.10 X-Y mount keyhole problem

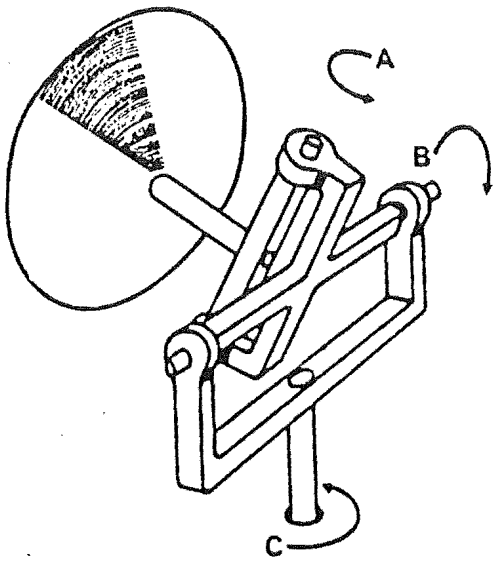

Fig. 2.11 Three-axis stabilization: cross elevation over elevation over azimuth.

A: cross-elevation axis
B: elevation axis
C: azimuth axis

source: Recommendations and reports of the CCIR (1978)

satellite communication using multi-axis antenna mount systems are discussed by Brown et al. (1970), Harries (1970), Brooks (1973) and Johnson (1978).

The three-axis stabilization mounting system is provided with three orthogonal axes with revolute joints (c.f. Fig. 2.11). The vertical axis movement is called training (azimuth), an orthogonal axis is called cross level (elevation), a third orthogonal axis in horizontal plane containing the line of sight is called the level (cross elevation). The level axis carries the antenna and other communication equipment and has the gyro stabilization reference unit mounted on it (c.f. section 2.7.1). One set of gyro and accelerometer combination is mounted on the level axis and one on the cross level axis to stabilize antenna against the ship motion. Detailed description of the construction and operation of the gyro accelerometer combination is discussed by Brown et al. (1970), Harries and Heaviside (1973), and Johnson (1978).

When the satellite is near the zenith, the cross level axis will take over the roll motion thus eliminating rapid movement of the azimuth axis. When the satellite is near the horizon the cross level axis will be parallel to the azimuth axis and will take out short term compass errors.

In the marine satellite communication system the antenna should be capable of sweeping through 360° training, -20° to 110° elevation and ± 30° cross level. The addition of the third axis increases the mechanical complexity of the mount. The extra axis and joints results in an increase in the total mass of the system to be moved. The complete mechanism requires a heavier supporting structure, additional gearing arrangements and complex control equipment. Each axis has different parameters and must be computer controlled with three different sets of parameters so that the singularities which cause the keyhole can be avoided by using the third degree of freedom.

2.5.3.2 Elevation over azimuth on stable platform

In ship-borne communication system, pointing a narrow beamwidth antenna at a satellite requires a stabilized platform to alleviate the ship motion. The detailed arrangement for a four axis tracking mount is shown in Fig. 2.12. The pitch and roll axis are used to stabilize the antenna against the ship motion and the elevation and azimuth axes are used for the tracking operation. The control of roll, pitch and elevation, azimuth axes is independent but the cost and complexity of the operation are greatly increased. A detail discussion can be found in the references CCIR report (1978) and Miya (1981).

2.6 SPECIAL REQUIREMENTS OF MARITIME SATELLITE COMMUNICATION

Maritime satellite communication has many special design requirements for continuous operation of the communication system in severe operating conditions. The major factors affecting the design of the maritime satellite communication system are torsional and linear forces on the antenna supporting structure due to wind and vibration, and the necessity to maintain an inertial plane against the ship motion. The frequencies used by maritime systems are specially allocated for the service, 1530 to 1544 MHz and 1026 to 1646 MHz for the link between the satellite and the ship. The link between the shore stations and the satellite operates in the 6/4 GHz bands (Pratt et al., 1986). The angle to which the ship may roll depends on the ship size and the state of the sea and a value of $\pm 25^{o}$ can be taken as a typical maximum roll value (c.f. CCIR report, 1978). Conventional methods used to stabilize the antenna against the dynamic motion of the ship are discussed in the section 2.7. Figure 2.13 shows the SKYNET 5 ship-borne antenna arrangement as an example of maritime communication system.

2.6.1 Problems Associated with Maritime Satellite Communication

The special problems associated with maritime communication are as follows:

1. Interference from high powered radars.

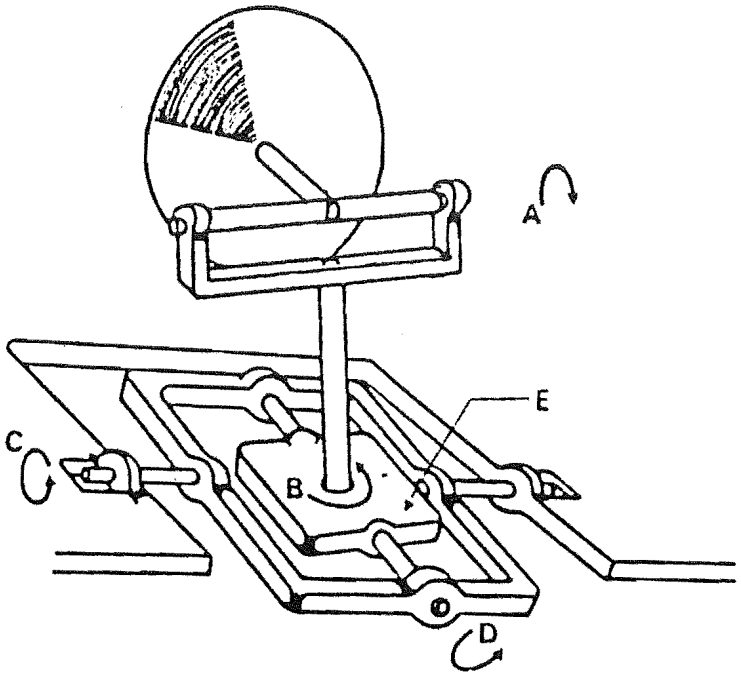

Fig. 2.12 Four axis stabilization: elevation over azimuth on stable platform

A: elevation axis B: azimuth axis
C: pitch axis D: roll axis
E: stable platform

source: Recommendations and reports of the CCIR(1978)

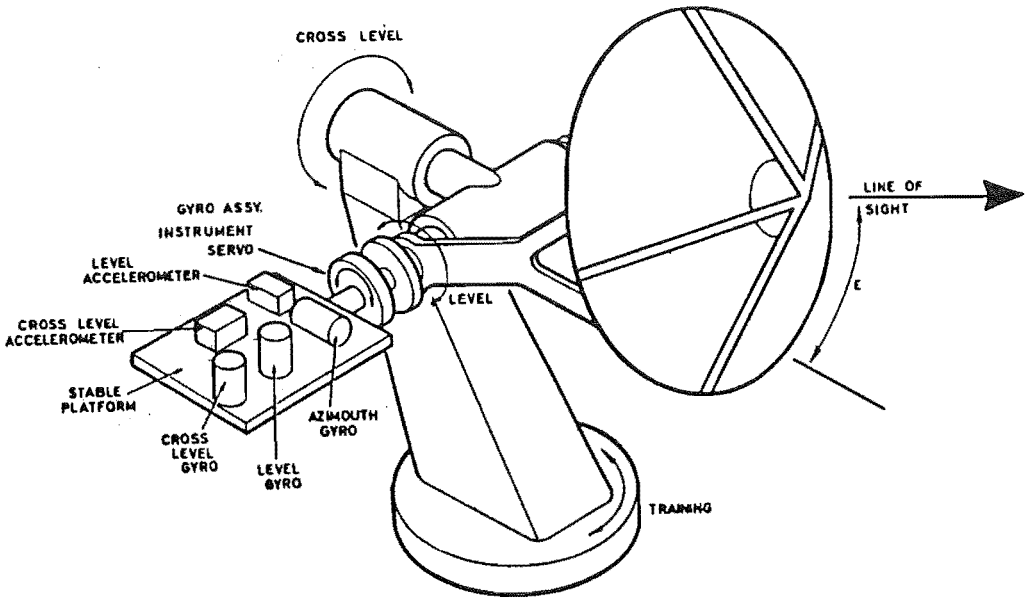

Fig.2.13 Skynet 5 : stabilization reference unit
source : Brown K R (1970)

2. Restricted space available for the antenna dish, supporting structure and control equipment.

3. Restrictions on the total weight of the communication system.

4. Effect of wind and severe vibrations caused by ship motion.

5. Variations in response and errors caused by roll, pitch and yaw of the ship.

6. Large coverage area required (typically from 20° elevation to 90° elevation) to maintain links with the satellites at different latitudes and longitudes.

7. Maintenance requirements for long periods at sea.

2.7 STABILIZATION METHODS

As discussed in the section 2.5.3, some form of antenna stabilization is required for maritime satellite communications systems to maintain the satellite link. The main types of stabilization methods are discussed in the following section.

2.7.1 Passive Stabilization

Passive stabilization utilizes the inertia of a pendulum or flywheel to stabilize a platform on which the antenna is mounted.

2.7.1.1 Compound pendulum stabilization

In this form of stabilization, the inertia of a compound pendulum is used to stabilize a platform on which the antenna is mounted. The period of the pendulum is much higher than roll period of the ship. This type of stabilization is discussed in detail by Kirby (1973). This stabilization method is the simplest and the cheapest of all the stabilization methods. Errors in the system can be up to ± 6° which are not acceptable for a high gain narrow beamwidth antenna. For a medium gain antenna of about 1-m diameter, this type of semi-stabilized platform can be used.

2.7.1.2 Flywheel stabilization

In this type of stabilization method,instead of a compound pendulum, two flywheels mounted on the x-y axes of the platform are used to provide stabilizing torques. The increased inertia allows the centre of gravity of the assembly to be nearer to the axis. The main disadvantage of this type of stabilization is that the whole assembly is heavy and occupies more space on the ship. The pointing errors of about $\pm 2^0$ using this type of stabilization units allows use of medium gain antennas only.

2.7.2 Active Stabilization

This method of stabilization uses a reference stabilization unit consisting of gyroscopes and level sensors to sense the ship's motion. The reference unit generates signals which drive the power servos to control each mounting axis. Pointing errors are limited to about $\pm 0.5^0$ using active stabilization methods (c.f. CCIR report, 1978).

2.7.2.1 Stabilisation reference unit

The function of stabilization unit is discussed in detail by Brown et al. (1970) and Harries (1970). A brief description is given here to explain the principle. The antenna stabilization reference unit is a two axis gyro vertical unit and a free azimuth unit. Three single axis gyros are mounted in the level, cross level and azimuth direction and two accelerometers in the level and cross level directions. The level and cross level gyros feed the corresponding servos and thus maintain the antenna in the established attitude in the vertical plane. The elevation angle is controlled by the angle set into the instrument servo. This elevation angle is with reference to true horizontal, so the instrument servo directly sets the antenna in elevation angle. Thus the reference stabilization unit maintains the antenna stable against ship motion, and the instrument servo rotates the antenna housing relative to the stabilization reference unit. The gyroscopes function as position sensors and the output torque is a function of input angular disturbance (c.f. Fig. 2.13).

2.8 ANTENNA ERROR DETECTION METHODS

After the satellite is acquired, variations in the satellite position can be detected by a number of error detection methods. Different antenna error detection techniques are discussed in brief in the following section to illustrate the principle. A comprehensive review of these techniques has been done by Hawkins et al. (1988).

In general, five classes of error detection mechanisms have evolved to meet the needs of various satellite communication stations. These can be described as:

1. Manual Tracking
2. Programme tracking
3. Monopulse or simultaneous sensing
4. Sequential amplitude testing
5. Electronic beam squinting

The principle of operation, advantages and limitations of the method are discussed in the following section.

2.8.1 Manual Tracking

In manual tracking each axis is controlled by the operator until the received signal strength is maximum. Thus the tracking accuracy, which is low, depends on the operator. Generally, if autotracking mode fails, manual tracking mode is used to maintain the contact with the satellite.

2.8.2 Programme Tracking

Programme tracking was the first method used in 1960's for tracking early satellites like TELSTAR. In programme tracking the direction of the antenna is determined by calculating the position of the satellite in terms of the "look angles". The exact look angles are calculated daily by using satellite

ephemeris data. In the case of ship-borne communication, the ship location should be accurately known. This information is used to drive the antenna positioning servo system which points the antenna in the required direction.

The tracking accuracies depend on the correct orbit predictions. Frequently operator intervention is necessary. In cases where high pointing accuracies are not a criterion, programme tracking can be used. Many earth stations use programme tracking as a back up system in case other systems fail.

2.8.3 Monopulse Tracking (Simultaneous Lobing System)

Monopulse tracking is one of the earlier and popular autotracking mechanisms. In this technique, the satellite beacon error signal, resolved in elevation and azimuth planes, drives the mounting servos to null this error . The antenna used in monopulse tracking system has a four horn feed system symmetrically arranged about the boresight axis which creates overlapping antenna patterns (c.f. Fig. 2.14). The received signal is split into four components by exciting all the four feeds and is then processed by a comparator to generate three different antenna pattern response characteristics.

The sum pattern is the sum of all four signals, the elevation difference pattern has two main lobes in the elevation plane with a deep null on the boresight axis (c.f. Fig. 2.15). The magnitude and the sign of error signal depend on the angle of boresight axis in that particular plane.

The tracking error signal is independent of the absolute value of the received signal and the error signal is approximately a linear function of the off axis angle. The tracking accuracy is very good, typically 0.005^{o} with a SNR of about 15 dB (c.f. Hawkins et al., 1988).

This type of tracking system is mainly employed by large earth stations such as INTELSAT and marine satellite communication systems such as SKYNET and for satellite to satellite communication.

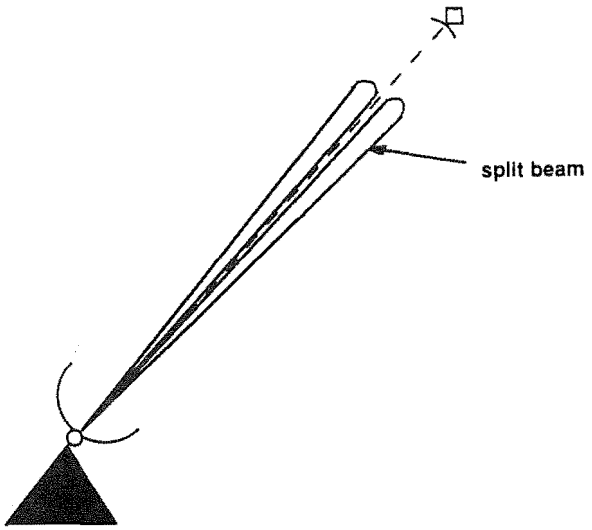

Fig. 2.14 Monopulse tracking system

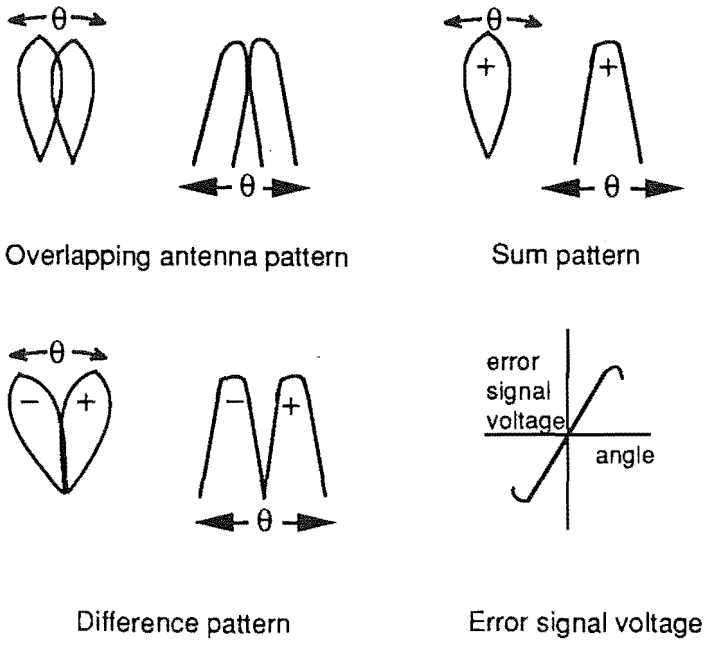

Fig. 2.15 Simultaneous lobing system

The complex wavefront processing to derive tracking error information and the use of a 4 or 8 channel receiver makes the system expensive. The four feed arrangement results in mechanically large systems.

2.8.4 Sequential Amplitude Testing

Conical scanning system and step track system employ sequential amplitude testing technique.

2.8.4.1 Conical scanning system

In conical scanning system an offset beam is continuously rotated about the boresight axis of the antenna either by rotating the complete antenna about the boresight axis or by rotating an offset feed (c.f. Fig. 2.16). The received signal in the beacon channel is modulated at a frequency equal to the rotation rate of the beam. The magnitude and plane of the modulation represents the amount and direction of the correction required. When the antenna points directly at the satellite, the line of sight and the rotation axis coincide and the conical scan modulation is zero.

Conical scanning suffers from AM interference. The requirements for rotating the antenna or an offset feed makes the system mechanically complex. The tracking accuracies are less than those obtained by the monopulse technique. The cost of such system is also high. Conical scanning is being superseded by the step track and electronic beam squinting (EBS) systems described in the next sections.

2.8.4.2 Step track (hill climbing) system

In 1970 the step track or hill climbing tracking technique was developed. This tracking technique (c.f. Fig. 2.17) offers a low cost method which gives similar accuracies as obtained by using the conical scan method . The system is equipped with a signal strength detector, timing generator and stepping motors. The signal strength is sampled and measured. The antenna is then rotated about the azimuth axis and the measurement repeated. The antenna is next rotated about the elevation axis and signal strength measured. By comparison of the signal strengths before and after the moves, the direction of the movement to align the antenna is determined.

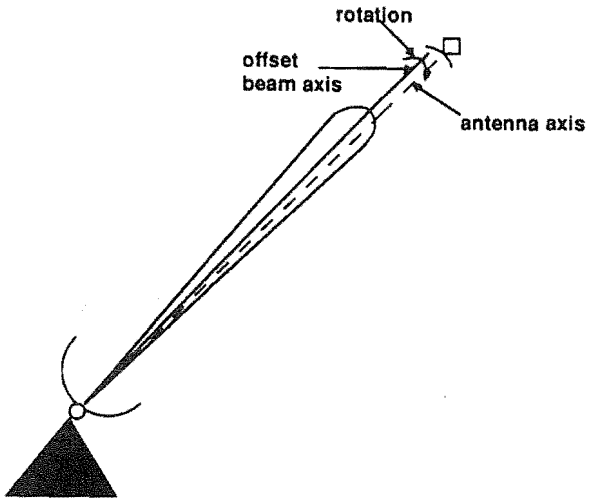

Fig. 2.16 Conical scanning tracking system

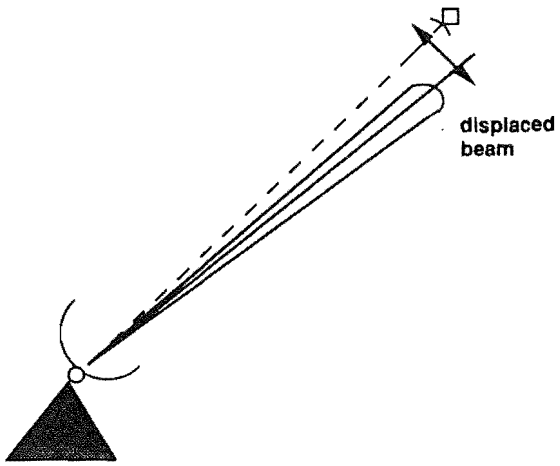

Fig. 2.17 Step track system

The limitations of the step track system are as follows: Even if the boresight axis is pointing accurately, the antenna axes will be moved. Therefore an average pointing error exists under perfect conditions. Secondly, the tracking mechanism does not work instantaneously. A dynamic lag always exists between the satellite position and the antenna position. This limits the achievable pointing accuracy to 0.05º (c.f. Hawkins et al., 1988). Thirdly, to match the pointing accuracy of a similar monopulse tracking system, the required SNR needs to be 15 dB higher. This is due to the susceptibility to AM interference or signal fading during sampling. Fourthly stepping of large antennas result in higher wear and tear of the servo systems and gearboxes during the execution of the search pattern. Thus for large antennas a nodding subreflector is preferred and this is then similar to the rotational subreflector used for some conical scan systems.

Considering all these limitations, the step track technique is used where lower cost of the communication system is required and the necessary pointing accuracy is not so high. For smaller earth stations and maritime satellite communication tracking systems, step track techniques are extensively used.

2.8.5 Electronic Beam Squinting (EBS)

Electronic beam squinting is the latest technique used for signal error detection. It consists of near simultaneous spatial measurement of beacon signal by using electronic switching techniques.

The tracking system antenna consists of four equally positioned parasite dipoles around a central dipole. Individual parasitic dipoles can be made to idle or can be short circuited. In practice each of them is short circuited in turn and the received beacon signal strength is measured in the receiver stage and stored along with its coordinate direction. This occurs in a millisecond time frame and the effects of signal fading can be averaged. The signal strengths in the single time frame are compared and the required coordinate position is computed to provide an error signal to drive the servos (c.f. Fig. 2.18).

EBS offers many advantages over other systems. It employs very high sampling rates. Pointing accuracies are very good, and are comparable

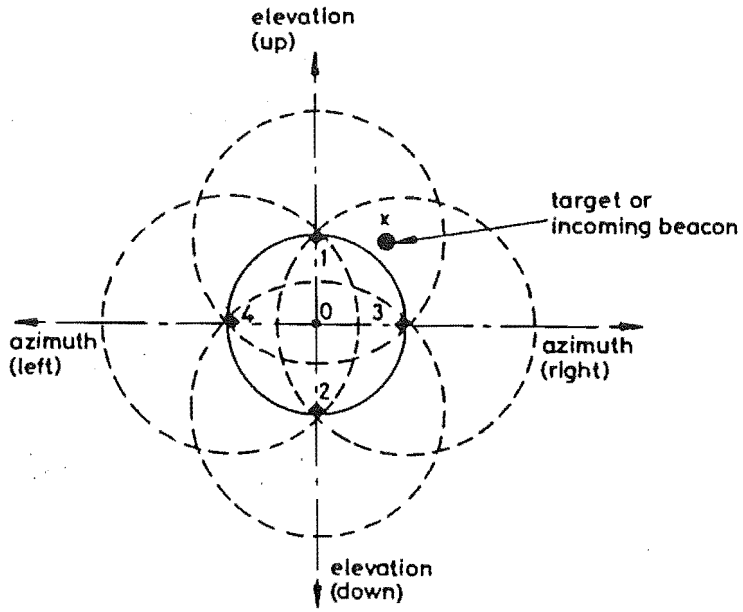

Fig. 2.18 Polar diagram showing directional location of secondary beam peak levels(1,2,3,4) relative to boresight (O) and incoming beacon (x) for EBS source: Hawkins G J (1988)

with traditional monopulse tracking system. The single channel tracking receiver makes the system comparatively cheap. The system is less susceptible to AM interference and has fast dynamic response. The reduced demand on servo mechanism results in reduced wear and tear and minimum maintenance costs.

2.9 BASIC QUANTITIES OF SATELLITE COMMUNICATION ANTENNAS

Various design parameters are used to optimize the performance of large antennas employed in an earth station. Some of the basic parameters are discussed briefly in the following section. A detail description can be found in the references Miya (1981) and CCIR report (1978).

2.9.1 Gain (G)

The antenna parameter of greatest interest to the system designer is the gain in the direction of the satellite. The gain of an antenna is defined as: "the ratio of the power per solid angle radiated in a given direction from the antenna to the power per unit solid angle radiated from an Isotropic antenna supplied with the same power" (c.f. Miya, 1981).

The gain G of an antenna having a physical aperture area of A is expressed by

$$G = \frac{4\pi}{\lambda^2} A \eta \qquad (2.1)$$

where η = aperture efficiency
λ = operating wavelength

Higher antenna gains are desirable because they produce higher gain to noise ratio and reduce the transmitting power of the satellite.

2.9.2 EIRP (Equivalent Isotropically Radiated Power)

EIRP is defined as the product of antenna input power P_T and its transmit gain G_T.

$$EIRP = P_T G_T \qquad (2.2)$$

The total EIRP from the satellite is limited by the cost of providing high satellite transmitter power and the fixed satellite antenna gain.

2.9.3 Directivity (D)

The degree that the radiated field is concentrated in one direction is called the directivity of an antenna. The antenna pattern is a recording on a chart of a measured directivity $D(\theta,\Phi)$ swept in a plane. The beamwidth can be determined by the antenna pattern recorded. The full angular width between the two points which are below the main beam peak by 3 dB is considered to represent the beamwidth and is called the Half Power Beamwidth (c.f. Fig. 2.19). Large antennas have higher gains but a narrow beamwidth and hence greater tracking accuracies are required. Beamwidth for a given aperture decreases as the frequency of the communication signal is increased (c.f. CCIR report, 1978).

2.9.4 Noise Temperature (T)

Noise temperature is a useful concept in receiver design, since it provides a method for determining total thermal noise generated by the active and passive devices in the receiving system. Miya (1981) gives the equation for the noise temperature T of a circular polarization receiving antenna as:

$$T = \frac{1}{4\pi} \int_{\theta=0}^{\pi} \int_{\Phi=0}^{2\pi} T_b(\theta,\Phi)\, G(\theta,\Phi)\, \sin\theta d\theta d\Phi \qquad (2.3)$$

where $G(\theta,\Phi)$ = gain of the antenna in the direction (θ,Φ).
$T_b(\theta,\Phi)$ = brightness temperature of the sky in the same direction.

To increase the gain to noise ratio for a given application, the lowest possible system noise temperatures need to be achieved.

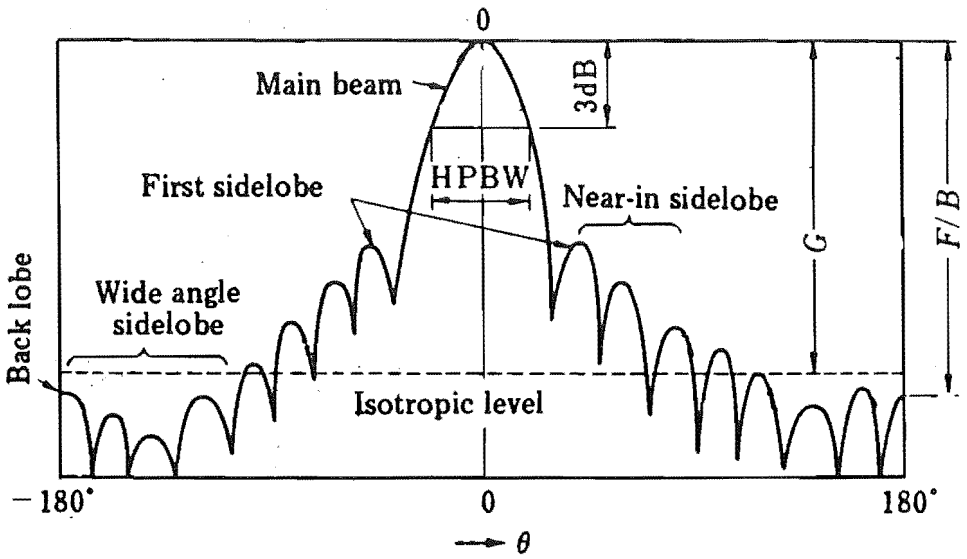

Fig. 2.19 Antenna radiation pattern showing half power beamwidth source: Miya K (1981)

2.9.5 Gain-to-Noise Ratio (G/T)

G/T is used as a "figure of merit". It is a measure of overall receiving system performance. The G/T ratio must be maximized within the constraints of antenna size and receiver cost. The optimum G/T for a given application is a compromise between the cost of large antenna, to increase G, and the cost of lower system noise, to decrease T, to achieve an optimum G/T.

2.9.6 Signal-to-Noise Ratio (SNR)

The equations to calculate the signal-to-noise ratio (SNR) are discussed by Miya (1981). The noise power P_N referred to the antenna input can be expressed as:

$$P_N = K\,Ts\,B \tag{2.4}$$

where K = Bolltzmann's constant (1.38×10^{-23} Joules/K)
B = frequency bandwidth, Hz
Ts = equivalent noise temperature in kelvin.

The receiving system noise temperature Ts is given by:

$$Ts = T + (Lf - 1)\,To + Lf\,Tr \tag{2.5}$$

where T = overall external noise
Lf = feed loss
To = temperature of the feed system
Tr = receive noise temperature

The carrier-to-noise ratio (C/N)r of the receiving system can be expressed as:

$$\left(\frac{C}{N}\right)_r = \frac{P_r}{P_n} = \frac{P_T G_T}{KB}\left(\frac{G}{T}\right)\left(\frac{\lambda}{4\pi d}\right)^2 \tag{2.6}$$

where P_r is the receive power of the antenna

The signal-to-noise ratio (SNR) of the earth station after demodulation can be expressed as:

$$\frac{S}{N} = G\left(\frac{C}{N}\right) \qquad (2.7)$$

where G = system gain.

2.10 EARTH STATION CLASSIFICATION

The following table summarizes the INTELSAT classification criteria for standard A, B and C type of earth stations.

Standard	A	B	C
Frequencies (GHz)	6/4	6/4	14/11
Polarization	Circular	Circular	Linear
G/T dBK^{-1}	40.7	31.7	$39 + 20 \text{ Log } \left(\frac{f}{11.2}\right)$
Typical dish diameter (m)	30	11-13	19
Antenna midband receive gain (dB)	61	51.5	65
Antenna midband transmit gain (dB)	64	54.1	66.4
Main reflector rms surface tolerance (mm)	1.0	0.8	0.6
Typical LNA noise temperature (K)	40	40	120

(Source: Pratt et al., 1986).

Table 2.1 Summary of INTELSAT Standard A, B, and C Earth Station Characteristics

2.11 SUMMARY

This chapter has presented a review of standard antenna mounting systems employed in the earth stations. The construction and "keyhole" problems associated with conventional mounting systems were discussed in detail. Special problems associated with maritime satellite communication systems were elaborated and the conventional methods used to solve these problems were discussed. A brief review of various antenna error detection methods used in autotracking was given. A further discussion on EBS is provided in chapter 5. Finally the various parameters affecting the design and performance of large earth station antennas were discussed. In particular, the effects of gain, noise temperature and frequency on the antenna beamwidth and hence tracking accuracy requirements were elaborated.

CHAPTER 3

SIX DEGREES OF FREEDOM PARALLEL LINKAGE ROBOTIC MANIPULATOR: GEOMETRIC AND KINEMATIC ANALYSIS

3.1 INTRODUCTION

In the previous chapter, the "keyhole" problems associated with conventional antenna mount systems have been described. It was pointed out that a high gain antenna mounting system used on a ship will experience difficulties in satellite communication because of the dynamic motion of the ship. As the trend towards large aperture, high frequency antennas continues, there is a corresponding increase in the need for an accurate antenna positioning mechanism.

A solution to the above problem was suggested by Dunlop and Azulpurkar (1988) during the research on modified Stewart platform mechanism. The Stewart platform (c.f. Stewart, 1965) is a parallel linkage mechanism which consists of six linear actuators constrained between a fixed base and a moving platform. Stewart platform has six degrees of freedom so an antenna mounted on the moving platform can be aimed anywhere in the visible hemisphere without any "keyhole" regions.

This chapter deals with the kinematic analysis of the parallel link mechanism based on the modified Stewart platform. Various characteristics of the parallel link manipulator are compared with a conventional serial link robot configuration. A method for the determination of the six actuator lengths for various orientations of the platform is outlined and the mechanical joint design is discussed. The singularity positions of the parallel linkage manipulator are elaborated.

3.2 ROBOTIC MANIPULATORS

A mechanism is a means of transmitting, controlling or constraining relative movements. A manipulator can be defined as a device which is capable of

grasping an object and changing its position and orientation in the space. The Robotic Institute of America defines an industrial robot as:

"a reprogrammable, multifunctional manipulator designed to move material, parts, tools or specialised devices through variable programmed motions for the performance of a variety of tasks."

The position of an object in the space is determined by three spatial coordinates (X, Y, Z) with reference to a fixed orthogonal frame and its angular rotations, pitch, yaw and roll (θ, Φ, α) around each of the three axes. Thus, to carry out a spatial manipulation task, a robotic manipulator is required to produce six independent controlled motions, three translational motions along the three orthogonal axes and three rotational motions about these axes. Thus, a general purpose manipulator should have six degrees of freedom (DOF) to carry out the required translational and rotational motions. The six DOF can be achieved by using six links connected to each other by suitable joints. Each of the six freedoms must be controlled separately.

Most of the present day industrial robots have designs which try to emulate the human arm, i.e. they are "anthropomorphic". In a human arm, the shoulder and the elbow joints position the arm in space and the wrist joint orients the hand to perform the operation of object grasping and manipulation. Likewise, most robotic manipulators have their actuators connected in series through revolute or prismatic joints, each joint representing a degree of freedom. The two types of joints used are: prismatic (or sliding pair) allowing pure translation of one link with respect to the other, or the revolute pair providing pure rotation between adjacent links.

There are many robotic configurations capable of providing the six degrees of freedom. According to the way how the links are connected to each other they can be classified as:

1. Serial link or open kinematic chain manipulators.

2. Parallel link or closed kinematic chain manipulators.

3. Hybrid - a combination of 1 and 2.

3.3 SERIAL LINK ROBOTIC MANIPULATORS

A schematic diagram of a conventional serial link manipulator is shown in Fig. 3.1. It has six fixed length links each of which can swing through an arc with respect to the preceding link thus positioning the end effector at the required position.

3.3.1 Advantages of a Serial Link Manipulator

The serial link manipulator which is constructed as an open kinematic chain has several advantages.

1. Large range of motion: Since the links are connected one after the other, the manipulator has a large work envelope. The work space of a typical anthropomorphic robot is shown in Fig. 3.2. The large work space also results in longer reach of the end effector.

2. The serial link manipulator has an ability to reach into small holes.

3. All the link joints are powered establishing a direct relationship between the number of joints and the degrees of freedom of the end effector.

3.3.2 Disadvantages of a Serial Link Manipulator

1. Each link carries the weight of the following link and its drive mechanism. Thus the links and joints need to be stiff and this further increases the total mass to be moved. This puts limits on the amount of weight that can be handled by the robot because of the cantilever construction. To reduce the moving mass and inertia, the motor drives are usually located on the first link of the robot.

2. All the errors arising in the joints are cumulative and the actual position of the end effector may be different from the predicted one. Thus some form of compensated actuation and sophisticated control technique need to be employed to alleviate the load dependent errors.

3. In a serial link manipulator, for a given position of end effector there exists more than one set of joint coordinates. Thus the kinematic indeterminacy

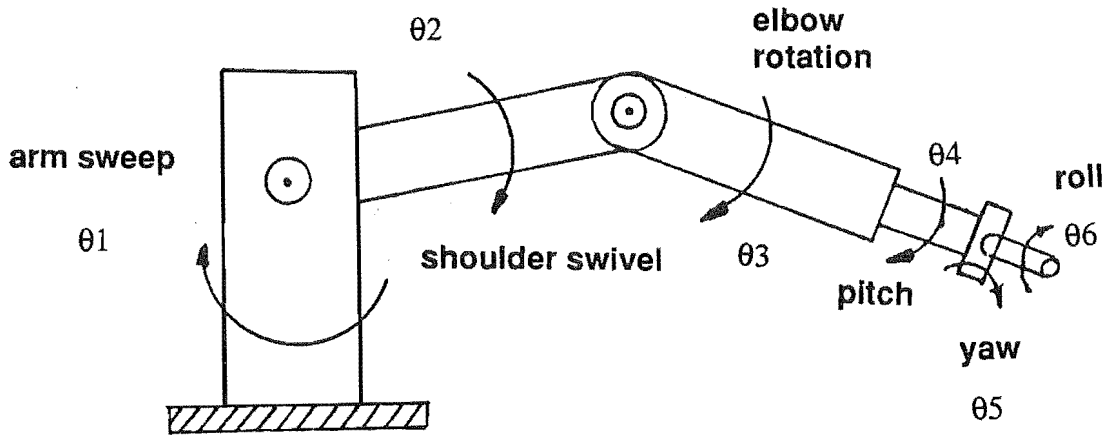

Fig. 3.1 A typical serial link robot with six degrees of freedom

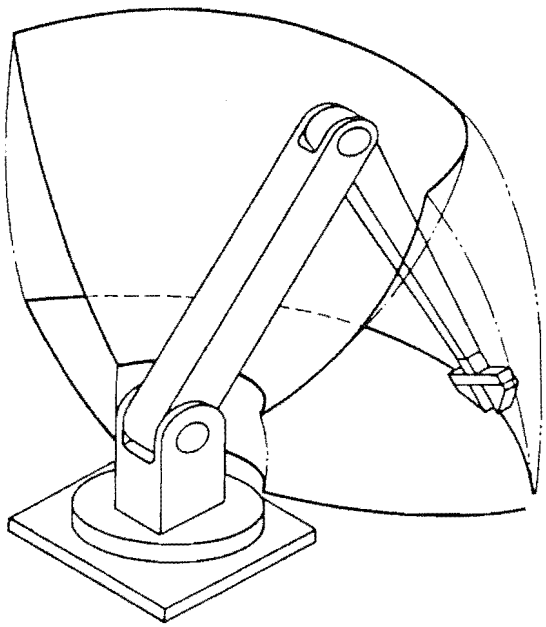

Fig.3.2 Anthropomorphic robot and the associated workspace

results in ambiguous positions of the links for a required end effector position.

3.4 AN ALTERNATIVE MANIPULATOR DESIGN

An alternative to the conventional serially linked open chain manipulator was originally suggested by Stewart (1965) for use as a 'flight simulator' (c.f. Fig. 3.3). He called the mechanism as "A platform with six degrees of freedom". Stewart's original design consisted of a triangular plane called the platform connected to the base with six extendable legs. The legs were connected to the platform through a three axis joint and to the base by a two axis joint. By controlling the length of each leg, the platform can be moved to the required position and orientation. Stewart envisaged the use of such a platform as a flight simulator, a stable platform on a ship subjected to pitch, roll and yaw motions, a new form of machine tool and a mechanism for automated assembly.

Hunt (1978, 1982, 1983) has further developed the kinematic geometry of a six degree of freedom parallel manipulator. He has applied the theory of screw systems to investigate the mobility and the singular positions of the parallel robotic structure (Hunt, 1980). He has reviewed many possible applicable parallel structures including the Stewart platform (Hunt, 1978). He has also listed the advantages of the parallel mechanism as being sturdier and less prone to accumulated errors due to the series connections, and also having less risk of unexpected linear dependence of the actuator freedom.

Fichter and McDowell (1980) suggested a robot arm based on the modified Stewart platform and have discussed the kinematic analysis of the parallel mechanism (1983, 1984). Fichter has presented a practical design of a Stewart platform based manipulator (1987). He suggested the possible applications of this robot in material handling, assembly, contour milling, painting, welding and as an antenna steering mechanism with a limited angular range. GEC developed a parallel topology manipulator controlled by a single board computer called 'GADFLY' for fast assembly operations (c.f. Powel, 1981, Potton, 1983).

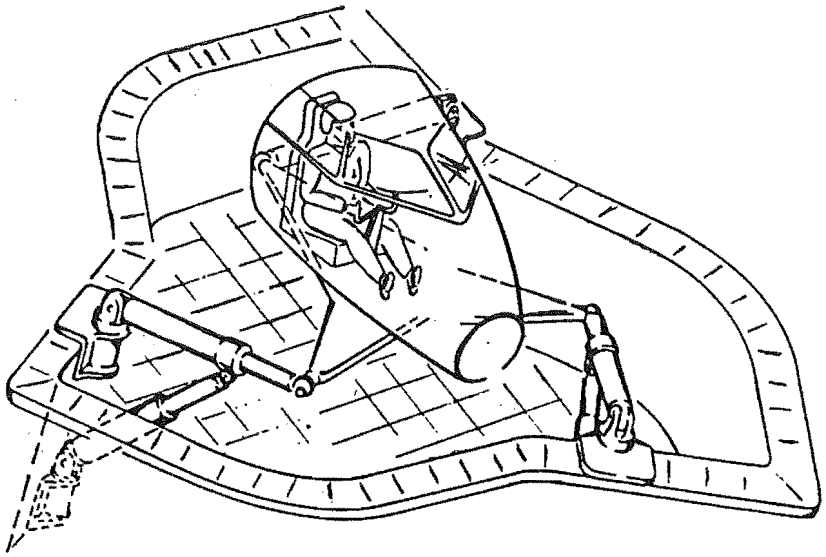

Fig. 3.3 Flight simulator based on the Stewart platform source: Stewart (1965)

McCallion and Pham (1979) used the parallel link mechanism for mechanised assembly. They suggested an assembly system consisting of industrial robots to handle large movements and a work station based on Stewart platform to perform the small and precise movements required for the final stage of the assembly operation. They established a one to one relationship between the platform's orientation and position and the actuator lengths. The six degree of freedom work station along with a compliant device was used to insert pegs of sizes ranging from 12 mm to 50 mm in diameter and 25 mm to 100 mm in length, into holes having diametral clearances from 12 μm to 24 μm and starting with misalignments between 1 mm to 2 mm and 1.5° to 2.5° (Pham, 1979).

A number of authors have carried out the number synthesis for the parallel mechanism (c.f. Pham, 1979, Hunt, 1980). Earl et al. (1982) have suggested module construction of kinematic structures to generate designs suitable for use in robot manipulators. Yang et al. (1984) have described an analytical method and computer aided procedure for analysing the kinematic characteristics of the parallel link mechanism. They have used ball and socket joints for the analysis and have given numerical methods for calculating the workspace of the mechanism in special cases. Inoue et al. (1985) have suggested the construction of a parallel manipulator in which the base and the platform are connected by a set of three pantographs instead of linear actuators. At the University of Canterbury, New Zealand, Rathbun (1986) developed an experimental NC milling machine with six degrees of freedom based on the Stewart platform mechanism (c.f. Fig. 3.4). Six electric step motors were used to drive the leadscrew actuators. The milling machine had a range of ± 100 mm in the linear axes and about ± 30° in the rotational axes. The milling machine controller was tested by machining rigid urethane foam blocks. The path synthesis and motion control calculations were performed by using a Z80 CPU. Cyclic angular errors were generated by the Hookes joints used to drive the leadscrews. These joints also jammed at some angles thus producing errors in the open loop control system.

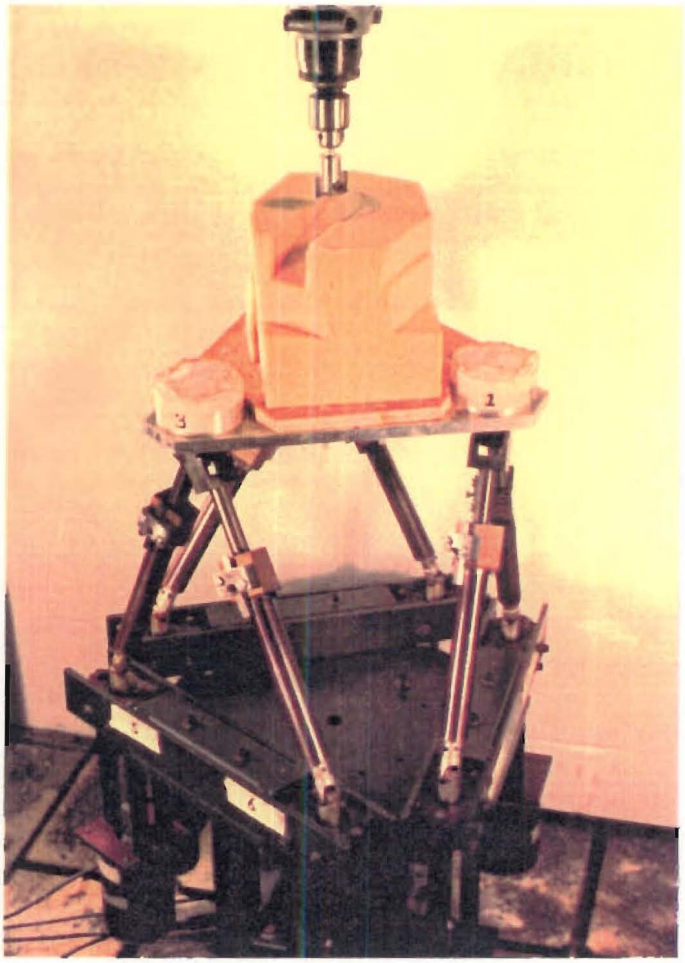

Fig. 3.4 Stewart platform: milling machine application

3.5 CONSTRUCTION OF A MODIFIED STEWART PLATFORM

Fig. 3.5 shows a modified Stewart platform in its simplest form. It consists of two bodies connected together by six actuators which can expand and contract. One body is called the base which is fixed and the other is called the platform which is movable. Each of the six actuators has one of its end points fixed to the base by a modified Hookes joint and the other to the platform by a three axis joint. Each actuator can expand and contract independently of the others thus positioning the platform with respect to the base. With the base fixed, the mechanism has six-degrees of freedom (c.f. Pham, 1979). The whole platform is moved to achieve the six degrees of freedom. Most conventional robots split the six DOF between the robot arm and the wrist. The arm positions the wrist in the 3D space and the wrist aligns the gripper. The limitations of work volume or motion of the mechanism are determined by the maximum and minimum actuator lengths, the size of the base and the platform and the joints range (c. f. section 5.3.1).

For a practical construction of the Stewart platform, the six points in the platform coincide in three pairs which are connected to six distinct points in the base (c.f. Fig. 3.6). Thus the platform is supported by three triangles $B_1B_2P_{12}$; $B_3B_4P_{34}$ and $B_5B_6P_{56}$. Such a triangulated system is capable of producing a very stiff structure. In each triangle the point Pij can lie anywhere in the plane of the supporting triangle Bi Bj Pij within the maximum and minimum limits of sides BiPij and BjPij. Each triangle can rotate about the axis BiBj allowing point Pij to lie anywhere along an arc. With this type of arrangement the platform load is supported by only tension or compression of the actuators. Each of the actuators produces a couple in opposite direction of that produced by the other actuator forming the triangle. Thus the couples counteract and eliminate torsion. Effectively the platform is supported by six pure forces (c.f. Fichter, 1987).

3.6 KINEMATIC STRUCTURE OF A PARALLEL MECHANISM

The kinematic structure of one of the actuators is shown schematically in Fig. 3.7. As seen from the Fig. 3.7 there are six joints in series. As discussed in previous paragraphs the joint between the platform and actuator is a RRR joint and that between the base and the actuator is a RR joint. The actuator

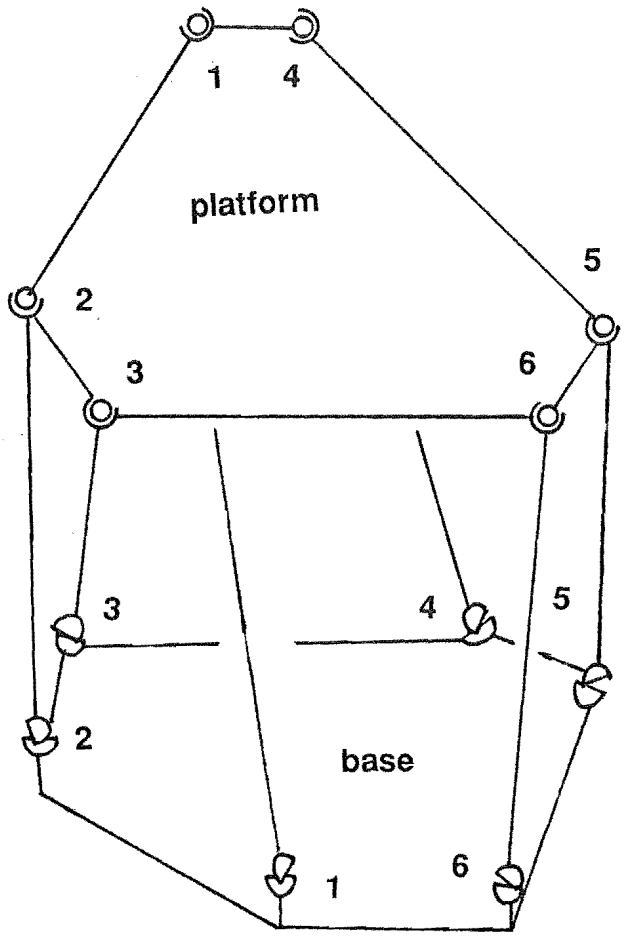

Fig. 3.5 General arrangement of the Stewart Platform

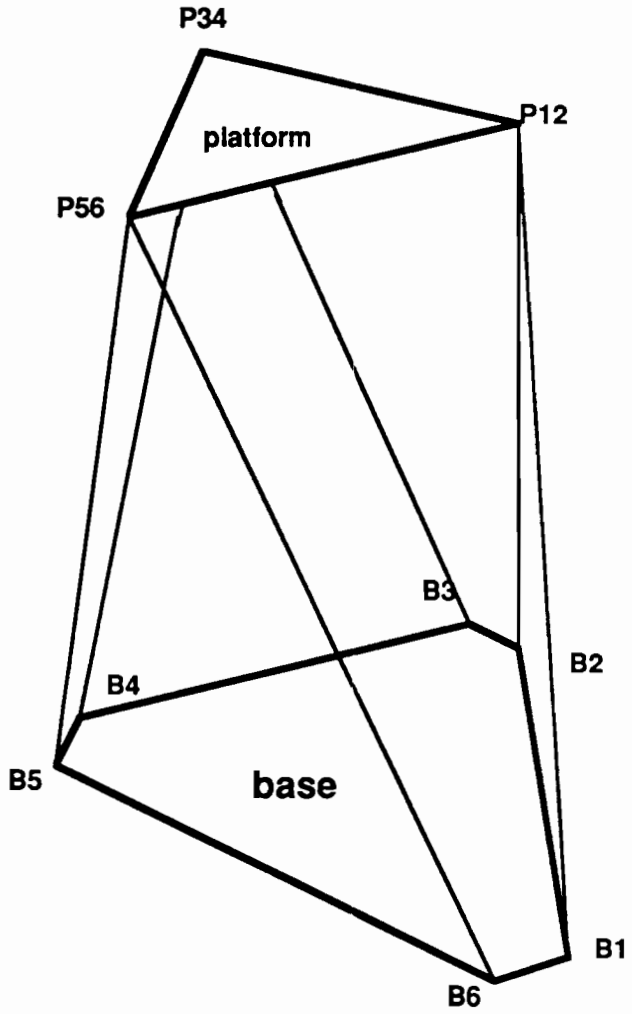

Fig. 3.6 Simplified Stewart platform construction

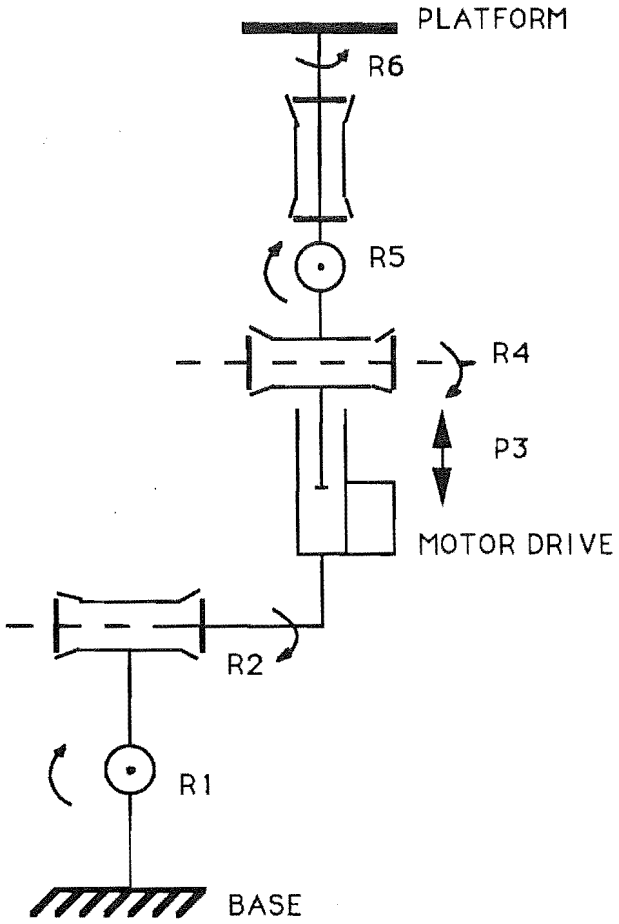

Fig. 3.7 kinematic structure of a parallel link mechanism

itself is a prismatic joint denoted by P3. In actual construction of such a mechanism the axes of the revolute joints R4, R5 and R6 are coincedent at a point Pij in the platform and the axes of the revolute joints R1 and R2 are coincident at a point Bi in the base.

3.7 KINEMATIC ANALYSIS

The kinematic analysis for a parallel mechanism involves calculation of the link lengths for the required position and orientation of the platform. In the following analysis the inverse problem for parallel mechanisms is discussed. A vector approach is used to determine the machine coordinates of the mechanism (L_i, i = 1 to 6) from the world coordinates (Φ, θ, α, x, y, z).

3.7.1 Vector Equations

The base and the platform of the general Stewart platform are arranged in a symmetric manner as shown in Fig. 3.8. A right handed orthogonal coordinate system is defined at a convenient place in each body. Each of the six points in the base is described by a position vector $\overline{BASE_i}$ with reference to the base coordinate system XYZ. Each of the six points in platform is described by a position vector $\overline{PLAT_i}$ with reference to the platform coordinate system xyz. The six points in platform coincide in three pairs. Thus the platform has three attachment points defined at the apex of an equilateral triangle. The base has six attachment points arranged symmetrically around base pitch circle radius 'Rb'. The platform pitch circle radius is 'Rp'. For platform with zero pitch, roll and yaw, the XYZ and xyz coordinate systems coincide and are shown in Fig. 3.8. This arrangement results in maximum stiffness of the structure. The adjacent base vectors subtend an angle of 2β. The angle β is selected such that there is no interference between adjacent actuators for any configuration of the system.

With reference to Fig. 3.9, the X components of six base vectors can be expressed in terms of Rb and β and are given by following equations:

$$
\begin{aligned}
\text{BASE (1,X)} &= \text{Rb Cos } (60^o + \beta) \\
\text{BASE (2,X)} &= \text{Rb Cos } (60^o - \beta) \\
\text{BASE (3,X)} &= \text{Rb Cos } (60^o - \beta) \\
\text{BASE (4,X)} &= \text{Rb Cos } (60^o + \beta) \\
\text{BASE (5,X)} &= -\text{Rb Cos } (\beta) \\
\text{BASE (6,X)} &= -\text{Rb Cos } (\beta)
\end{aligned}
\qquad (3.1)
$$

Similarly the Y components of the six base vectors can be expressed in terms of Rb and β and are given as:

$$
\begin{aligned}
\text{BASE (1,Y)} &= \text{Rb Sin } (60^o + \beta) \\
\text{BASE (2,Y)} &= \text{Rb Sin } (60^o - \beta) \\
\text{BASE (3,Y)} &= -\text{Rb Sin } (60^o - \beta) \\
\text{BASE (4,Y)} &= -\text{Rb Sin } (60^o + \beta) \\
\text{BASE (5,Y)} &= -\text{Rb Sin } (\beta) \\
\text{BASE (6,Y)} &= \text{Rb Sin } (\beta)
\end{aligned}
\qquad (3.2)
$$

These vectors are expressed with reference to the fixed orthogonal coordinate system, XYZ embedded in the base.

With reference to Fig. 3.10, the x components of the six platform vectors are expressed in terms of Rp and are given by following equations.

$$
\begin{aligned}
\text{PLATFORM (1,x)} &= -\text{Rp Cos } (60^o) \\
\text{PLATFORM (2,x)} &= \text{Rp} \\
\text{PLATFORM (3,x)} &= \text{Rp} \\
\text{PLATFORM (4,x)} &= -\text{Rp Cos } (60^o) \\
\text{PLATFORM (5,x)} &= -\text{Rp Cos } (60^o) \\
\text{PLATFORM (6,x)} &= -\text{Rp Cos } (60^o)
\end{aligned}
\qquad (3.3)
$$

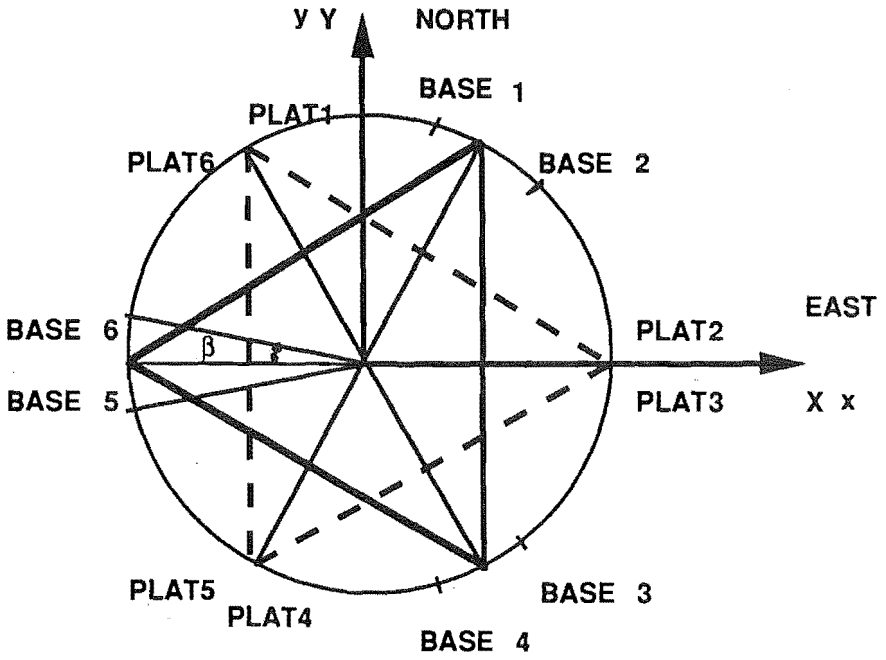

Fig.3.8 Base and platform orientation

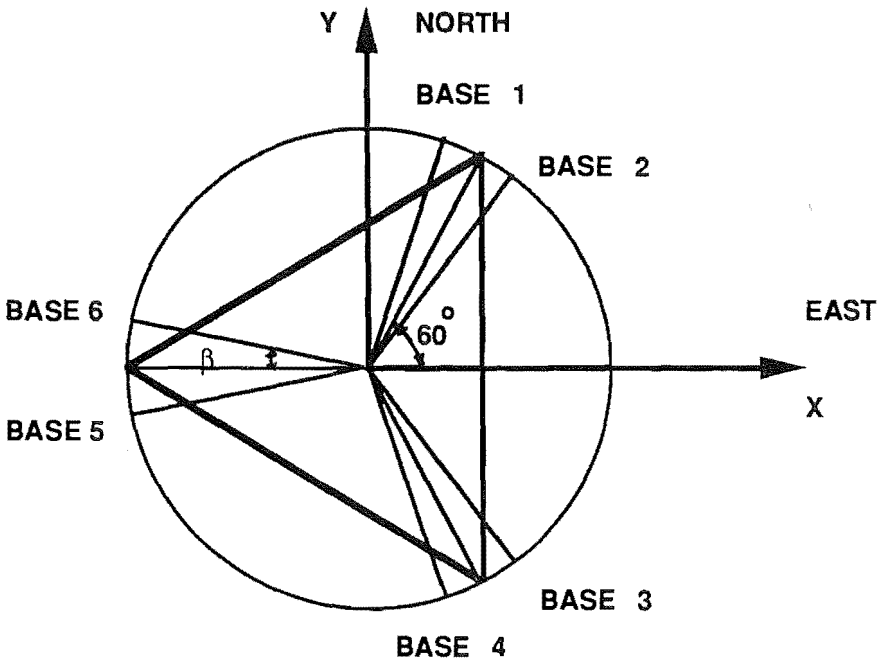

Fig. 3.9 Base Vectors

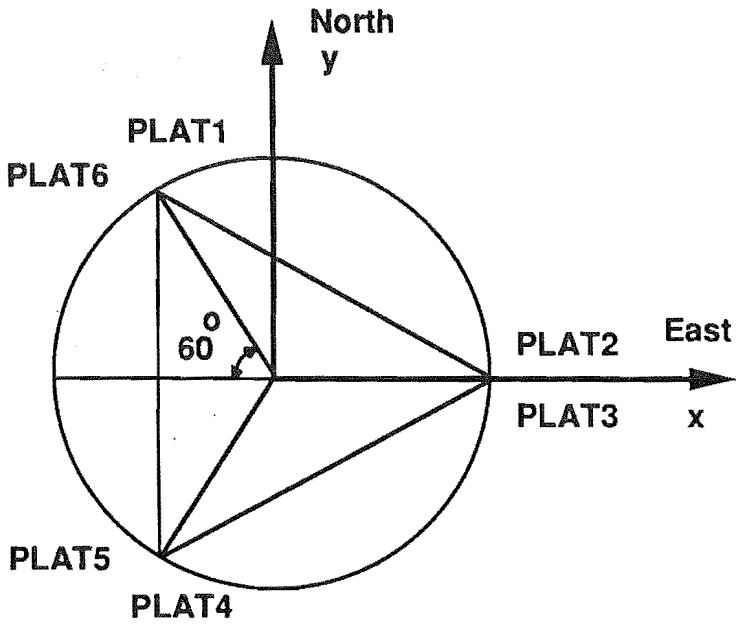

Fig. 3.10 Platform vectors

Similarly the y components of the six platform vectors are given as:

$$\begin{aligned} \text{PLATFORM (1,y)} &= \text{Rp Cos (30°)} \\ \text{PLATFORM (2,y)} &= \text{O} \\ \text{PLATFORM (3,y)} &= \text{O} \\ \text{PLATFORM (4,y)} &= -\text{Rp Cos (30°)} \\ \text{PLATFORM (5,y)} &= -\text{Rp Cos (30°)} \\ \text{PLATFORM (6,y)} &= \text{Rp Cos (30°)} \end{aligned} \qquad (3.4)$$

For all platform vectors z = 0.

3.7.2 Vector Transformation

The homogeneous coordinate representation of objects in the three dimensional space is a (3 + 1) space entity. The fourth coordinate for each vector is a scale factor. When each component of the vector is multiplied by the scale factor the direction and magnitude of the vector does not change. A point vector $Xi + Yj + Zk$ is represented in homogeneous coordinates as a column matrix.

$$\bar{B} = [X\ Y\ Z\ 1]^T \qquad (3.5)$$

The transformation of a space is a 4 x 4 matrix and represents translation and rotation of vectors. The transformation F of a vector $\bar{B}$ to a vector $\bar{P}$ is represented by the matrix product:

$$\bar{P} = F\bar{B} \qquad (3.6)$$

Matrix transformation can be used to transform around a closed chain in a mechanism. If a coordinate system (Xi Yi Zi) is fixed in the link i then the transformation matrix F (i, i + 1) transforms the coordinates of vector $\bar{B}$ in system i to its coordinates in system i + i. A set of transformations applied to a body in the space will give the final position and orientation of the body.

3.7.2.1 Translation transformation

The transformation T corresponding to a translation by a vector Ai + Bj + Ck is given by:

$$T = \text{Trans}(Ai + Bj + Ck) = \begin{bmatrix} 1 & O & O & A \\ O & 1 & O & B \\ O & O & 1 & C \\ O & O & O & 1 \end{bmatrix} \qquad (3.7)$$

Given a vector $\bar{B}$ (X, Y, Z, 1), its transformation vector $\bar{V}$ is given by

$$\bar{V} = T\bar{B} = \begin{bmatrix} 1 & O & O & A \\ O & 1 & O & B \\ O & O & 1 & C \\ O & O & O & 1 \end{bmatrix} \begin{bmatrix} X \\ Y \\ Z \\ 1 \end{bmatrix} = \begin{bmatrix} X+A \\ Y+B \\ Z+C \\ 1 \end{bmatrix} \qquad (3.8)$$

The translation transformation can be viewed as addition of two vectors Xi + Yj + ZK and Ai + Bj + CK. During the translation transformation the orientation of the body does not change.

3.7.2.2 Rotation transformation

The transformations corresponding to rotations about the X, Y, Z axes by the angles Φ, θ, α respectively are given as follows:

$$\text{Rot}(X, \Phi) = \begin{bmatrix} 1 & O & O & O \\ O & C\Phi & -S\Phi & O \\ O & S\Phi & C\Phi & O \\ O & O & O & 1 \end{bmatrix} \qquad (3.9)$$

$$\text{Rot}(Y, \theta) = \begin{bmatrix} C\theta & O & S\theta & O \\ O & 1 & O & O \\ -S\theta & O & C\theta & O \\ O & O & O & 1 \end{bmatrix} \qquad (3.10)$$

$$\text{Rot}(Z, \alpha) = \begin{bmatrix} C\alpha & -S\alpha & O & O \\ S\alpha & C\alpha & O & O \\ O & O & 1 & O \\ O & O & O & 1 \end{bmatrix} \qquad (3.11)$$

Where CΦ and SΦ represent Cos (Φ) and Sin (Φ) and Cθ and Sθ represent Cos (θ) and Sin (θ) respectively. The transformation R which consists of rotation Φ about the Z axis followed by rotation θ about Y axis can be expressed in the reference coordinate frame (X, Y, Z) as:

$$R = \text{Rot}(Y,\theta)\ \text{Rot}(Z,\Phi) \qquad (3.12)$$

The same set of rotations can be viewed as a rotation Φ about the Z axis followed by rotation θ about the new Y' axis.

$$Rr = \text{Rot}(Z,\Phi)\ \text{Rot}(Y',\theta) \qquad (3.13)$$

In general, if we post multiply a transformation representing a frame by a second transformation, we make that transformation with respect to the frame axes determined by the first transformation. Where as premultiplication results in the transformations with respect to the fixed coordinate system (c.f. Paul, 1981).

3.7.3 Euler Angles

Euler angles are three independent parameters which uniquely determine the orientation of one rigid body relative to the reference coordinate system. Orientation is mostly specified by a sequence of rotations roll, pitch and yaw or else by the Euler Angles. Euler angles describe any possible orientation in terms of a rotation Φ about Z axis followed by a rotation θ about the new Y' axis and finally a rotation α about the new Z" axis (c.f. Fig. 3.11). The Euler transformation E(Φ, θ, α) can be evaluated by multiplication of the three rotation matrices.

$$R(\Phi,\theta,\alpha) = \text{Euler}(\Phi,\theta,\alpha) = \text{Rot}(Z,\Phi)\ \text{Rot}(Y',\theta)\ \text{Rot}(Z'',\alpha) \qquad (3.14)$$

$$= \begin{bmatrix} (C\Phi C\theta C\alpha - S\Phi S\alpha) & (-C\Phi C\theta S\alpha - S\Phi C\alpha) & (C\Phi S\theta) & O \\ (S\Phi C\theta C\alpha + C\Phi S\alpha) & (-S\Phi C\theta S\alpha + C\varnothing C\alpha) & (S\theta S\alpha) & O \\ (-S\theta C\alpha) & (S\theta S\alpha) & (C\theta) & O \\ O & O & O & 1 \end{bmatrix}$$

3.7.4 Specification of Position

Once the platform orientation is specified by the Euler Angles (Φ,θ,α), the final position can be fixed by multiplying $E(\Phi,\theta,\alpha)$ by a translation transform corresponding to a vector $\bar{T}$. The position of the platform relative to the base is defined by a translation that may be written as a vector $\bar{T}$, from the origin of the base coordinate system to the origin of the platform coordinate system. Each linear actuator is represented by a vector and vector algebra is used to find out various lengths and angles as discussed in the following section.

3.8 DETERMINATION OF ACTUATOR LENGTHS

The orientation of the antenna dish can be specified in the Euler angle coordinates E (Φ, θ, α) or RPY (roll, pitch and yaw) coordinates. A vector normal to the platform plane passing through the xyz coordinate system origin can be pointed anywhere in the space by rotating the platform by an angle Φ about the Z axis, followed by an angle θ about the new Y' axis and finally by an angle α about the new Z" axis. When applied to a moving satellite, the Azimuth look (Az) is measured as a bearing from the true North and is ($90 - \Phi^{o}$). The elevation look angle (El) is measured above the horizon and is ($90 - \theta^{o}$). The final rotation angle α is set equal to ($-\Phi$) to untangle the six links. The Euler transformation equation (3.14) is then written as:

$$\text{Euler}\,[90^{o} - Az,\ 90^{o} - El,\ Az - 90^{o}] \qquad (3.15)$$

The rotations are performed in one operation instead of one after other to avoid the actuator links colliding with each other. These rotations are followed by a translation $\bar{T}$ to the final XYZ axis position as shown in Fig. 3.12. The transformation is given by the following equation:

$$\begin{aligned} & T = \text{Trans}\,(A, B, C) \\ \text{Where} \quad & A = L\,C\Phi\,S(\theta/2) \\ & B = L\,S\Phi\,C(\theta/2) \\ & C = L\,C(\theta/2) \end{aligned} \qquad (3.16)$$

L = the distance between the platform and base centroids

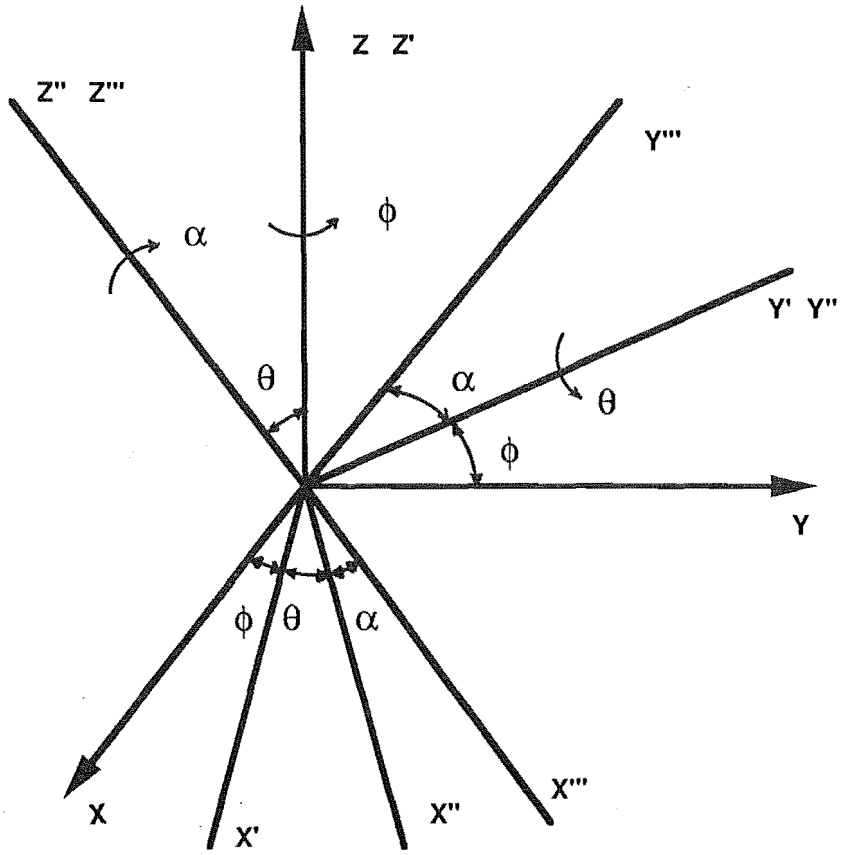

Fig. 3.11 Euler angles

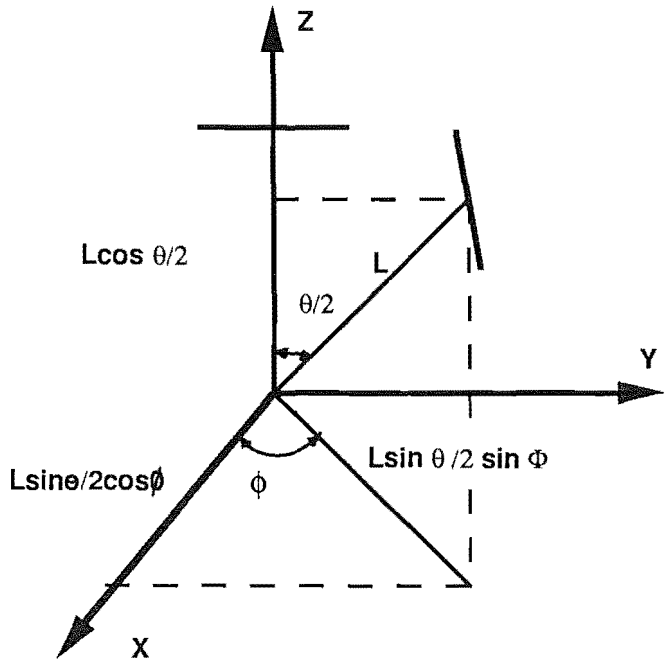

Fig. 3.12 Translation components for platform position specification

These translation coordinates are obtained by giving rotations to the platform such that the vector $\bar{T}$ moves along a hemisphere and makes equal angles (ζ) with the base and the platform.

The six platform joint position vectors $\overline{RPLATFORMi}$, where i = 1 to 6, are obtained by rotating the corresponding joint vectors $\overline{PLATFORMi}$ through the Euler angles (Φ, θ, α). Mathematically:

$$\overline{RPLATFORMi} = R(\Phi, \theta, \alpha)\,\overline{PLATFORMi} \qquad (3.17)$$

The six platform joint vectors $\overline{RPLATFORMi}$ are translated by T (A, B, C). The translated platform vectors are given by:

$$\overline{TPLATFORMi} = T(A, B, C) + R(\Phi, \theta, \alpha)\,\overline{PLATFORMi} \qquad (3.18)$$

In the matrix form

$$\begin{bmatrix} TPLATFORMix \\ TPLATFORMiy \\ TPLATFORMiz \\ 1 \end{bmatrix} = \begin{bmatrix} Li\ C\Phi\ S(\theta/2) \\ Li\ S\Phi\ C(\theta/2) \\ Li\ C(\theta/2) \\ 1 \end{bmatrix} + \begin{bmatrix} RPLATFORMix \\ RPLATFORMiy \\ RPLATFORMiz \\ 1 \end{bmatrix} \qquad (3.19)$$

The actuator lengths are calculated as the vector difference between $\overline{BASEi}$ and $\overline{TPLATFORMi}$.

In the vector form:

$$\overline{Vi} = \overline{BASEi} - \overline{TPLATFORMi} \qquad (3.20)$$

Thus the magnitude of each actuator length is given by:

$$Vi = \sqrt{Vx^2 + Vy^2 + Vz^2} \qquad (3.21)$$

Thus the actuator lengths can be calculated for all the positions of the platform for each azimuth and elevation angle as the platform moves in the hemispherical work envelope.

3.9 DIRECT AND INVERSE PROBLEM FOR SERIAL AND PARALLEL LINKAGE MANIPULATORS

For a parallel link manipulator given the required six end effector coordinates (Φ, θ, α, x, y, z), the six link lengths (joint coordinates) can be easily calculated using matrix transformations as discussed in previous paragraphs. In order to position the end effector at a desired location in the space the joint coordinates need to be calculated. Thus a closed form solution exists for the inverse problem in case of a parallel link manipulator. But for the direct problem, to determine the six end effector coordinates (Φ, θ, α, x, y, z) from the six link lengths, an iterative method needs to be applied.

For a conventional serial link robot the inverse problem involves calculating the joint coordinates (θ_1, θ_2, θ_3, θ_4, θ_5, θ_6) from the given end effector position. This is usually done by evaluating the kinematic equations obtained by multiplication of transformation matrices (c.f. Paul, 1981). However a closed form solution exists for calculating the end effector coordinates from the joint coordinates.

3.10 DETERMINATION OF THE JOINT ANGLES

The design of the joints between the platform and the actuators and the base and the actuators is critical for maximising the range of motion. Since the platform should be capable of moving through a hemisphere, the rotation limits of the joints should not restrict the motion of the platform. An analytical model is developed in the following section to determine the various physical constraints such as rotation range of the joints of the whole mechanism.

The top joint connects a pair of actuators to the platform. The centre lines of both the actuators and the local vertical axis must be coincedent to allow a single point connection in the platform. Thus the two actuators and base line form a triangle which simplifies the kinematic analysis and reduces the amount of computation required for the inverse kinematic transformations. A ball joint would limit the range of motion. Thus design of a joint capable of rotating about Az axis (c axis), El axis (b axis) and the platform 'a' axis is required (c.f. Fig. 3.15).

In order to avoid interference between the actuators which form a triangle, the minimum angle which the pair of actuators can make with each other must be calculated (c.f. Fig. 3.13). Referring to Fig. 3.13 these angle are nothing but the angles between the actuator pairs 1-6, 2-3 and 4-5. So the angles $\Psi_{1\text{-}6}$, $\Psi_{2\text{-}3}$ and $\Psi_{4\text{-}5}$ can be calculated from the vectors $\bar{V}_i$, i = 1 to 6 as follows:

$$\Psi_{1\text{-}6} = \cos^{-1}\left(\frac{\bar{V}1 \bullet \bar{V}6}{|\bar{V}_i|\ |\bar{V}6|}\right) \qquad (3.22)$$

Similarly the angle between actuators 2 and 3 ($\Psi_{2\text{-}3}$) and between actuators 4 and 5 ($\Psi_{4\text{-}5}$) can be calculated.

Next is the angle between the actuators and the Platform a, a' and a" axes (local elevation axes). Referring to Fig. 3.13, it is clear that in order to achieve the maximum range of motion, the actuators should be able to make as small angle as possible with the platform local elevation axes.
As seen from Fig. 3.13, vector $\overline{n_{16}}$ is normal to the plane of the actuator vectors $\bar{V}_1$ and $\bar{V}_6$. Therefore $\overline{n_{16}}$ can be expressed as a cross product of $\bar{V}_1$ and $\bar{V}_6$.

$$\overline{n_{16}} = \bar{V}_6 \times \bar{V}_1 \qquad (3.23)$$

$\bar{P}$ is a vector normal to the platform which can be expressed as:

$$\bar{P} = [A\ \ B\ \ C'\ \ 1]^T \qquad (3.24)$$

Where, A, B, C' are given by:

$A = C\Phi\, S\theta$, $B = C\Phi\, C\theta$, $C' = S\theta$

platform 'a' axis (along vector $\overline{m_{16}}$) is normal to the plane of vectors $\bar{P}$ and $\overline{n_{16}}$. Therefore $\overline{m_{16}}$ can be expressed as:

$$\overline{m_{16}} = \bar{P} \times \overline{n_{16}} \qquad (3.25)$$

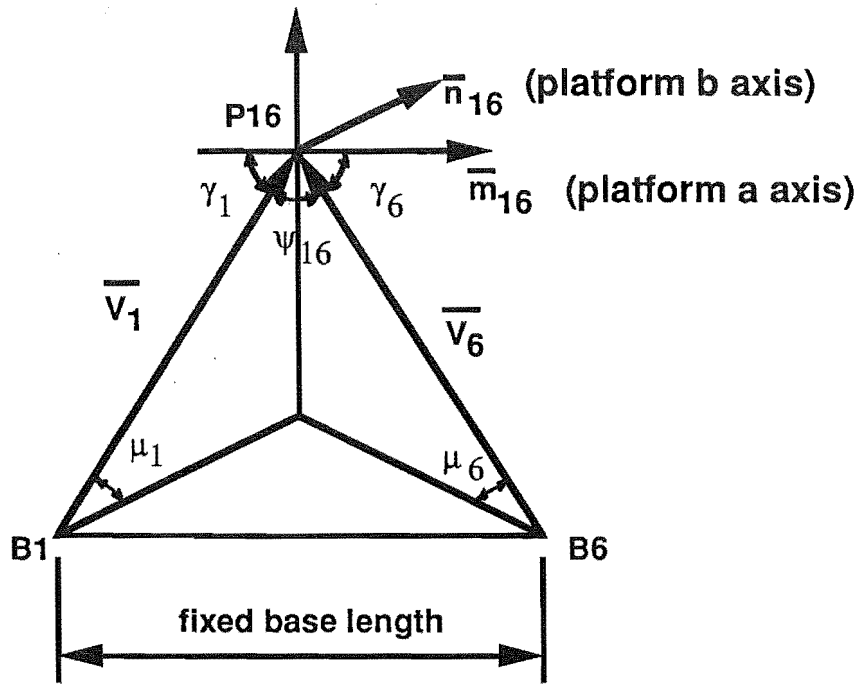

Fig. 3.13 Vector diagram showing the platform axes and the actuator triangle

Now the angle between the actuator 1 and the platform 'a' axis can be easily worked out as follows:

For actuator 1,

$$\gamma_1 = \text{Cos}^{-1}\left(\frac{\bar{m}_{16}.\bar{V}_1}{|\bar{m}_{16}|\ |\bar{V}_1|}\right) \qquad (3.26)$$

For actuator 6,

$$\gamma_6 = \text{Cos}^{-1}\left(\frac{\bar{m}_{16}.\bar{V}_6}{|\bar{m}_{16}|\ |\bar{V}_6|}\right) \qquad (3.27)$$

To verify the values of angles $\Psi_{1\text{-}6}$, γ_1 and γ_6 the following relation between them can be used.

$$\Psi_{1\text{-}6} + \gamma_1 + \gamma_6 = 180^o \qquad (3.28)$$

Similar procedure can be followed to calculate the angles between the actuators 2 and 3 and the platform 'a" axis, actuators 4 and 5 and the platform 'a"' axis.

The angle between the actuator centre line and the base as seen from the Fig. 3.13, is nothing but the angle between vectors $\bar{V}_i$ and their projection in the X-Y plane (base plane). Therefore, given $\bar{V}_i = (V_{xi}, V_{yi}, V_{zi})$ then the angle μi is given by:

$$\mu i = \tan^{-1}\left(\frac{Vzi}{\sqrt{Vxi^2 + Vyi^2}}\right) \qquad (3.29)$$

The angle μi needs to be evaluated so that the outer edge of the gearbox does not interfere with the base plate (c.f. Fig. 3.14). Fig. 3.14 shows schematically an actuator triangle and the RRR joint between the platform and the actuator pair and the RR joint between the actuator and the base.

This concludes the analysis of the joint angles.

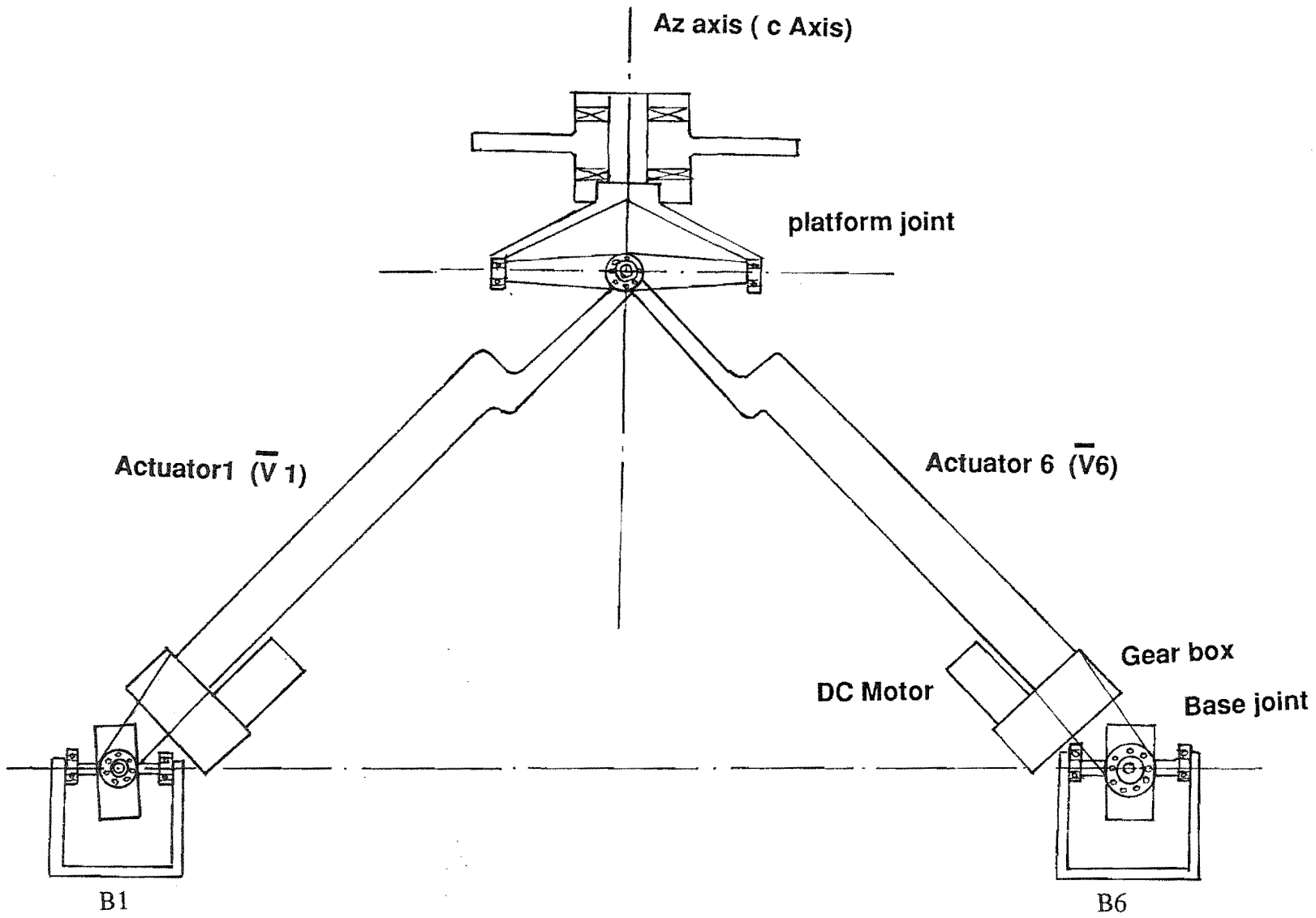

Fig. 3.14 Schematic drawing of the joints and the actuator triangle

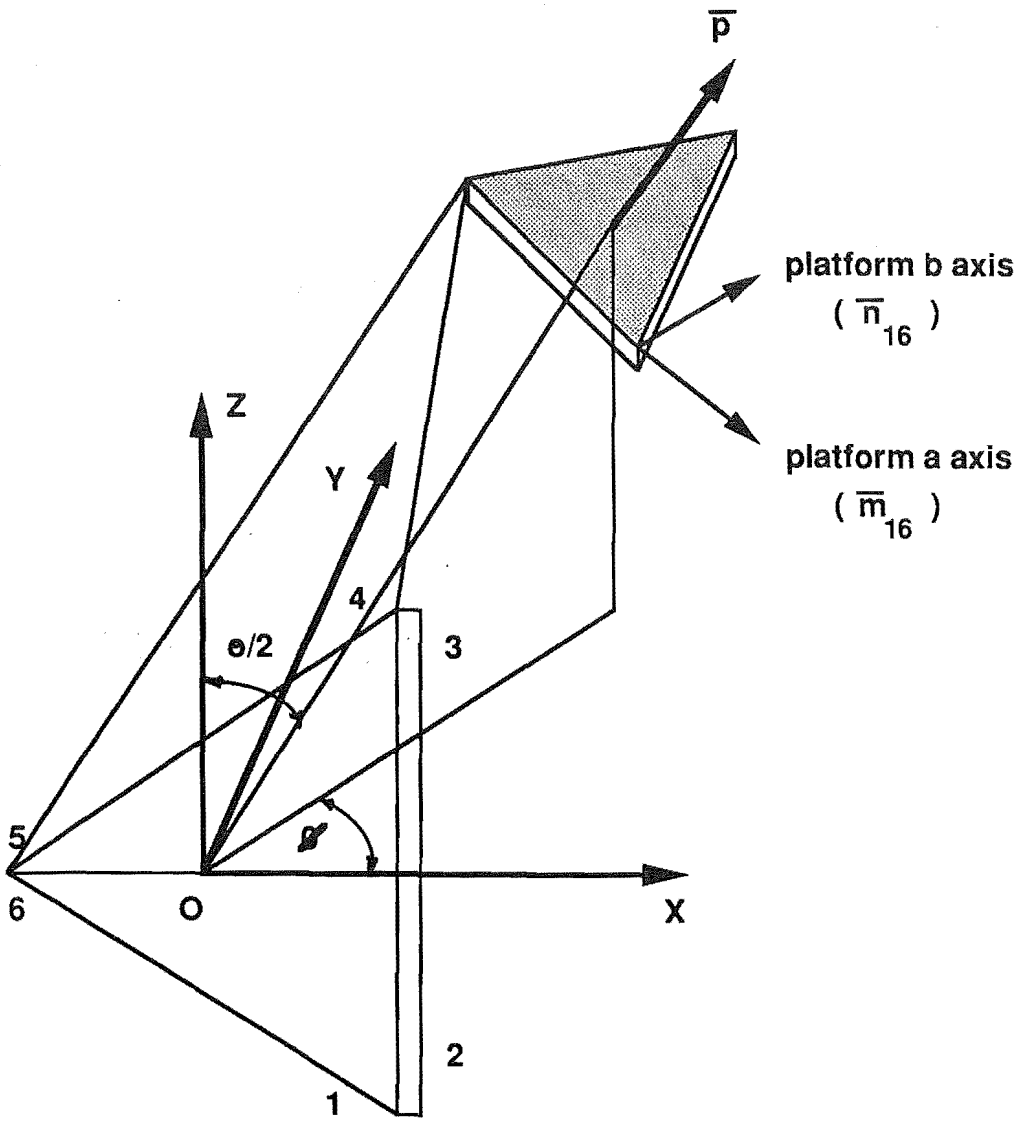

Fig. 3.15 Schematic diagram showing platform orientation and platform axes

3.11 SINGULARITY CONSIDERATIONS

The singular positions of a mechanism can be defined as positions where normal equations of the mechanism motion do not hold. Most conventional robot mechanisms have several singular positions. When robot's positioning trajectory passes close to a singular position, the mechanism will loose a degree of freedom or a degree of constraint depending on whether it is an open kinematic chain or a closed kinematic chain mechanism. In the design of any practical robot manipulator, the path followed by the end effector should not pass through any singularity position. This condition restricts the usable work envelope of a robot manipulator. In the following section the singularity positions of serial link and parallel link robot manipulators are discussed.

3.11.1 Singularity positions of a Serial Link Manipulator

A series connected manipulator is said to be in a singular position when it loses one or more degrees of freedom for a given position and orientation of the actuators. Hunt (1982) illustrates the conditions under which a system of series connected actuators will loose their freedom by constructing a matrix of the plücker coordinates for the actuators.

3.11.1.1 Plücker coordinates

Consideration of point coordinates does not help us to express in determinant or matrix form a condition for the loss of an end effector degree of freedom (singular position) for a general six actuator manipulator.

If a line vector $\overline{V_1V_2}$ is represented in the XYZ coordinates system, the direction of the line is given by its direction cosines l, m, n. To fix the actual location of the line in the XYZ system the moments of the line vector (denoted by P,Q,R) about the X,Y and Z axes are used. Thus the line vector $\overline{V_1V_2}$ can be represented by coordinates [l, m, n, P, Q, R] called the 'Plücker coordinates'. If the direction ratios (L, M, N) of the line are used then the Plücker coordinates are denoted by (L, M, N, P, Q, R).

3.11.1.2 Linear dependence of series connected manipulator freedoms

For a general series connected six actuator manipulator the 6 x 6 plücker coordinate matrix can be expressed as: (Hunt, 1982).

$$D = \begin{bmatrix} L_1 & M_1 & N_1 & P_1 & Q_1 & R_1 \\ - & - & - & - & - & - \\ - & - & - & - & - & - \\ - & - & - & - & - & - \\ - & - & - & - & - & - \\ - & - & - & - & - & - \\ L6 & M6 & N6 & P6 & Q6 & R6 \end{bmatrix} \qquad (3.30)$$

If the determinant D=O, indicating the linear dependence of the rows, then the manipulator will be in a singular position loosing one of the degrees of freedom.

As shown by Hunt (1982), at any instant the rank of the 6 x 6 matrix of the Plücker coordinates is equal to the end effector freedom of the manipulator.

3.11.2 Singular Positions of a Parallel Linkage Manipulator

In a parallel linkage manipulator, the singular position will result in gain of one or more degrees of freedom. In such a singular position the manipulator structure will become instable. The unstability of the mechanism results from the fact that in a singular position, the motion of the platform about an axis of singularity is instantaneously unconstrained. In the following discussion, two different methods of determining the singular positions of a parallel linkage manipulator are outlined.

3.11.2.1 'String-line' property of the actuators

'String-line' property can be used to determine the configurations of the mechanism where the normal degrees of freedom will change. According to Hunt (1982), whenever a line can be found intersecting all six joint axes the end effector loses one freedom. As seen from Fig. 16 (b) a line through point

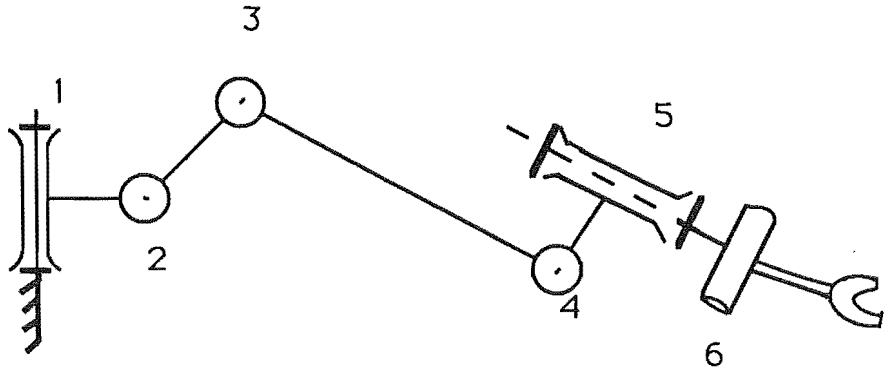

Fig. 3.16 (a) Robot arm with six serially connected actuators

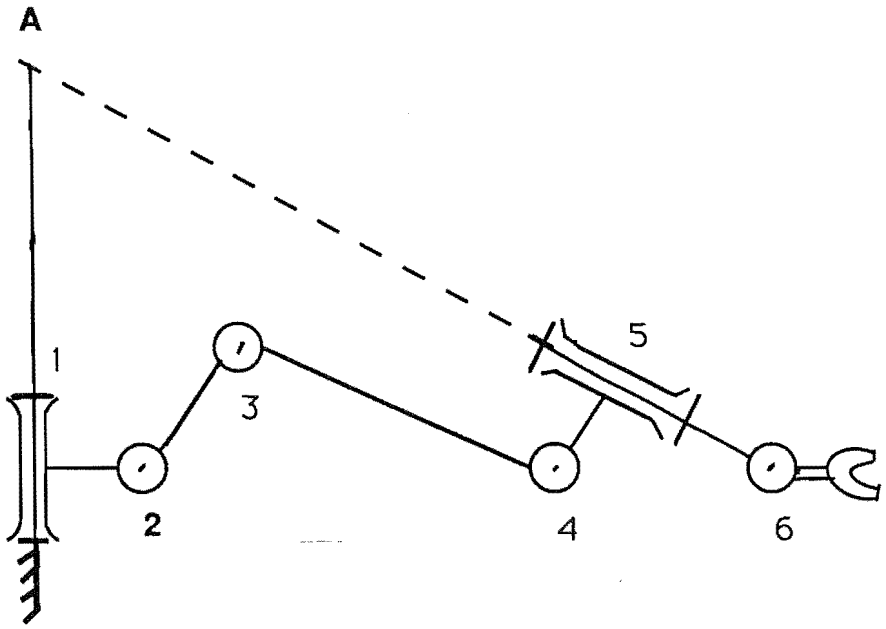

Fig. 3.16(b) Loss of end effector degree of freedom for the robot arm shown in Fig. 3.16 (a)

A normal to the plane of the paper intersects all the joint axes and the end effector looses one degree of freedom.

3.11.2.2 Singularity Positions of a Practical Stewart Platform

Using the 'string-line' property, if a configuration of the Stewart platform can be found such that all the six lines of action of the forces are linearly dependent (intersect an axis) then the platform will be in a singular position.

In Fig. 3.17, the platform plane P_{12} P_{34} P_{56} has been rotated about the Y axis till it becomes coplanar with the supporting triangle P_{34} B_3 B_4. It is easy to see from Fig. 3.17 that all the six actuators intersect the line P_{12} P_{56}. As shown by Hunt (1982) this configuration will result in the linear dependence of the six actuator vectors. The mechanism will gain an extra degree of freedom about the axis P_{12} P_{56}. This extra degree of freedom is pure rotation about the axis P_{12} P_{56}. What it means in practical terms is that in this configuration the rotational stiffness of the platform is low about the axis P_{12} P_{56} and any attempt to change the length B_3 P_{34} or B_4 P_{34} may result in inverting the platform after moving through the singularity.

Fichter (1987) gives the required angle of rotation about the Y-axis as follows:

$$R_Y = \tan^{-1}\left(\frac{-Tz}{Tx - R_B\, C_{AB3}}\right) \qquad (3.31)$$

where Tx, Tz : translations along X and Z directions
R_B : base radius
C_{AB3} : cosine of angle between X axis and the line joining B_3 and the origin.

By symmetry two more singular configurations of the mechanism can be obtained by rotating the platform plane about the combination of X and Y axes. The mechanism will gain an extra degree of freedom about the axes P12 P34 and P34 P56 respectively.

Fig. 3.19 shows the Stewart platform in another singular position. This configuration can be arrived at by rotating the platform plane about the z axis

keeping it parallel to the base plane. Starting from any position, an angle of rotation of 90° in either direction will result in the singular position (Fichter, 1987). In this singular position the platform has gained an extra degree of freedom which is a screwing motion about the platform z axis. All the six lines of action of forces along the actuators will intersect the z axis.

Another way of looking at the singularity positions is by comparing the similarity between a regular octahedron and the parallel linkage structure formed by the Stewart platform.

To simplify the discussion on stiffness and singularity considerations, only three attachment points on the base and on the platform are considered. As shown in Fig. 3.18, the three base attachment points A, B and C define an equilateral triangle ABC on the base and the three attachment points a, b, c define equilateral triangle abc on the platform.

From Fig. 3.18 the modified Stewart platform can be seen as a regular octahedron made of eight triangles. After examining various positions of the solid formed by these triangles, it is observed that the singularity positions occur when two adjacent triangles become coplanar and the structure is no longer an octahedron. The following configurations of the mechanism will result in a singular position:

1. The platform triangle abc is coplanar with a triangle formed by two points in the base plane and a common point joining the actuators in the platform plane. Three different singularity positions are possible (c.f. Fig. 3.17).

2. The base triangle ABC is coplanar with a triangle formed by two points in the platform plane and a common point joining the actuators in the base plane. Again, there are three different singularity positions possible.

3. When the platform triangle abc is rotated through 90° keeping it parallel to the base plane, the adjacent triangles $P_{12}B_3B_4$ and $P_{34}B_3B_4$ become coplanar and the mechanism is in a singular position (c.f. Fig. 3.19). Two different singularity positions can be arrived at by rotating the platform in clockwise or anti-clockwise direction.

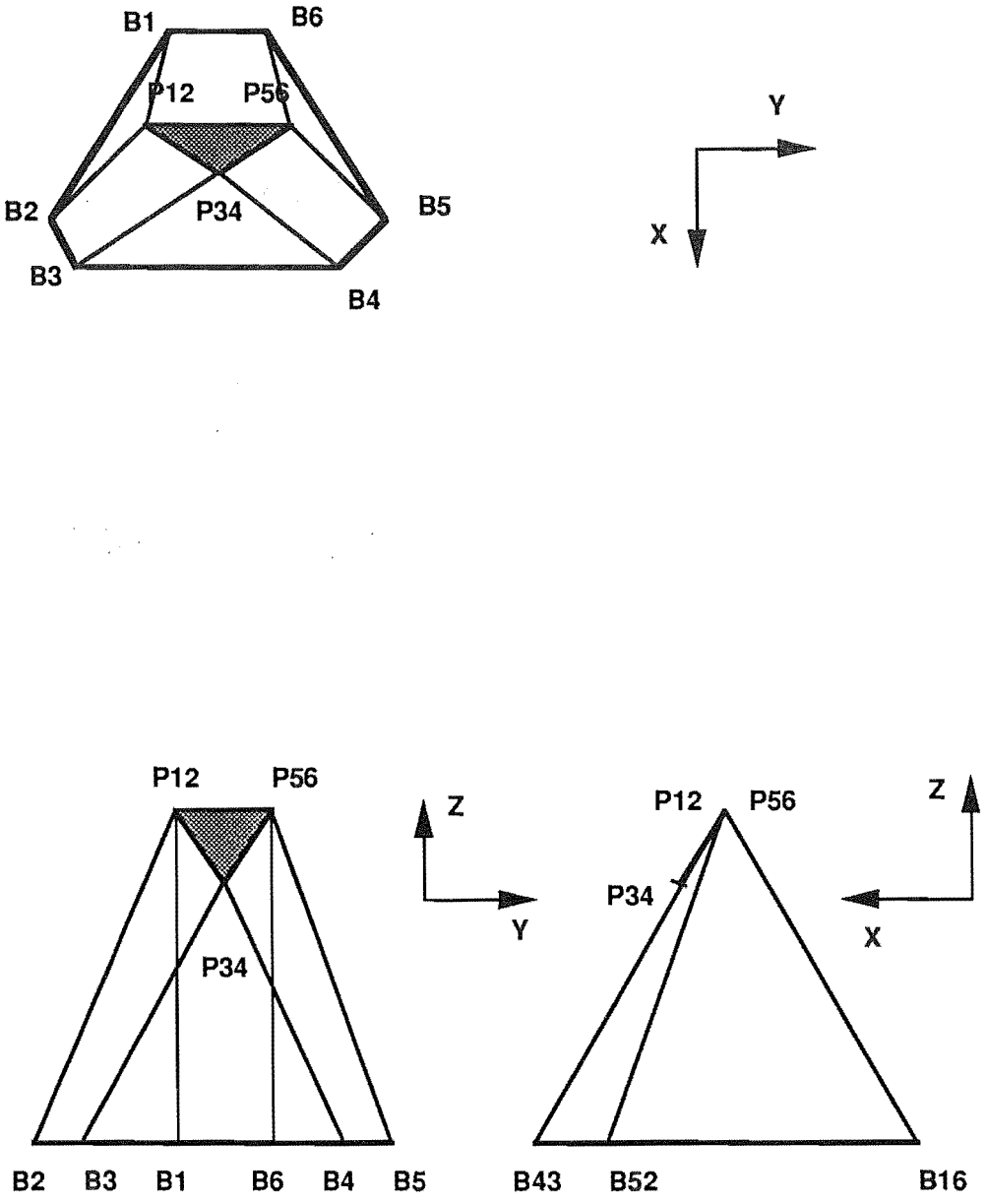

Fig.3.17 The top,front and right side view of the Stewart platform in a singular position

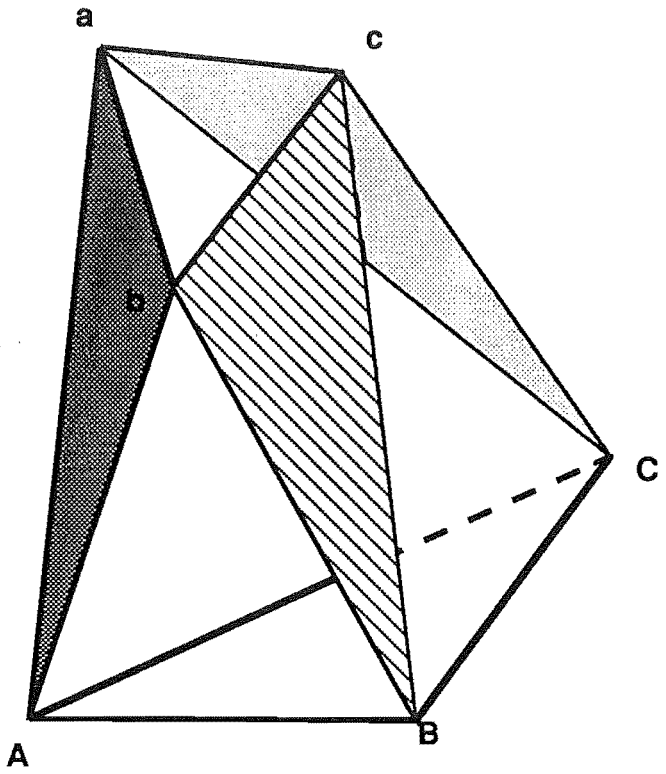

Fig. 3.18 Stewart platform : octahehedron formed by the base, platform and six triangles

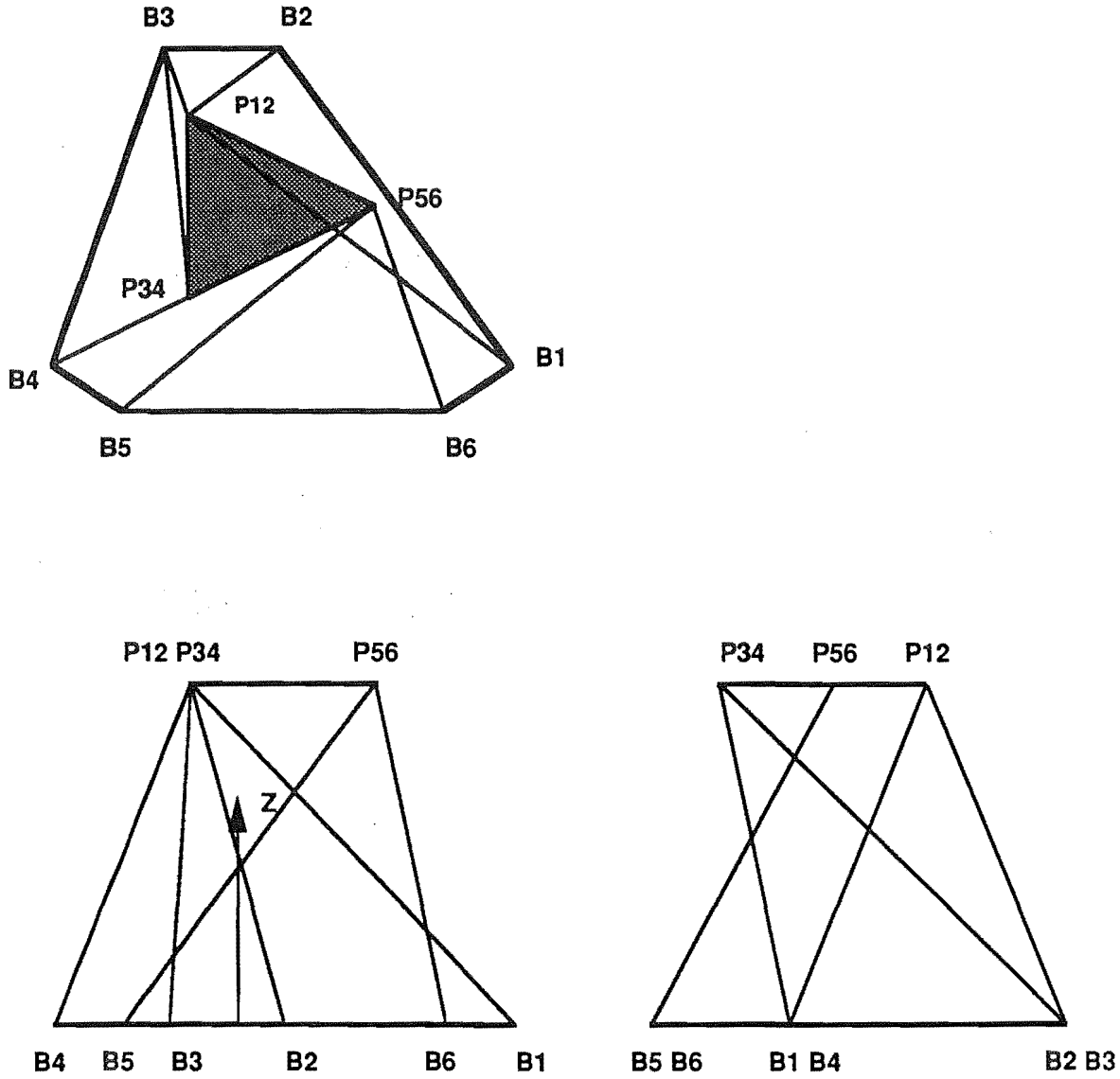

Fig. 3.19 The top,front and right side view of the Stewart platform in another singular position

Thus, there are eight singularity positions of the mechanism when the base is fixed. By symmetry, eight more singularity positions can be found by allowing the platform below the base.

For a practical construction of the Stewart platform described in Chapter 4, 8 of these combinations are eliminated because the platform is above fixed base. Three more of these combinations are eliminated because of the actuator length and mechanical joint limits. Six degrees of freedom of the mechanism are used to move the platform so that the remaining five singularity regions are avoided.

3.12 SUMMARY

This chapter outlined the advantages and disadvantages of a conventional serial link manipulator. An alternative closed kinematic chain manipulator design based on the Stewart platform mechanism was described. The general arrangement and kinematic structure of a modified Stewart platform was discussed. Kinematic analysis for solving the vector equations of the parallel mechanism for the actuator lengths was performed. The joint angles between the actuators and the base, and the actuators and the platform were calculated. Finally the singularity positions of the parallel linkage manipulator were discussed.

CHAPTER 4

COMPUTER CONTROL HARDWARE DESIGN

4.1 INTRODUCTION

To eliminate the "keyhole" problems and the difficulties experienced by the ship mounted tracking antennas, an antenna mount based on the modified Stewart Platform concept and employing the principles of Parallel Robotic Manipulator is developed as a ground and maritime antenna mount system (c.f. Fig. 4.1). Such an antenna mount with proper joint designs, computer control and a closed loop feedback control system can provide an accurate, fast dynamic response and structurally strong tracking system for land and marine use. In the following chapter, the design and operation of the actuating systems, computer control hardware and the multi-motor controller used in the construction of the novel antenna mount are discussed. This antenna mount is referred as "Robotic Satellite Tracking Platform" (RSTP) in further discussion.

4.2 A NOVEL ANTENNA MOUNT DESIGN PRINCIPLE

Six DC motor driven leadscrew actuators form the parallel link structure of the RSTP. When an antenna is mounted on the moving platform, the boresight axis can be locked on to the satellite by adjusting the actuator lengths. The azimuth and elevation look angle information is converted into the six actuator lengths by the control programme (c.f. section 5.4.2). The algorithm, for the rotational and translational coordinate transformation was discussed in chapter 3. All the six axes of the antenna mount are computer controlled. A six axis motor controller based on Hewlett-Packard HCTL-1000 motion control microprocessor is used to control the motion of the RSTP (c.f. section 4.4.3). The six degrees of freedom of the parallel mechanism result in a complete hemispherical work envelope for the RSTP without any keyhole problems near the zenith or the horizon. The RSTP actuating system details are given in the following section.

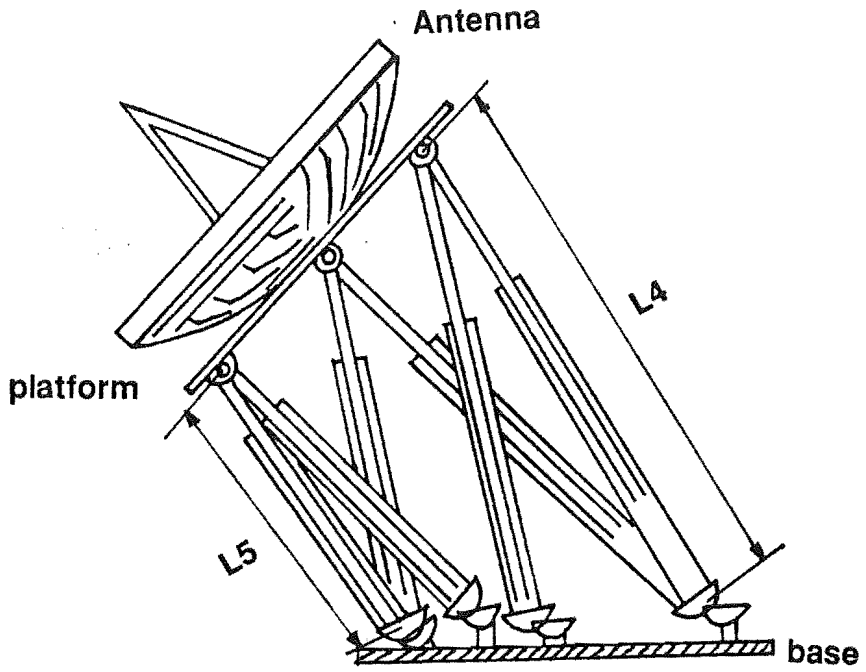

Fig. 4.1 Stewart platform based antenna mount

4.3 ACTUATING SYSTEMS

Actuators are the devices that make the robot move. The most commonly used actuators in the robot construction are: Hydraulic cylinders, pneumatic cylinders, DC motors and step motors.

Hydraulic cylinders operate at very high pressures. A high force to weight ratio is the major advantage of hydraulic actuators. Hydraulic drives are relatively insensitive to the load disturbances and have a fast dynamic response. The high stiffness allows accurate control to be achieved. These advantages of hydraulic actuators are offset by the high cost of the system and space required for the piping work.

The major types of electric motors used in robots are: stepping motors, brushless DC motors and DC motors. Stepping motors using open loop control are particularly popular for microcomputer controlled small robots. Brushless DC motors are expensive and hence could not be used for the prototype RSTP. Permanent magnet DC motor driven actuators offer many advantages. They provide a wide range of operating characteristics to suit the application and are relatively inexpensive. They operate on low voltage and through proper gearing, high torques can be generated. Considering the load and speed characteristics, ease of control and economy, Electrac Series 100 linear actuators (c.f. Warner Electric Catalogue, 1986) driven by permanent magnet DC motors are selected for the construction of the prototype robotic platform. The linear actuator details are given in the following section. A general discussion on the DC motor drives for the robot application follows in the section 4.3.2.

4.3.1 Linear Actuators

The Electrac Series 100 linear actuators offer a reasonable expansion ratio, adequate axial force and its gearbox housing has enough room for the encoder assembly and related wiring. The ball screw of the actuator consists of a bearing with an internal thread located on the leadscrew. The rotational motion of the DC motor is transmitted via the gear train to the leadscrew. The leadscrew moves the bearing linearly which in turn moves

the extension tube in and out of the cylindrical housing (c.f. Fig. 4.2a and 4.2b). The ball bearing construction results in higher efficiency and increased position accuracy. The actuator specifications are as follows:

Drive	:	24 V DC motor
Load capacity	:	500 lbs
Stroke length	:	24"
Retracted length	:	36.37"
Lead screw pitch	:	0.2"
Gear reduction ratio	:	1:5
Expansion ratio	:	1.66

The actuator extension speed vs load curve is shown in Fig. 4.3 (c. f. Warner catalogue,1986).

The original gearbox housing of the Electrac Series 100 actuator is modified to accommodate the encoder assembly (c.f. Fig 4.22) and direct fitting to the mounting bracket bearing assembly (c.f. Fig. 5.4).

4.3.2 DC Motor Drives

Depending upon the mechanism used to develop the magnetic field, the DC motors can be classified as permanent magnet or electromagnet DC motors. Electromagnet DC motors can be further classified as: DC shunt motor, DC series motor, compound motor or separately excited motor, according to the method used for exciting the field windings.

Normally permanent magnet DC motors are used as "servo" motors in robot application. In such a motor the torque τ_m is related to the magnetic flux Φ and armature current I_a and is given by the relation:

$$\tau_m = K_p \Phi I_a \qquad (4.1)$$

where K_p is the proportionality constant.

Since Φ remains constant in the steady state, the torque developed is directly proportional to the armature current.

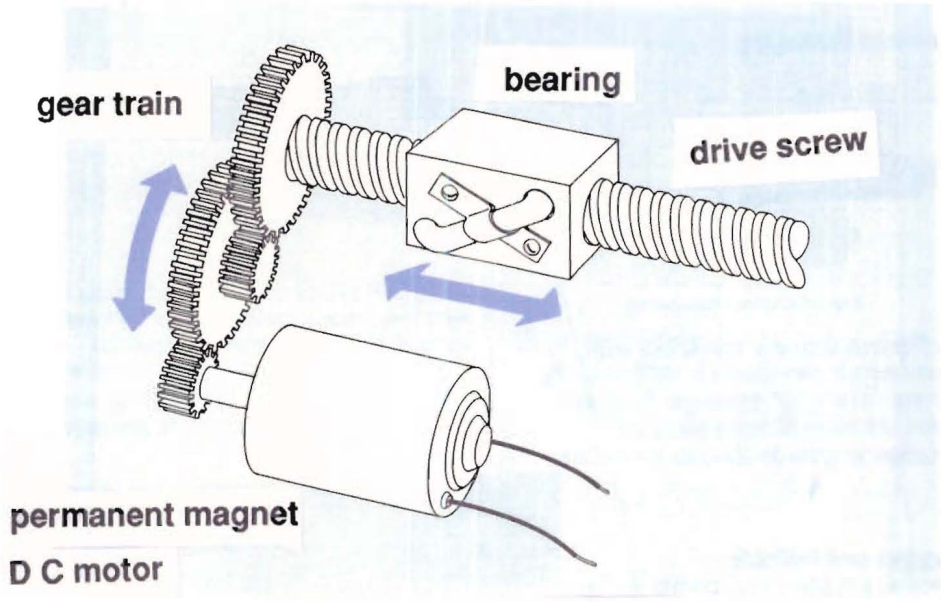

Fig. 4.2 (a) Schematic diagram of the Electrac series 100 linear actuator

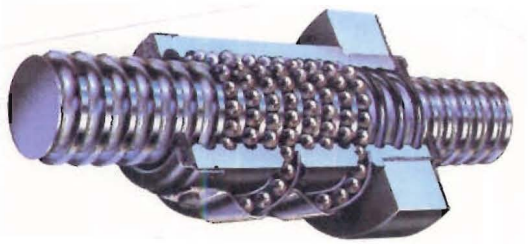

Fig. 4.2 (b) Cut section of the Electrac series 100 ball bearing screw

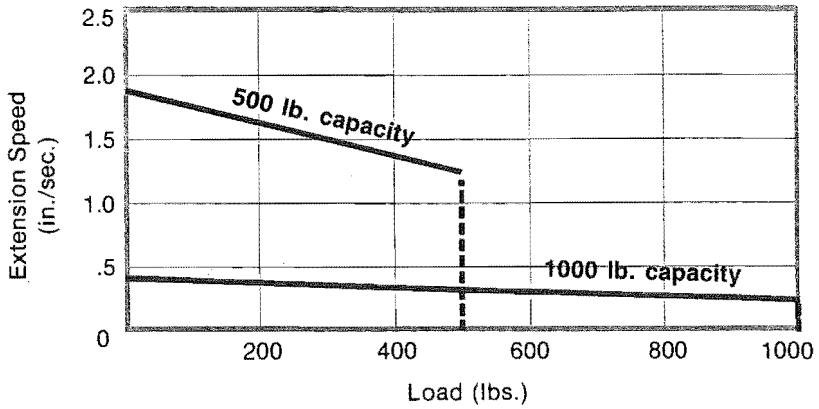

Fig.4.3 Load-speed characteristic curve for the Electrac series 100 linear actuator

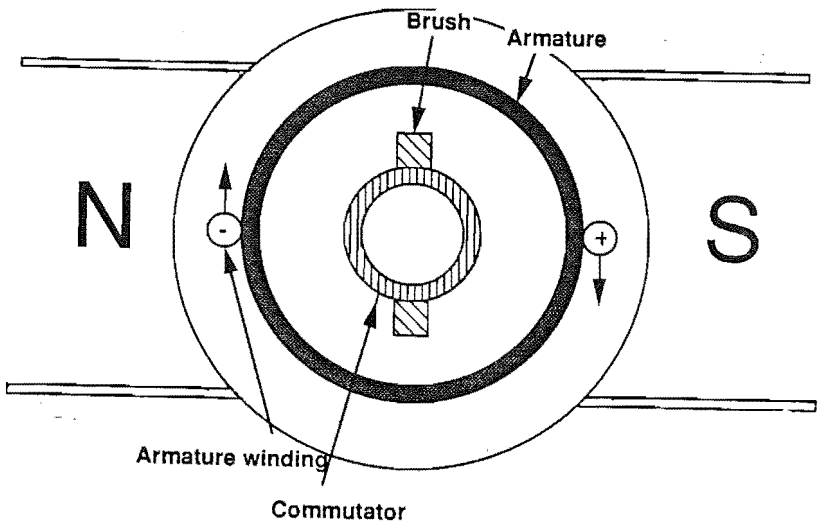

Fig. 4.4 Schematic diagram of a D C motor

The back emf E induced in the armature can be expressed as:

$$E = K_p \Phi \omega \qquad (4.2)$$

where ω is the shaft angular velocity.

The voltage relations between the external voltage V_m, back emf E and the voltage drop in the armature ($I_a R_a$) can be linked as:

$$V_m = E + I_a R_a \qquad (4.3)$$

Equations (4.1), (4.2) and (4.3) form the mathematical model for the DC motor operation. These simple mathematical relationships give ease of control in the incremental motion servo systems. Since there is no power dissipated in the permanent magnetic field, this type of motor has high efficiency and is compact in size.

4.3.2.1 Motor specifications for the RSTP

As mentioned in the section 4.3, the Electrak Series 100 linear actuators are driven by permanent magnet DC motors. The motor specifications are as follows: (c.f. Warner Catalogue,1986).

Input	:	24V DC
Current draw	:	9.1 amps at 500 lbs (Full load)
Duty cycle	:	25% on time at rated load per cycle
Measured resistance	:	0.9 Ω
Measured inductance	:	12 mH
Gearing ratio	:	motor shaft: load shaft = 1:5

Fig. 4.5 gives the relationship between the current drawn and load capacity for the DC motor.

4.4 RSTP CONTROL SYSTEM HARDWARE

The RSTP motion is controlled by a computer. This section outlines the control system hardware details. The overall arrangement of the control

system used for the computer control of the robotic platform is shown schematically in Fig. 4.6. The control system hardware consists of:

1. Host processor
2. Servo drives for DC motors
3. Motor controller card
4. Motor drives with encoders for feedback
5. Power supply

The operation of each part is discussed in the following section.

4.4.1 The Host Processor

An IBM PC AT-compatible personal computer (Zenith Z-286) is used as a host processor. The Zenith Z-286 incorporates Intel's 80286 16-bit microprocessor, an 80287 numeric coprocessor, a 16-bit I/O data bus and a 24-bit address bus. The address bus is capable of addressing up to 16 M byte of memory. The 640K (base + expansion) RAM was extended to (640K + 1024K) by plugging in a 1024 K extended memory card into the memory expansion slot. The 286 processor runs at 8 MHz clock speed performing approximately 0.01 MFLOPS.

The "expansion slot" or the I/0 channel of the Zenith Z-286 was used to accept the multi-motor controller Printed Circuit Board. The I/0 channel is an extension of the Intel 286 microprocessor bus. A 62-pin edge connector provides 8-bit bidirectional data bus, 20-bit address bus, I/0 read, write and memory control lines. Interfacing of the host processor with the multi-motor control adapter is discussed in detail under interfacing of the HCTL-1000 (c.f. section 4.4.3.3). In addition to act as a card cage for the multi-motor control adaptor, the host processor contains the main control programme which governs the overall operation of the RSTP.

4.4.2 Servo Drives for DC Motors

Servo control for robots refers to the type of control in which the manipulator motion is under constant supervision by a computer and requires real time trajectory generation and feedback. The DC motor can be driven by a

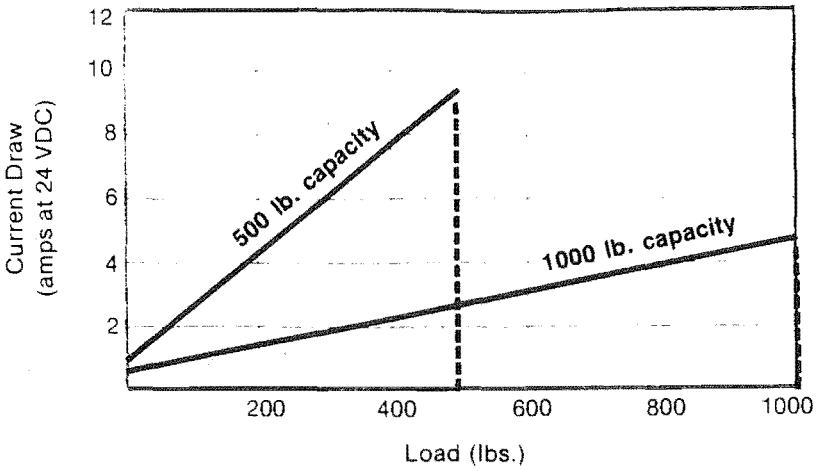

Fig. 4.5 Load-current characteristic curve for the Electrac series 100 D C motor

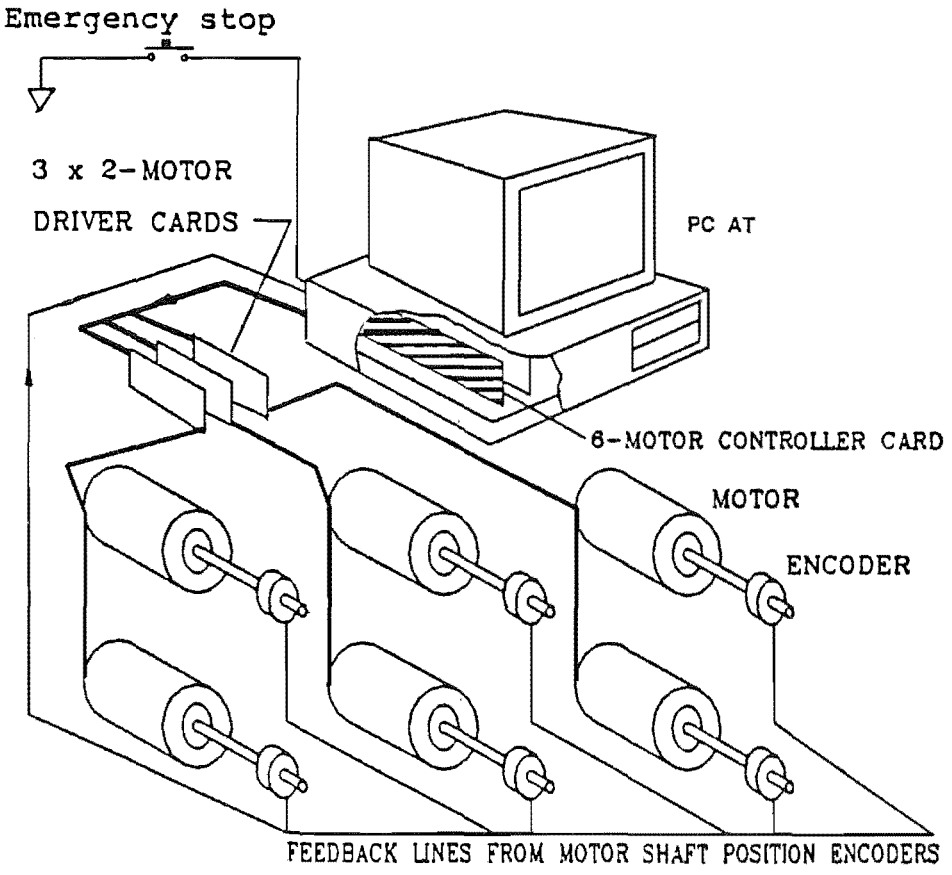

Fig. 4.6 Schematic structure of the RSTP control system

controllable DC current or voltage source. Linear amplifiers or switching amplifiers provide such a controllable voltage or current source.

Linear servo amplifiers employ an operational or differential amplifier to drive a power stage which in turn drives the DC motor. Linear amplifiers control the motor voltage or current by controlling the voltage applied to the motor. There must be a voltage drop across the transistors which is equal to the difference between the supply voltage and the required motor voltage with the appropriate amount of current flowing through. Therefore a significant amount of power is dissipated in the output transistors. The power dissipation is greatest when running the motors under low speed and high torque conditions where motor back emf is low and the current is high. The DC motors used to drive the RSTP linear actuators require low speed and high torque. Therefore, switching (PWM) amplifiers are used in the design of the servo drives for the RSTP.

4.4.2.1 PWM servo drives

A Pulse Width Modulated (PWM) signal contains a pulse train in which the duration of each pulse is proportional to the amplitude of the signal generating the pulse train (c.f. Fig. 4.7 b). Switching amplifiers control the motor voltage by varying the duty cycle (or pulse width) of the voltage applied to the motor. Since the transistors operate in on-off mode, very little power is dissipated in either state of the transistors.

The PWM servo drive for the RSTP DC motors consists of a H-Bridge circuit with four switching transistors and a motor arranged as shown schematically in Fig. 4.8. According to their configuration, PWM amplifiers can be divided into three categories: Bipolar, Unipolar and Limited Unipolar. The three operating modes of the PWM amplifiers are shown in Table 4.1.

4.4.2.2 Bipolar PWM servo drive

The HCTL-1000 outputs motor command in two forms: An 8-bit motor command which can be connected to a DAC to drive a linear amplifier or PULSE and SIGN output to drive a PWM amplifier. The PWM signal has a frequency of the external clock frequency/100 (18.432 KHz in this application). The duty cycle is resolved to 1 part in 100. The duty cycle and

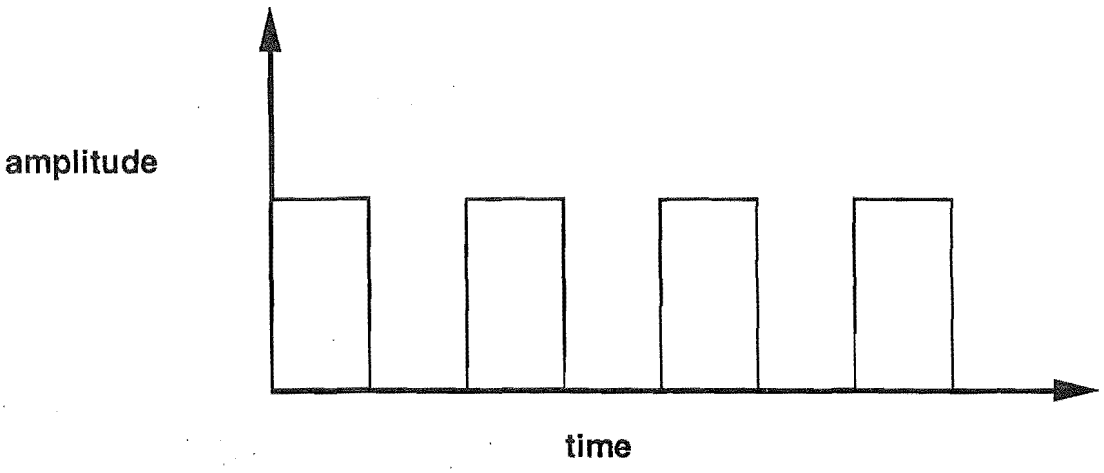

Fig. 4.7 (a) Carrier signal for bipolar mode
(c.f. Table 4.1 and Fig. 4.8)

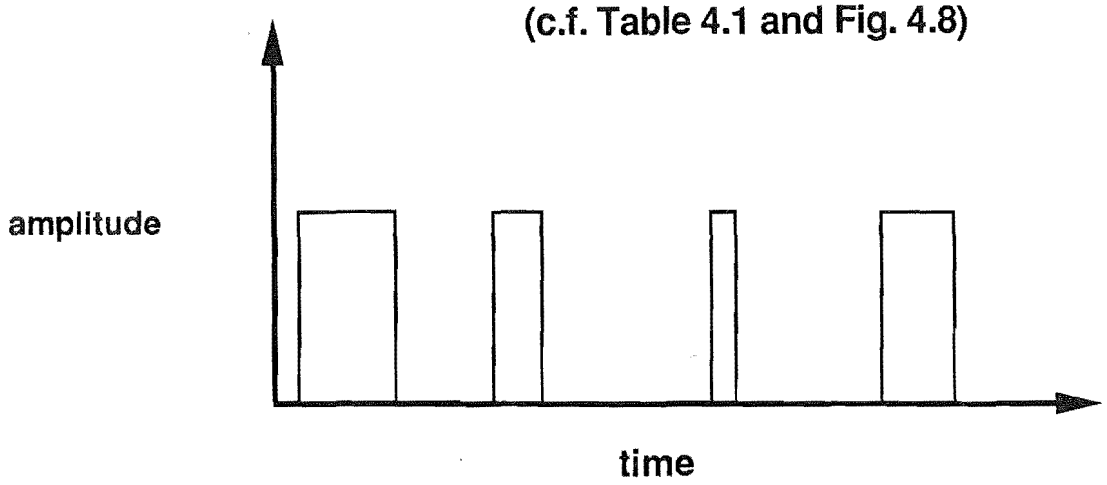

Fig. 4.7 (b) Pulse Width Modulated Signal

Operation Mode and Input Voltage V_{in}	Transistors Condition and Motor Voltage	
	"On" Phase	"Off" Phase
Bipolar mode	F_1 , F_4 on F_2 , F_3 off $V_m = V_s$	F_2 , F_3 on F_1 , F_4 off $V_m = -V_s$
Unipolar $V_{in} > 0$	F_1 , F_4 on F_2 , F_3 off $V_m = V_s$	F_2 , F_4 on F_1 , F_3 off $V_m = 0$
Unipolar $V_{in} < 0$	F_2 , F_3 on F_1 , F_4 off $V_m = -V_s$	F_2 , F_4 on F_1 , F_3 off $V_m = 0$
Limited unipolar $V_{in} > 0$	F_1 , F_4 on F_2 , F_3 off $V_m = V_s$	F_4 on F_1 , F_2 , F_3 off $V_m = 0$ if $I_{AB} > 0$ $V_m = V_s$ if $I_{AB} < 0$ $0 < V_m < V_s$ if $I_{AB} = 0$
Limited unipolar $V_{in} < 0$	F_2 , F_3 on F_1 , F_4 off $V_m = -V_s$	F_2 on F_1 , F_3 , F_4 off $V_m = 0$ if $I_{AB} < 0$ $V_m = -V_s$ if $I_{AB} > 0$ $-V_s < V_m < 0$ if $I_{AB} = 0$

Table 4.1 The Operation Modes of PWM Amplifiers

polarity of the PWM command is determined by the 2's complement contents of the HCTL-1000 register RØ9H. The SIGN pin of the HCTL-1000 gives polarity of the command. Low output on SIGN pin indicates positive polarity.

4.4.2.3 Interfacing the servo drive

The output from the PWM ports of the HCTL-1000 circuits is translated and amplified through the logic circuit for the bipolar motor drive and gives control signals to the H-bridge amplifier circuit (c.f. Ma Li, 1989). HCPL-2530 Dual High Speed Optocouplers are used to isolate the motor drive from the computer so as to protect the computer from the current or voltage surges. The Optocoupler contains a pair of LEDs and integrated photon detectors with electrical isolation between input and output. The logic circuit for the bipolar motor drive consists of U3, U4 and U5 logic gates as shown in Fig. 4.10. U5 is a ULN 2823, an 8-channel Darlington Transistor Integrated Circuit. It can sink current up to 500 mA and can withstand voltages to 90V. It provides sufficient gate drive to saturate the FETs.

The power stage of the PWM servo drive consists of power MOS FETS (MTP15NØ5E) arranged in an H-bridge pattern as shown in Fig. 4.9. The MTP15NØ5E offers very high switching frequency (up to 5 MHz). The parasitic diode connected between the source and the drain provides voltage clipping and a current path for both unipolar and bipolar drives. The four 16V, 4.745 A, 1W Zener diodes limit the gate-source input voltage of the FETs. When using a 24V power supply for the FETs and the motor drive, a 36V power supply is used to drive the gate inputs to ensure sufficient input voltage to saturate the FETs. The detail design of the PWM drive power stage is discussed by Ma li (1989) who developed the electronics for the drives.

4.4.2.4 Limited unipolar PWM servo drive

The bipolar operation mode of the PWM amplifier (shown in Fig. 4.8) was recommended in the HCTL-1000 application notes. During tests on the bipolar PWM servo drive, it was found that the motors were unable to supply the necessary torque when the duty cycle was less than 60%. This greatly reduced the operating range of the motor and the motor stopped before the

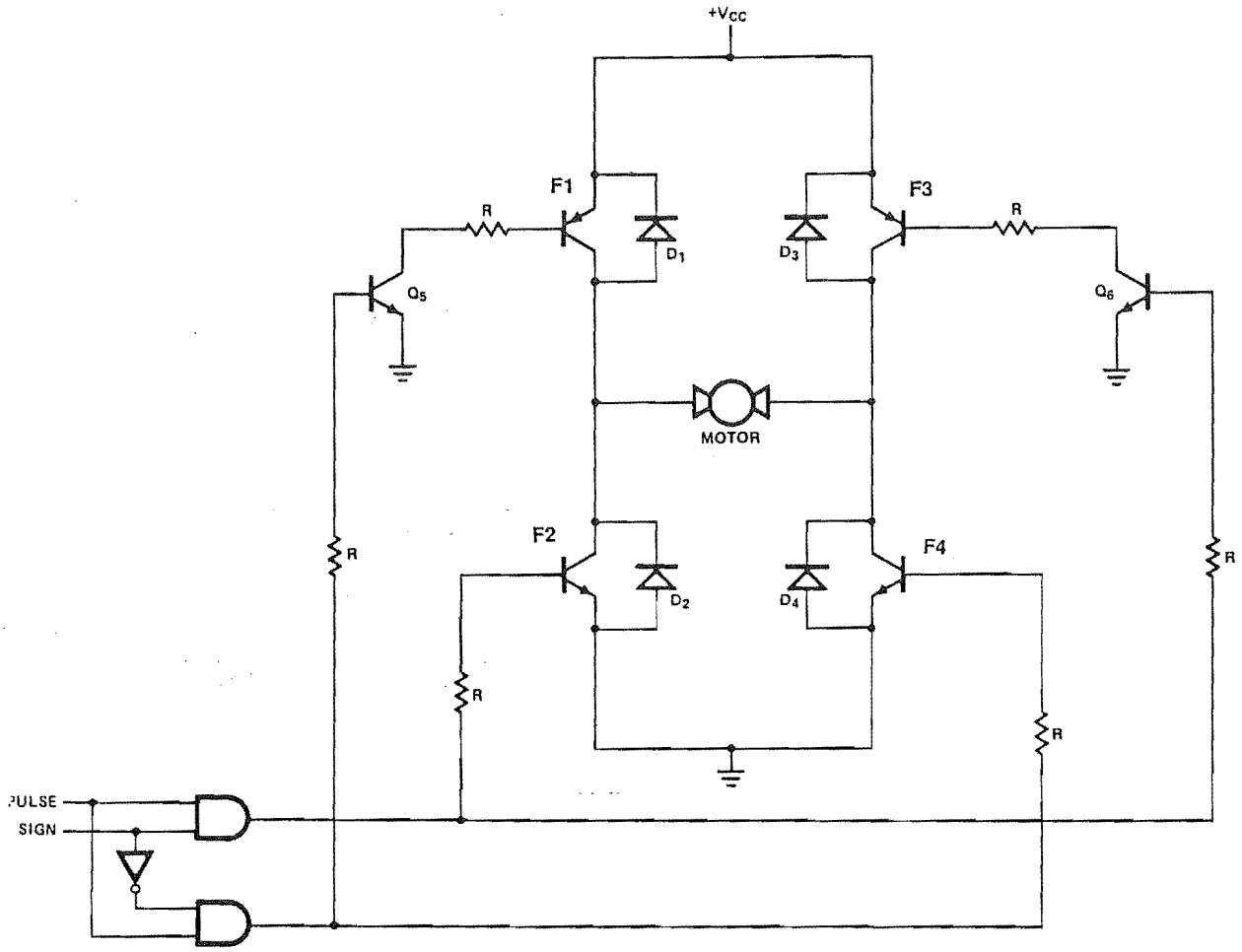

Fig. 4.8 Recommended Bipolar H-Bridge amplifier interface for the HCTL-1000

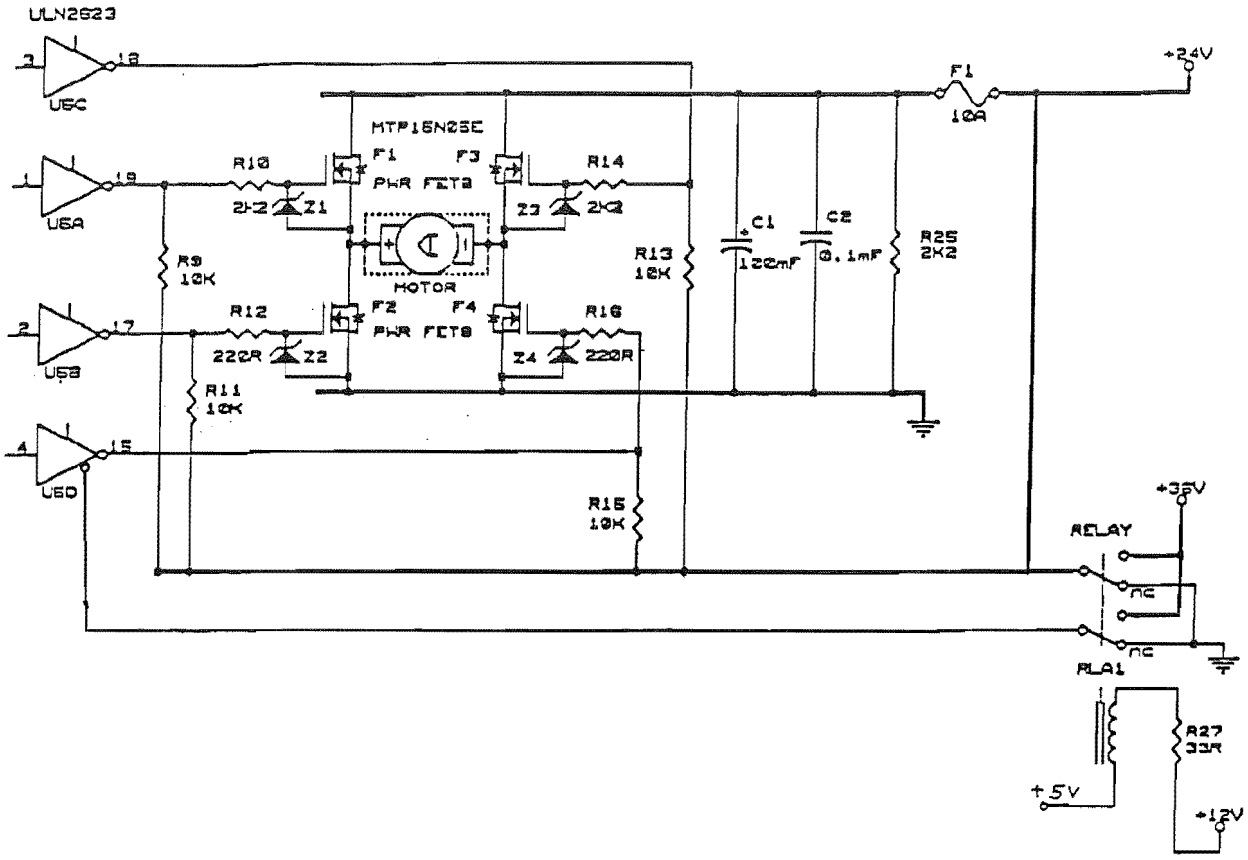

Fig. 4.9 Power stage of the motor drive

command position was reached. The limited Unipolar mode was then used instead of the bipolar mode for the PWM drive.

Under the limited unipolar drive mode, the threshold of duty cycle under which the motor can be driven was found to be 20% for 24V DC motor supply (c.f. Ma Li, 1989). Thus the operating range of the motor is greatly increased under the limited unipolar mode of the servo drive.

For a limited unipolar PWM servo drive, F1 and F4 are turned ON while F2 and F3 remain OFF during the ON time. During the OFF time, F4 remains ON and F1 is turned OFF with F2 and F3 OFF. This does not allow current reversal as can happen in the ordinary unipolar drive. The logic circuit for the limited unipolar PWM servo drives is shown in Fig. 4.10. Fig. 4.11 shows the control box containing the three servo drive cards for the RSTP.

To allow one pair of transistors to turn off before the other pair is turned ON, the PWM port of the HCTL-1000 has a sign reversal inhibit option. When the bit zero in the status register (RØ7H) is set, the pulse output for one PWM period after the sign polarity reversal is inhibited (c.f. Fig. 4.12). This prevents both FETs between the supply voltage and ground being ON at the same time.

4.4.3 Multi-Motor Controller Adapter

The multi-motor controller adapter (c.f. Dunlop and Ma Li, 1988) consists of six HCTL-1000 microprocessors plus decoder and control logic for the address and data access commands from the host processor. Logic buffers and a square wave clock generator (1.8432 MHz frequency) complete the controller. The adapter is plugged into an expansion slot of the host processor. Fig. 4.13 shows the schematic diagram of the controller adapter interface with the host processor and the motor drives. Fig. 4.14 shows a close up view of the actual adapter developed for the RSTP application. A 96-pin connector soldered on the controller PCB is used to Input and Output signals for the motor drives (c.f. Fig.4.20).

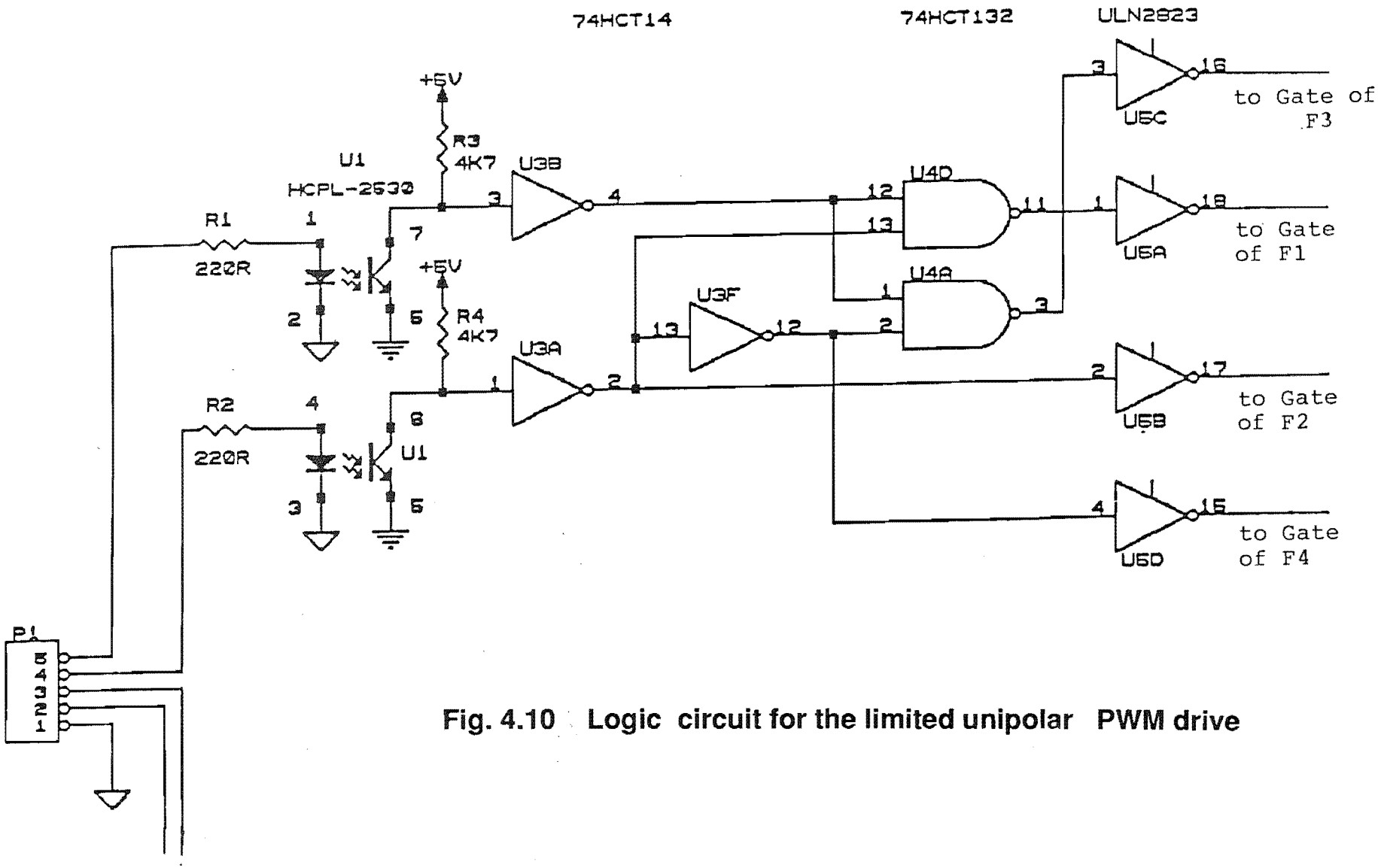

Fig. 4.10 Logic circuit for the limited unipolar PWM drive

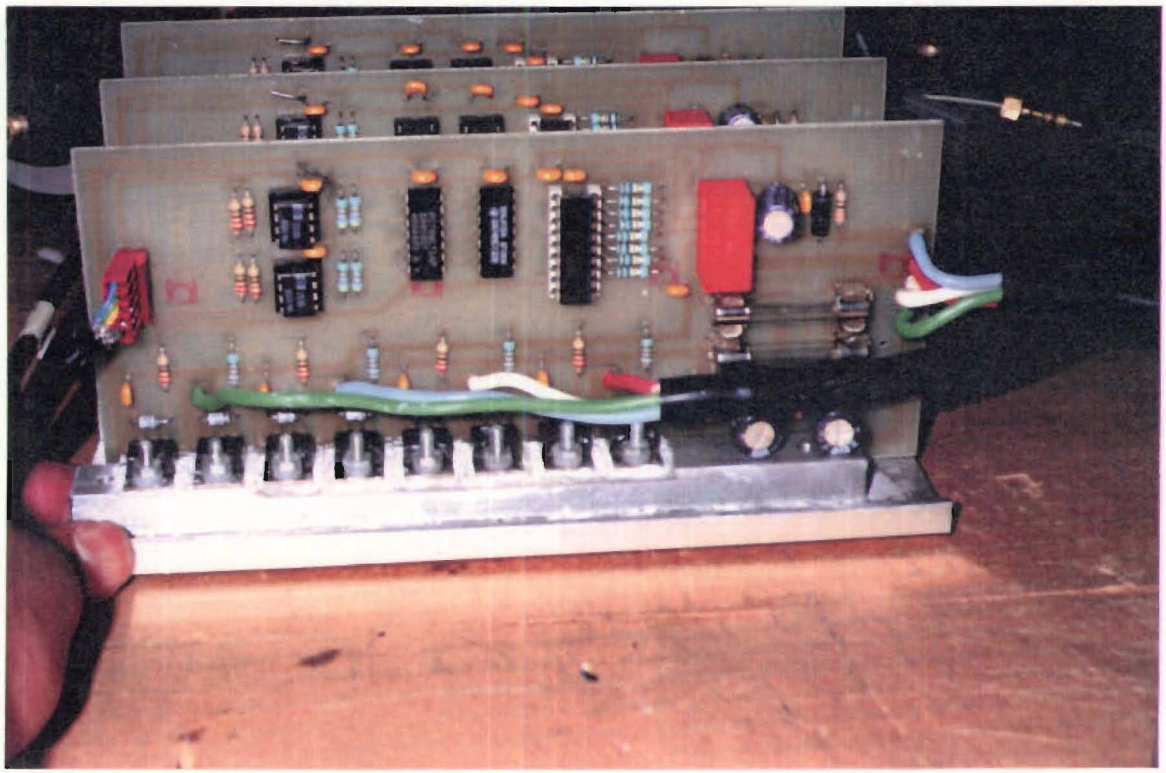

Fig. 4.11 3X2 servo cards for the RSTP motor drive

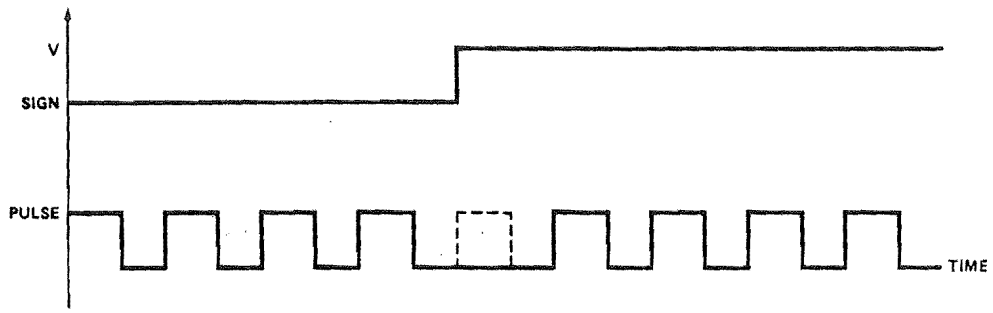

Fig. 4.12 Sign reversal inhibit for the PWM port

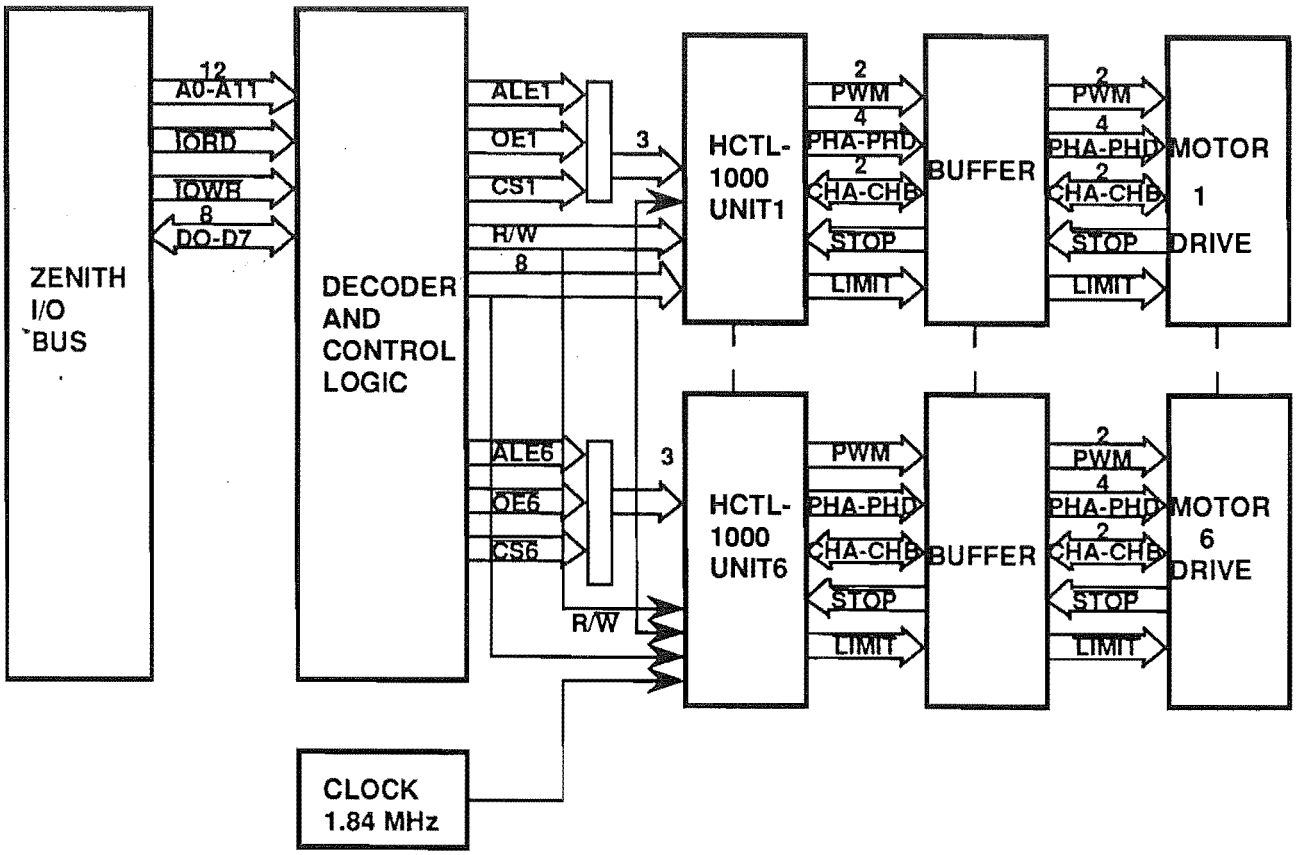

Fig.4.13 Computer and motor interfaces for the motor controller

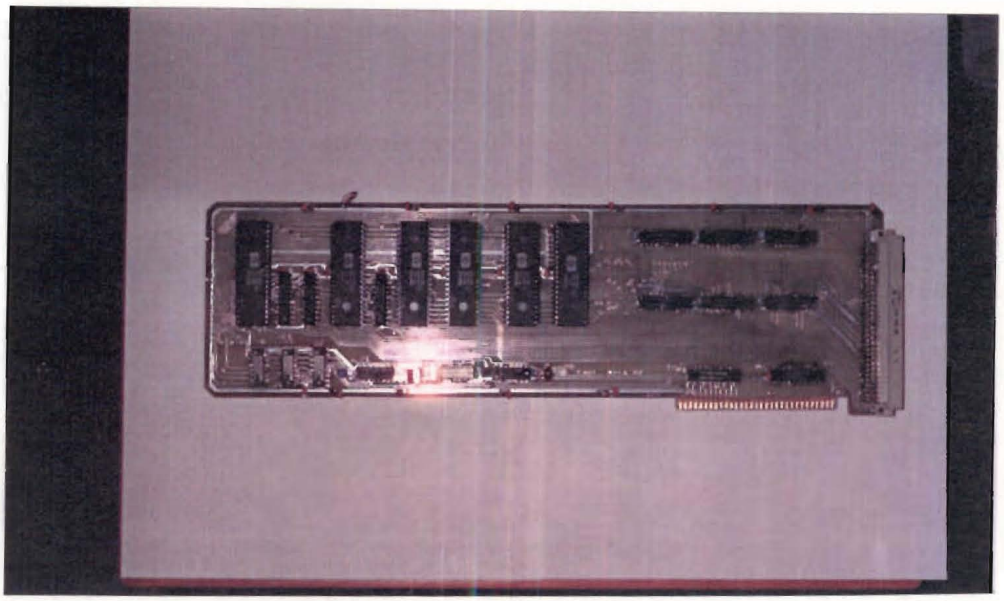

Fig. 4.14 Six-motor controller adapter for the RSTP

4.4.3.1 HCTL-1000

The HCTL-1000 is a general purpose motion control chip made by Hewlett-Packard. It provides 24-bit position accuracy and can be used to control hydraulic cylinders, DC motors, DC brushless and stepper motors. It performs all the time-intensive computation for digital motion control, thereby freeing the host processor for other tasks. Fig. 4.15 shows schematically the system block diagram incorporating HCTL-1000. For the robotic platform application six HCTL-1000 units are used to drive the six DC motors. The internal construction, operation and interfacing of the HCTL-1000 with the host processor and the motor drives is discussed in the following section.

4.4.3.2 HCTL-1000 construction and operation

The HCTL-1000 is a digitally sampled data system. While information from the host processor is accepted asynchronously with respect to the control functions, the motor command is computed on a discrete sample time basis. The HCTL-1000 provides the position and velocity control by using a bank of 64 8-bit internal registers. 32 of these registers are user accessible and are configured by the user to suit the application. The configuration of these registers is discussed under the software implementation in chapter 5 (section 5.4). Fig. 4.16 shows the functional block diagram of the 32 user accessible registers. The internal structure of the HCTL-1000 is shown in Fig. 4.17.

The HCTL-1000 receives the input commands from the host processor and position feedback from the incremental encoder with quadrature output. The embedded microprocessor accumulates the quadrature pulses to generate the actual position. It then compares the desired position (velocity) to the actual position (velocity) and computes the error signal which is input to a programmable digital filler $D_1(z)$. The filter outputs a motor command as a PWM signal and a direction signal at the PWM port and as an 8-bit signal for a DAC at the motor command port. The HCTL-1000 has two emergency flags, $\overline{\text{LIMIT}}$ and $\overline{\text{STOP}}$, which allow operation of the HCTL-1000 to be interrupted under emergency conditions. The flags are hardware set flags. The $\overline{\text{LIMIT}}$ flag can be set by pressing an emergency stop button located on the control panel of the RSTP.

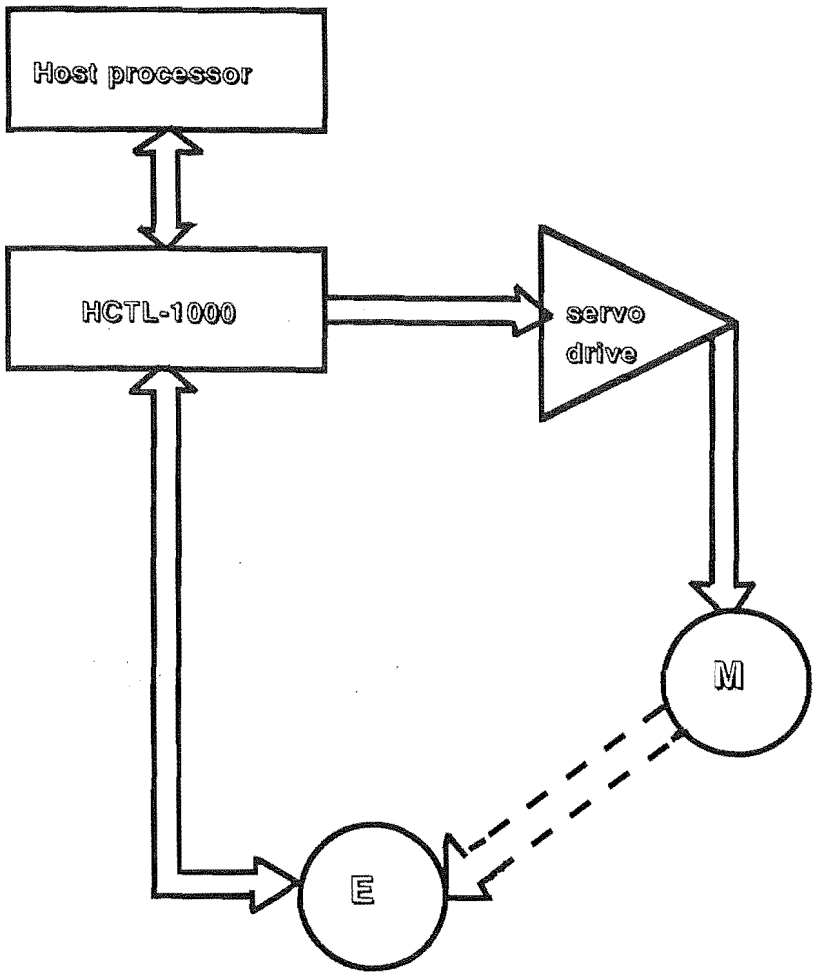

Fig. 4.15 Control system block diagram

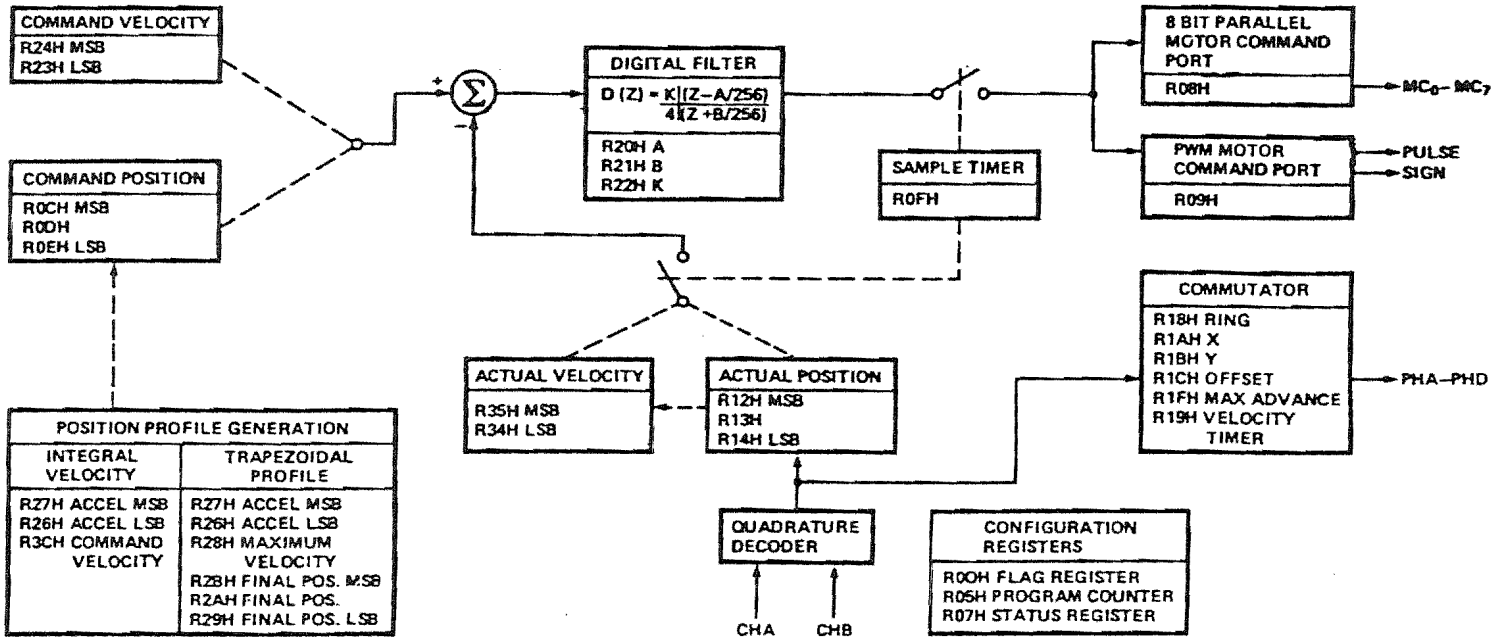

Fig. 4.16 HCTL-1000 user accessible registers block diagram

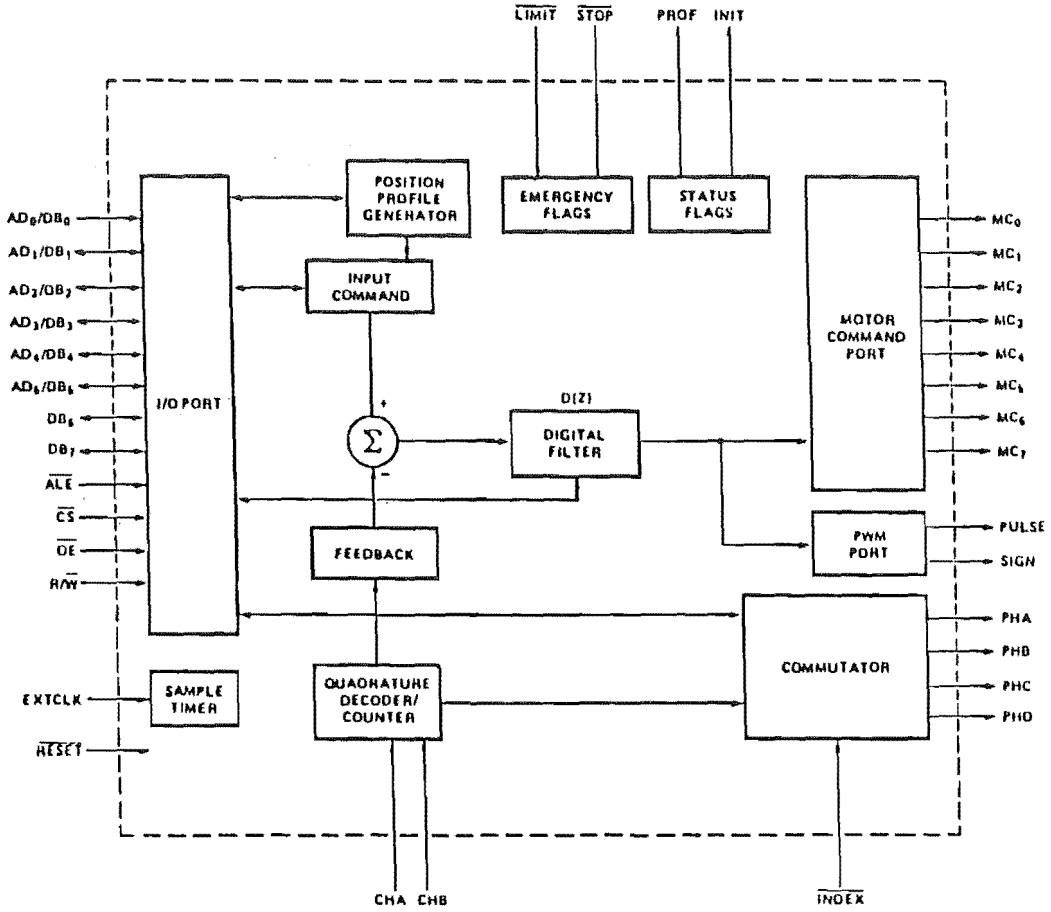

Fig. 4.17 HCTL-1000 internal block diagram

4.4.3.3 Interfacing the HCTL-1000

A Zenith Z-286 IBM PC type computer serves as a card cage for the controller adapter. The expansion slot of the Zenith system board has a 62-pin edge connector which accepts the controller adapter. Fig. 4.18 shows the I/O signals used for interfacing the HCTL-1000 with the host processor. The controller is addressed by using I/O mapped address space. A total of 768 I/O device addresses are available to I/O channel cards The controller adapter can occupy 32 I/O addresses from 300-31FH. The HCTL-1000 occupies only 12 I/O addresses, from 300H to 305H and from 308H to 30FH.

The data to and from the HCTL-1000 registers is accessed by using an 8-bit address/data multiplexed bidirectional bus. The control bus of HCTL-1000 contains 4 I/O lines: $\overline{ALE}$ (address latch enable), $\overline{CS}$ (chip select), $\overline{OE}$ (output enable) and R/$\overline{W}$ (read/write). These control lines control the data transfer between the HCTL-1000 registers and the host processor. The timing configurations for the data transfer and the control signal decoding procedures are discussed in detail by Ma Li (1989). The PWM and SIGN signals are used for drives of DC motors or hydraulic cylinders PHA-PHD and $\overline{INDEX}$ output supplies four commutator signals to provide phase switching information to step or DC brushless motors (c.f. Fig. 4.19).

Fig. 4.19 shows the I/O signals of HCTL-1000. The signals from HCTL-1000 go to the buffer chips U15-U23 (74LS244, octal tri-state buffer). The buffers provide improved noise rejection. The buffer pinout is shown in Fig. 4.20. A 96-pin connector soldered on the controller board interfaces the buffer chips with the motor drives (c.f. Fig. 4.20).

4.4.4 Feedback System Components

For a closed loop control system, measurement of the controlled parameters is essential to provide a feedback signal. For sensing the position of the robot end effector, various analog and digital techniques can be used. The use of an optical encoder provides a completely digital mechanism for determining the position of an actuator.

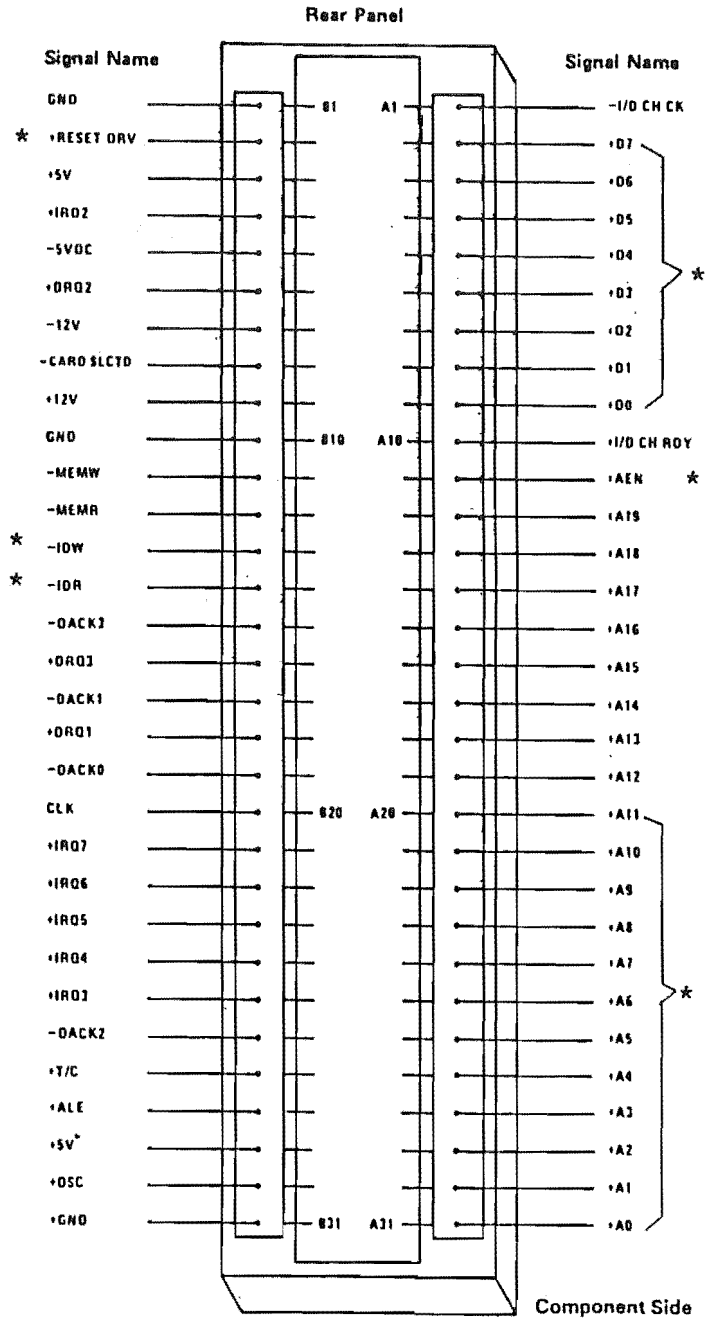

Fig. 4.18 The Zenith Z-286 I/O channel pinout
* signals used in the motor controller

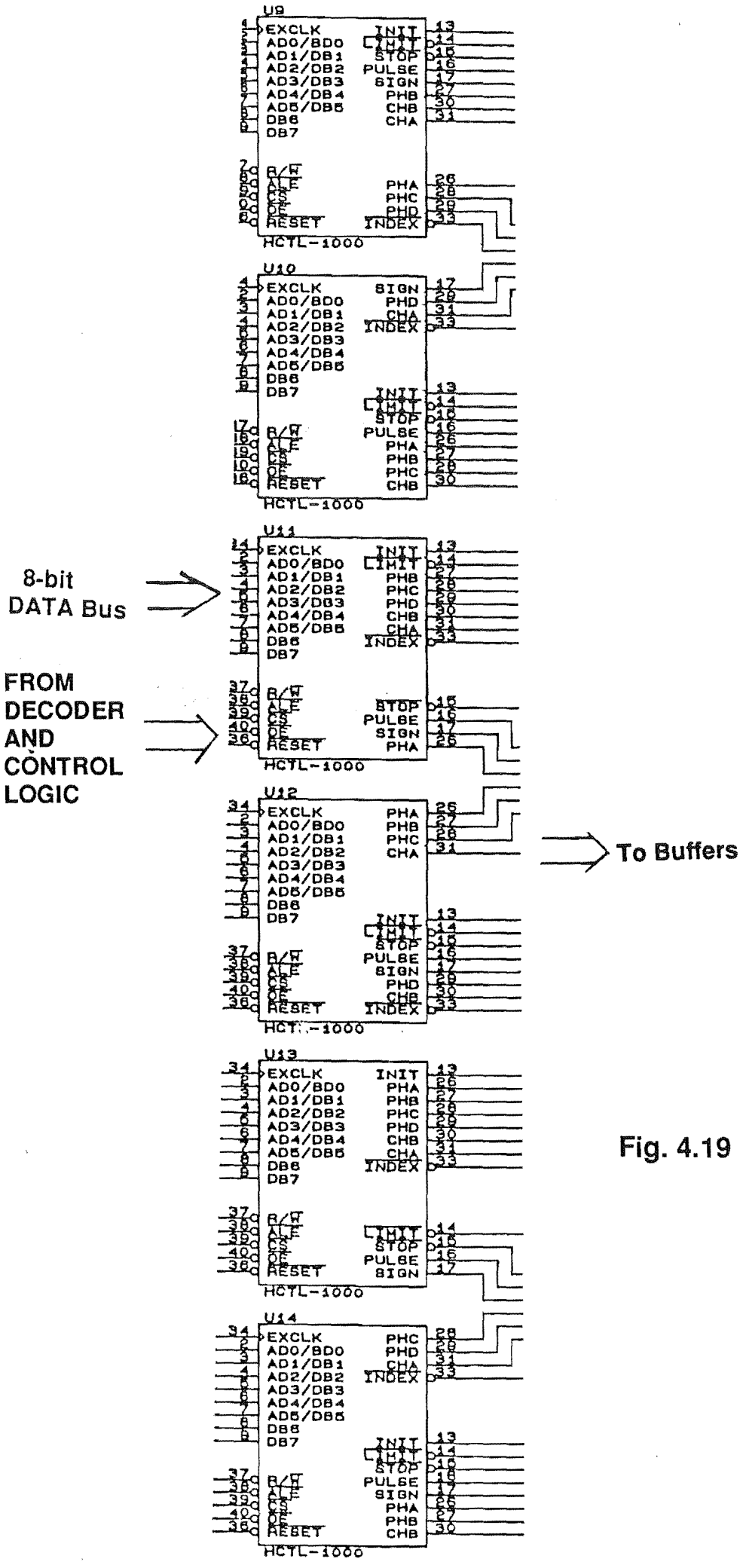

Fig. 4.19 The HCTL-1000 I/O signals

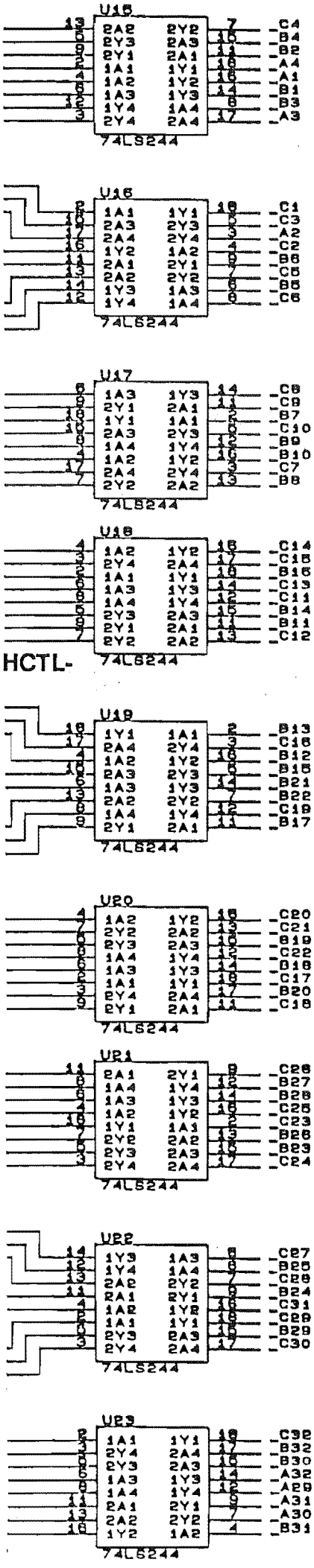

FROM HCTL-1000

96-PIN CONNECTOR

	C	B	A	
FROM U6	PHA	PHB	SIGN	1
	INDEX	STOP	PHD	2
	PHC	CHB	CHA	3
	INIT	LIMIT	PULSE	4
FROM U10	PHD	CHA	+5V	5
	INDEX	SIGN	+5V	6
	PHC	STOP	+5V	7
	INIT	CHB	+5V	8
	LIMIT	PHA	+5V	9
	PULSE	PHB	+5V	10
FROM U11	PHD	CHA	+5V	11
	INDEX	SIGN	+5V	12
	PHC	STOP	+5V	13
	INIT	CHB	+5V	14
	LIMIT	PHA	+5V	15
	PULSE	PHB	+5V	16
FROM U12	PHD	CHA	GRND	17
	INDEX	SIGN	GRND	18
	PHC	STOP	GRND	19
	INIT	CHB	GRND	20
	LIMIT	PHA	GRND	21
	PULSE	PHB	GRND	22
FROM U13	PHD	CHA	GRND	23
	INDEX	SIGN	GRND	24
	PHC	STOP	GRND	25
	INIT	CHB	GRND	26
	LIMIT	PHA	GRND	27
	PULSE	PHB	GRND	28
FROM U14	PHD	CHA	SIGN	29
	INDEX	STOP	PHB	30
	PHC	CHB	PHA	31
	INIT	LIMIT	PULSE	32
	C	B	A	

PIN ASSIGNMENT
96-PIN CONNECTOR ON PCB

Fig. 4.20 The buffer and controller socket pinout

4.4.4.1 Digital measurement of position and velocity

For measuring the position and velocity of a robot joint digitally, an optical shaft encoder and special purpose hardware to interface the encoder to the computer is used. There are two basic types of optical shaft encoders: Absolute and Incremental. For absolute encoders a special gray code is used to eliminate the errors which can occur with binary codes. In the gray code, at any point on the scale, only one bit changes at a time, this reduces bit slew errors and hence the counting errors. For better resolution, an absolute encoder requires more sensors and is therefore much more expensive than the incremental encoder.

An incremental encoder employs three sensors. Two of them produce pulses which are 90° out of phase with each other and the third sensor is focussed on the reference point. The pulse pattern produced by the two sensors indicates the direction, the position being determined by counting the number of pulses after the reference sensor is activated. A counter is incremented or decremented according to the direction of travel. Fig. 4.21 shows a block diagram of a Hewlett-Packard 6000 series incremental optical encoder. The construction of an incremental encoder is much simpler, but extra hardware is required for interfacing and decoding the output signal. It is possible to get an angular resolution of 0.648 seconds of arc with a pulse rate of 2000,000 per revolution.

In case of an incremental encoder, the frequency of the pulses sent by the encoder is proportional to the speed. The microprocessor can directly compute velocity by sampling position signal. Alternatively, a DC tachogenerator is coupled to the joint for which the velocity is to be measured. The generated voltage is proportional to the speed and the direction is given by the polarity of the output.

4.4.4.2 Encoder for the RSTP

The feedback in the RSTP control system is achieved by using optical incremental encoders. The position of each linear actuator is measured by mounting an optical incremental encoder on the actuator leadscrew shaft. A pair of Optoelectronics OPB 960 slotted optical switches (optocouplers) are employed as the encoder. The encoder is a metal disc with 50 equally

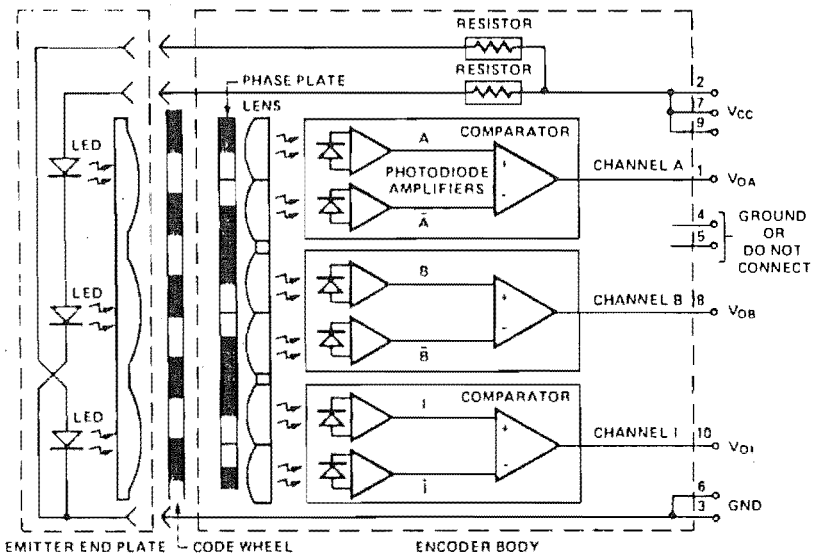

Fig. 4.21 Hewlett-Packard 6000 series optical shaft encoder

spaced radial slots and is mounted directly on the actuator shaft. The two optocouplers are fixed to the motor bracket on opposite sides of the slotted metal wheel (c.f. Fig. 4.22). The position of the encoder can be adjusted by loosening some Allen screws. The complete encoder assembly is enclosed in the gearbox housing.

Each encoder channel consists of an integrated circuit with two photodiodes, an amplifier, a comparator and a LED light source. The LED source transmits light through the metal disc only when the slots in the metal wheel are in line with the LED source. When the photodetectors receive the light the output will be high, otherwise it is low. When the disc rotates, two trains of rectangular pulses are output from the two channels. The output of channel B (CHB) is in quadrature to the output of channel A (CHA). The direction of rotation is determined by which channel is leading (c.f. Fig. 4.23).

The quadrature phase shift between CHA and CHB will enable the 50 slot metal wheel to output 200 edges/revolution. The Electrac Series 100 actuator leadscrew has 0.2" pitch. This gives a linear resolution of

$$\frac{0.2}{200} = 0.001" \ (25.4\ \mu m).$$

Thus the position counter will be incremented or decremented for every 0.001" (25.4 μm) movement of the actuator.

4.4.4.3 Encoder interface

The signals from CHA and CHB are output to the quadrature decoder/ counter in the HCTL-1000 as feedback signals for the actuator shaft position. The input pins on the decoder has a Schmidt trigger buffer to filter out unwanted noise spikes. The decoder detects the direction of rotation by decoding the relative pulse edges of CHA and CHB and counts the number of pulse edges in 2's complement form. This number is stored in the position registers R12H, R13H and R14H. It represents current position of the actuator in thousands of an inch.

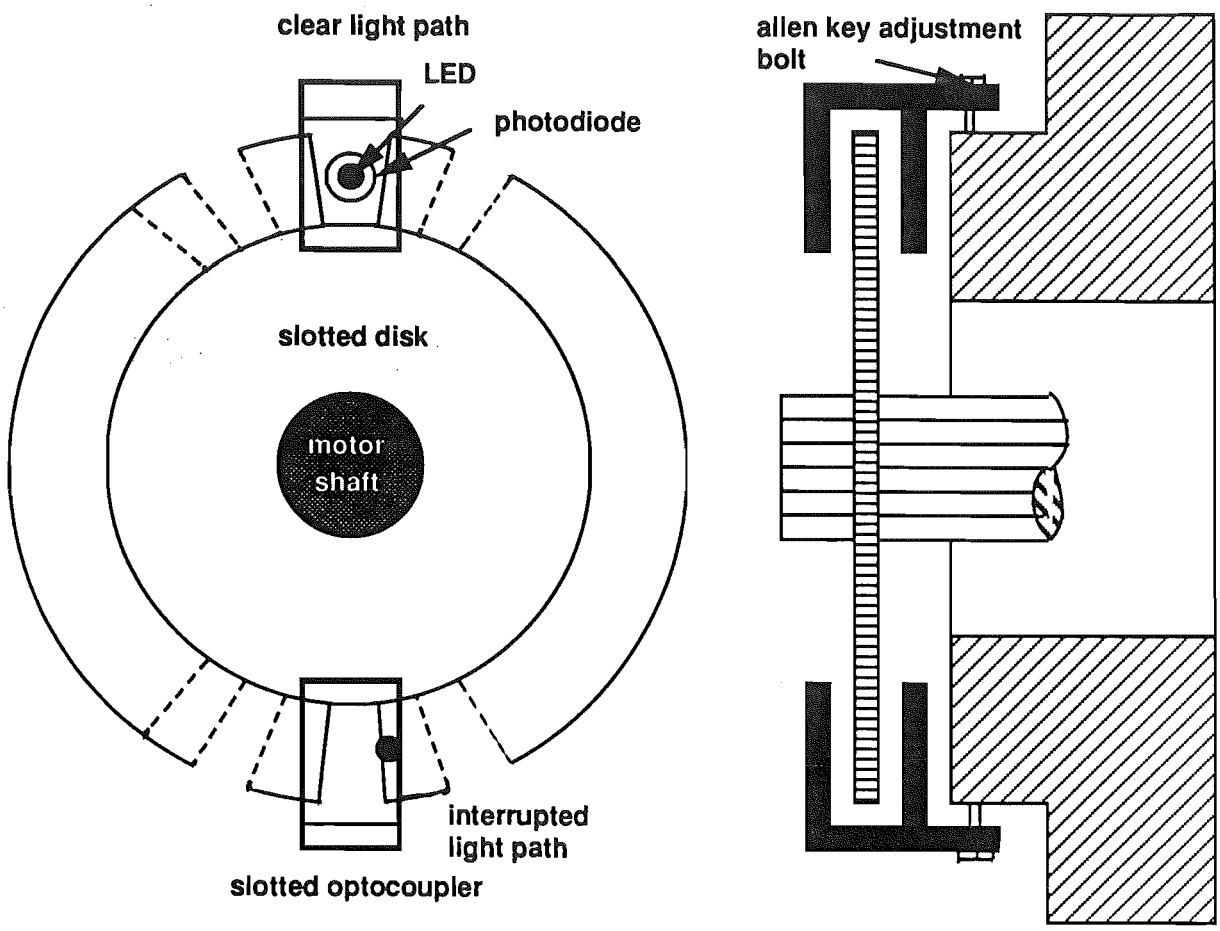

Fig. 4.22 The encoder and the slotted metal wheel mounting assembly arrangement

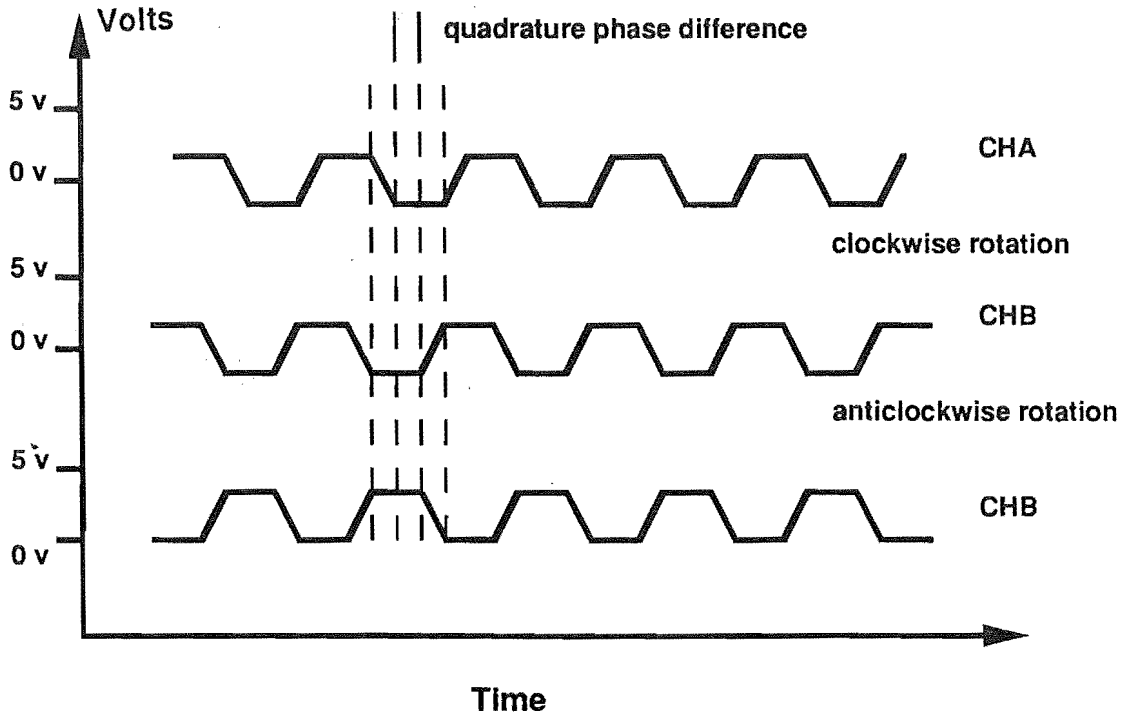

Fig. 4.23 CHA and CHB output for clockwise and anticlockwise rotation

4.4.4.4 Encoder adjustment

For accurate counting of the pulses, CHA and CHB of each pair of encoders must be adjusted to precisely 90° (electrical) apart. The adjustment for the correct phase shift of the two channels was carried out by using an oscilloscope. The CHA and CHB output of the encoder was connected to the two channels of an oscilloscope and the actuator slowly extended/retracted. The resulting waveforms were observed on the scope and the position of the two optocouplers mechanically adjusted using the Allen screws till correct phase shift and equal mark/spece ratio was obtained.

The linear resolution of the encoder can be increased considerably by mounting it on the motor shaft instead of the leadscrew shaft of the actuator. This will enable the encoder to rotate at the motor speed rather than the leadscrew speed. Thus for a gearing ratio of 1:5 between the motor and the leadscrew shaft, the linear resolution for the similar system will be $\frac{0.2"}{5 \times 200}$ = 0.0002" (5.08 μm). But the backlash in the gear train will seriously affect the accuracy of position measurement.

4.4.5 The Power Supply

The power supply unit for the RSTP consists of two 12V traction batteries connected in series to form a 24V DC supply. Two banks of 24V batteries, two 12V DC power supplies along with the relay, ON/OFF switches and a battery charger constitute the power supply system. The schematic circuit diagram in Fig. 4.24 shows the required + 36V, + 24V and + 12V voltage supplies. The supply voltage to the DC motor drives can be increased to 36V and the gate input voltage to 48V by adding the third 12V battery in series (shown by dashed line in Fig. 4.24). Fig. 4.25 shows the power supply unit for the RSTP.

Two 24V battery banks are provided for continuous operation. When one bank is supplying the necessary voltage the second bank can be charged. The 24V DC supply is connected between the source and drain of the FETs and 36V supply is used to drive the gate inputs. The extra 12V ensures sufficient gate voltage to saturate the FETs.

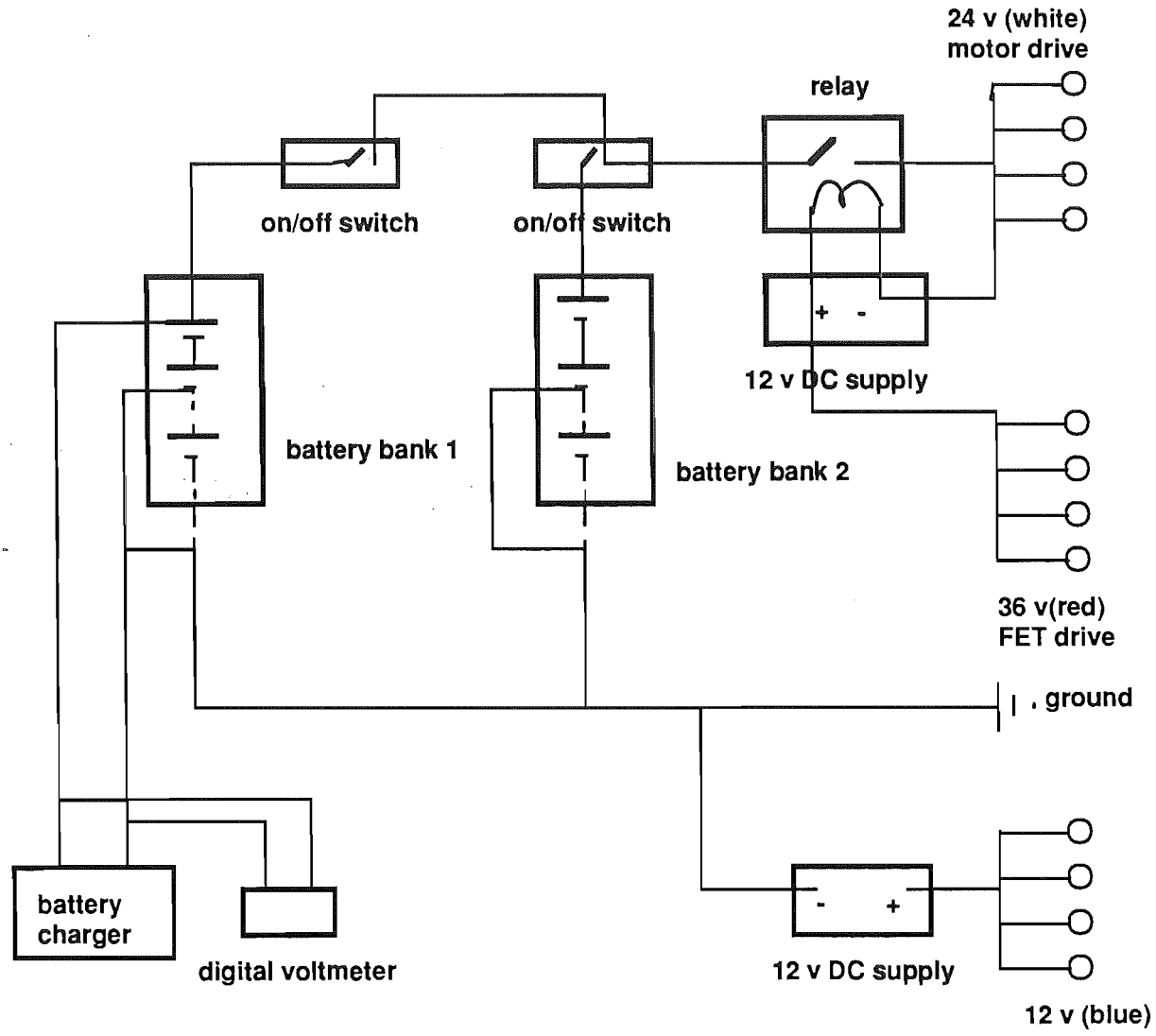

Fig. 4.24 Schematic diagram of the RSTP power supply unit

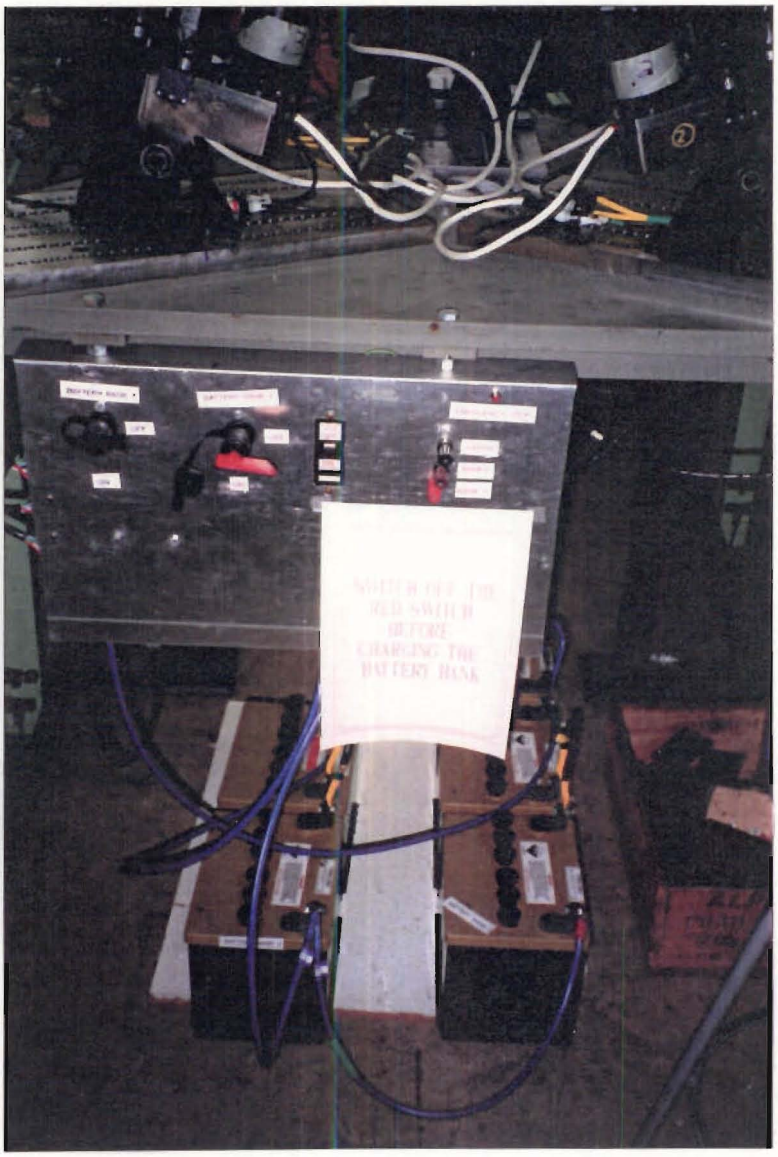

Fig. 4.25 The control panel and the power supply unit for the RSTP

4.5 PATH CONTROL OF THE RSTP

Different strategies are used to control the trajectory followed by the end-effector during movement from one command position to another. There are three main trajectory generation methods.

1. Point to point control.

2. Acceleration and deceleration ramp control.

3. Continuous path control.

4.5.1 Point to Point Control

PTP (point to point) control requires stating the coordinates of the starting and destination points. In coordinated PTP control all the robot axes are driven simultaneously at controlled speeds, so that they reach their destination simultaneously. The successive destination points can be chosen close enough so that the motion of the end effector is smooth. The time interval between successive steps is determined by the speed of the processor and the number of calculations which must be carried out at each step.

Linear interpolation is used to calculate the coordinates of intermediate points on the desired path. Linear interpolation will result in a straight line motion between successive points. If the interpolated points are close enough, the actual path followed by the manipulator will be close to the desired path.

The position control mode in HCTL-1000 offers PTP control. The details of achieving coordinated PTP control using the position control mode are discussed in detail under the software implementation in Chapter 5 (c.f. section 5.4).

4.5.2 Acceleration and deceleration ramps

Abrupt changes in the velocity and acceleration values result in the vibration of the manipulator and deviation from the required path. The vibrations can

be reduced by accelerating to the required velocity at a controlled rate and decelerating when approaching the destination. The successive values of the required velocity are increased at a constant rate (Δv) till the maximum programmed value is reached (c.f. Fig. 4.26). The profile generator in the HCTL-1000 profiles the velocity trajectory after the final destination, maximum velocity and acceleration values are specified by the user. The details of the trapezoidal control mode operation are discussed under the software implementation in chapter 5 (c.f. section 5.4).

4.5.3 Continuous Path Control

Continuous path motion is another form of PTP control where a continuous smooth curve is fitted between the starting and destination point. The result is a smooth continuous motion over the controlled path. There is a gradual change of velocity and acceleration between points. Cubic spline interpolation is one of the techniques which can be used for generating a smooth curve in the continuous path control.

4.6 CONTROL MODES OF HCTL-1000

HCTL-1000 executes one of the four position control algorithms selected by the user. The four control modes are:

1. Position control
2. Proportional velocity control
3. Trapezoidal profile control
4. Integral velocity control

Control flags FØ, F3 and F5 in the flags register (RØØH) determine which control mode is executed. The following section gives a brief description of each control mode. Details of the algorithms to execute these control are discussed in chapter 5 under the software implementation section (c.f. section 5.4).

4.6.1 Position Control Mode

Position control performs point to point position moves with no velocity profiling. The host processor specifies a 24-bit position command, which the

controller compares with the 24-bit actual position. The position error is calculated, the full digital lead compensation is applied and the motor command is output. The actual and command position data is 24-bit two's complement data stored in six 8-bit registers. The position is measured in encoder quadrature counts.

4.6.2 Proportional Velocity Control Mode

In proportional velocity mode, the algorithms takes a user specified command velocity, calculates the actual velocity and computes the velocity error. The velocity error is multiplied by K/4 and output as a motor command. The dynamic pole and zero lead compensation are not used.

The command and actual velocity are 16-bit two's complement words. The units of velocity are encoder quadrature counts/sample time. The controller tracks the command velocity continuously until new mode command is given.

Internally, the controller performs velocity profiling through position control. From the user specified command velocity and acceleration, the controller internally generates position profiles. This system has zero state velocity error. This results in difficulty in achieving loop stability compensation .

4.6.3 Integral Velocity Control Mode

Integral velocity control performs continuous velocity profiling which is specified by a command velocity and command acceleration. Once the specified velocity is reached, the HCTL-1000 will maintain that velocity until a new command is specified. The command velocity is an 8-bit two's complement word and the acceleration is a 16-bit scalar word. The units of velocity are quadrature counts/sample time and the units of acceleration are quadrature counts/(sample time)^2.

4.6.4 Trapezoidal Control Mode

Trapezoidal profile control performs point to point position moves and profiles the velocity trajectory to a trapezoidal or triangle. After the desired final position, maximum velocity and acceleration values are specified, the

controller computes the necessary profile to conform to the command data. Fig. 4.27 shows the possible trapezoidal/triangular trajectories using HCTL-1000.

The command data for this control mode is a 24-bit two's complement word, the command acceleration is a 16-bit scalar word and the maximum velocity is a 7-bit scalar word.

4.7 SUMMARY

A novel antenna mount design was suggested for improved satellite tracking operation. This chapter described the method for employing the Parallel Robotic Mechanism for the tracking application. The computer control feedback system hardware was described in detail. The operation and interfacing of the multi-motor controller based on six Hewlett-Packard HCTL-1000 motion control chips was detailed. Finally various trajectory generation schemes using HCTL-1000 control modes were described. The main limitation of the controller was the inability to control the acceleration derivatives or jolts and thus control the mechanical forces setting up vibrations.

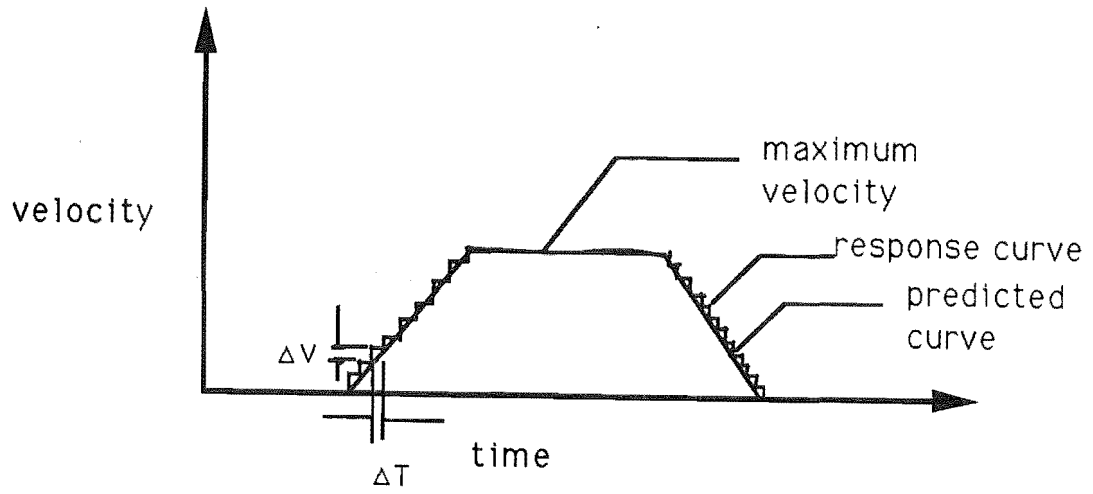

Fig. 4.26 Acceleration and deceleration ramp

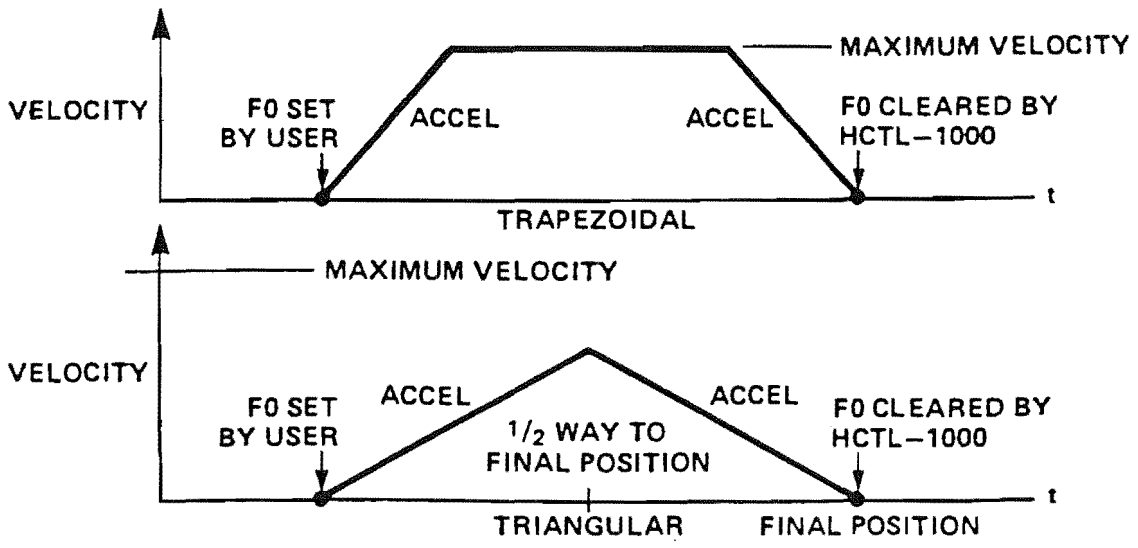

Fig. 4.27 Trapezoidal and triangular profile mode of the HCTL-1000

CHAPTER 5

RSTP: MECHANICAL HARDWARE DESIGN AND SOFTWARE IMPLEMENTATION

5.1 INTRODUCTION

The discussion of a prototype RSTP based on the design principles described in chapter 3 and incorporating the computer control techniques discussed in chapter 4 is developed for various applications in general and the satellite tracking application in particular. This chapter discusses the mechanical hardware and the software implementation details of the RSTP. A variable geometry set up incorporating provisions for changing the sizes of base and platform is described. A computer programme is developed to model the variable geometry configuration. The simulation programme 'CHECKANT.PAS' calculates actuator lengths and various joint angles for a range of base and platform sizes. These values are checked against the physical mechanical constraints of the mechanism and an optimum configuration is selected.

Under the the software implementation section, the functions of various software routines to control the RSTP movement are described. The software consists of orbital satellite bearing calculations, main control programme and numerous custom library routines. Various applications of RSTP are outlined with the emphasis being on low cost maritime applications for high gain antennas.

5.2 MECHANICAL HARDWARE

The prototype RSTP consists of an asymmetrical hexagonal baseplate, six Electrac Series 100 actuators, six mounting brackets, a triangular platform and the top joint subassemblies (c.f. Fig. 5.1). In the following section the construction of each part is described.

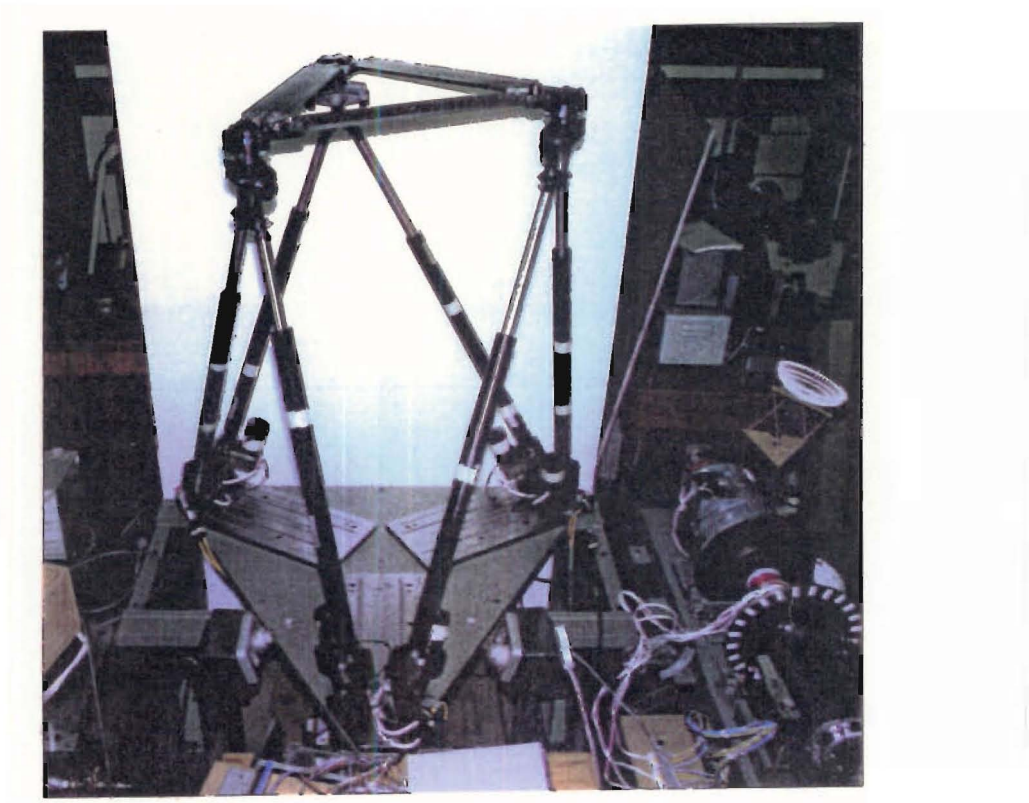

Fig. 5.1 The prototype RSTP

5.2.1 The Platform and Baseplate

The baseplate is fabricated from a solid steel plate and is of asymmetrical hexagonal shape. It incorporates a series of mounting holes so that the base radius 'Rb' can be varied to change the RSTP configuration (c.f. Fig. 5.2). The baseplate is supported on a fabricated mounting frame.

The base pitch circle radius 'Rb' can be written as:

$$Rb = \sqrt{\{[109.40 + (\text{Number of mounting hole} - 1) \times 12.5 - 50]^2 + [55.5]^2\}} \text{ mm}$$

$$\cos \beta = \frac{\text{Norminal offset (55.5 mm)}}{Rb} \qquad (5.1)$$

There are 43 mounting holes on the baseplate, giving Rb a range of 59.4 to 584.4 mm.

The platform plate consists of three steel plates bolted to support plate and is of triangular shape. It also incorporates a series of mounting holes so that the platform pitch circle radius 'Rp' can be varied to change the RSTP configuration.

The platform pitch circle radius 'Rp' is calculated by using following formula:

$$Rp = \frac{[(\text{Number of mounting hole} - 1) \times 10.825 + D + 100]}{\cos 30^{\circ}} \qquad (5.2)$$

where, D = Distance between the centre of the plate and the number of mounting hole.

The platform pitch circle radius 'Rp' can be varied from 127 to 802mm.

The procedure 'ANTENNA-PARAMETERS' in the main control programme calculates the 'X' and 'Y' components of platform and base vectors for the user supplied values of 'Rb' and 'Rp'.

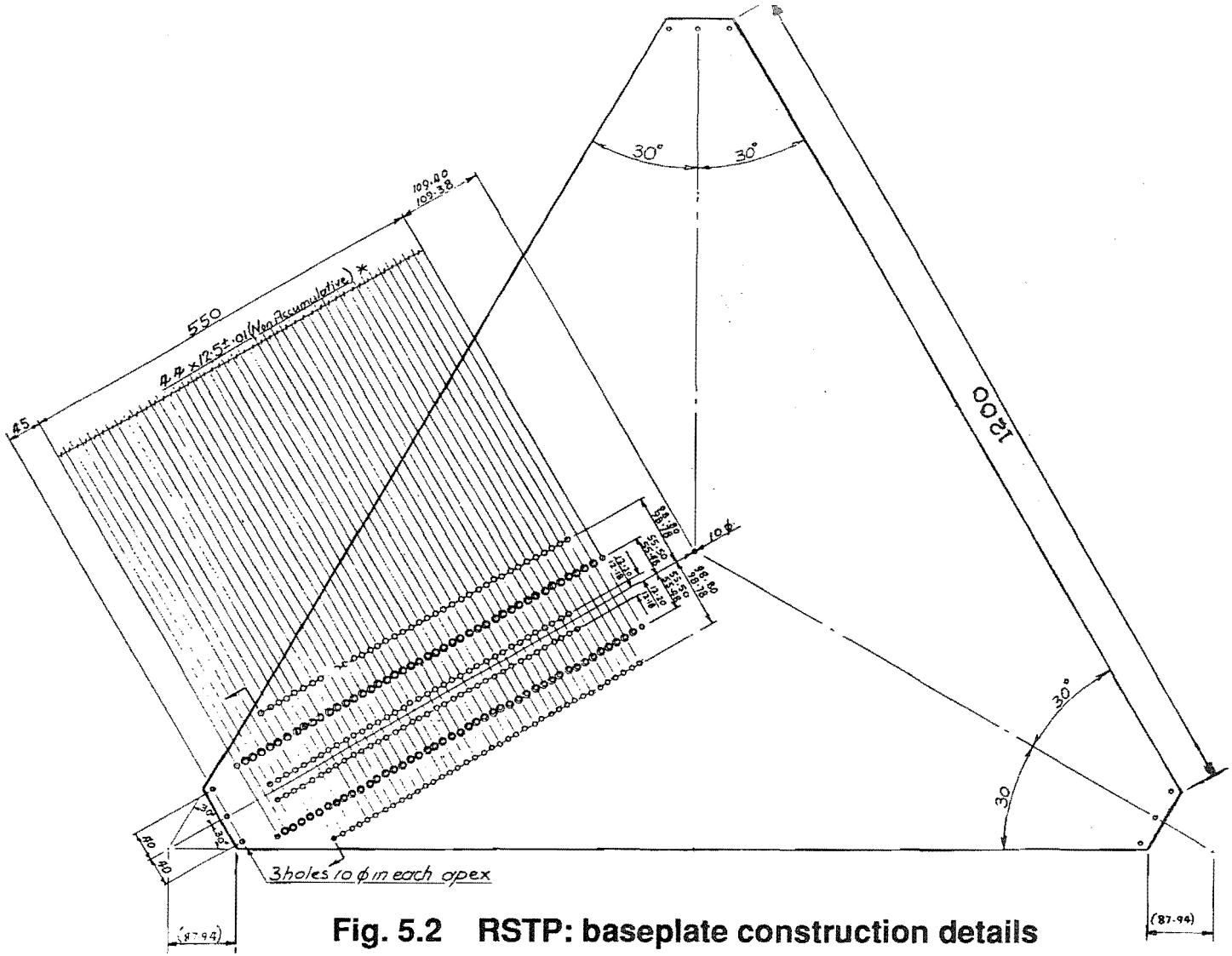

Fig. 5.2 RSTP: baseplate construction details

Drawing G R Johnson

5.2.2 Actuator and Mounting Bracket Subassembly

As mentioned in Chapter 4, the RSTP uses linear actuators to move the platform. The minimum and maximum nominal actuator length is 923.798 mm (36.37") and 1533.398mm.(60.37") respectively (c.f. Warner Catalogue, 1986). When the mounting bracket and top joint assemblies are taken into account the maximum and minimum lengths of each actuator are as tabulated in table 5.1. The accuracy of the measurement of the actuator lengths is $\pm$ 0.01 mm. The actual measurement of these lengths is essential for the initial setting up of the RSTP. During the RSTP movement, each actuator extension is calculated and checked with the allowable extension. If the calculated extension is found to be outside the permissible range, an error is generated and motion of the robot stopped immediately. In the 'HOME POSITION' of the RSTP all the actuators must have known identical lengths. The procedure 'HOME POSITION' in the main control programme drives the actuators so that all of them are of exactly the same length in the 'HOME POSITION'.

	Actuator 1	Actuator 2	Actuator 3	Actuator 4	Actuator 5	Actuator 6
Actuator length, mm	1026.62	1026.78	1022.80	1026.00	1026.00	1027.80
top joint bearing Φ, mm	40.132	40.080	40.080	40.106	40.055	40.132
Mounting bracket bearing Φ, mm	49.022	49.174	49.047	49.174	49.022	49.149
Actuator length between bearing centres, mm	982.043	982.153	978.240	981.360	981.460	983.160

Table 5.1 Table showing the measured actuator lengths

Each actuator and motor assembly unit is fixed to the baseplate using a specially designed mounting bracket (c.f. Fig. 5.3). The mounting bracket design incorporates a modified Hookes joint which allows rotation in the plane of the triangle formed by the actuators and about the side of the base forming the triangle. The mounting bracket design enables the rotation of each actuator in the plane of the triangle until the actuator centre line makes an angle of 30° (μ_i) with the baseplate. At μ_i = 30° the gearbox face will touch the baseplate. The main control programme calculates the angle μ_i for each RSTP orientation and sets an error flag if μ_i becomes less than 30°

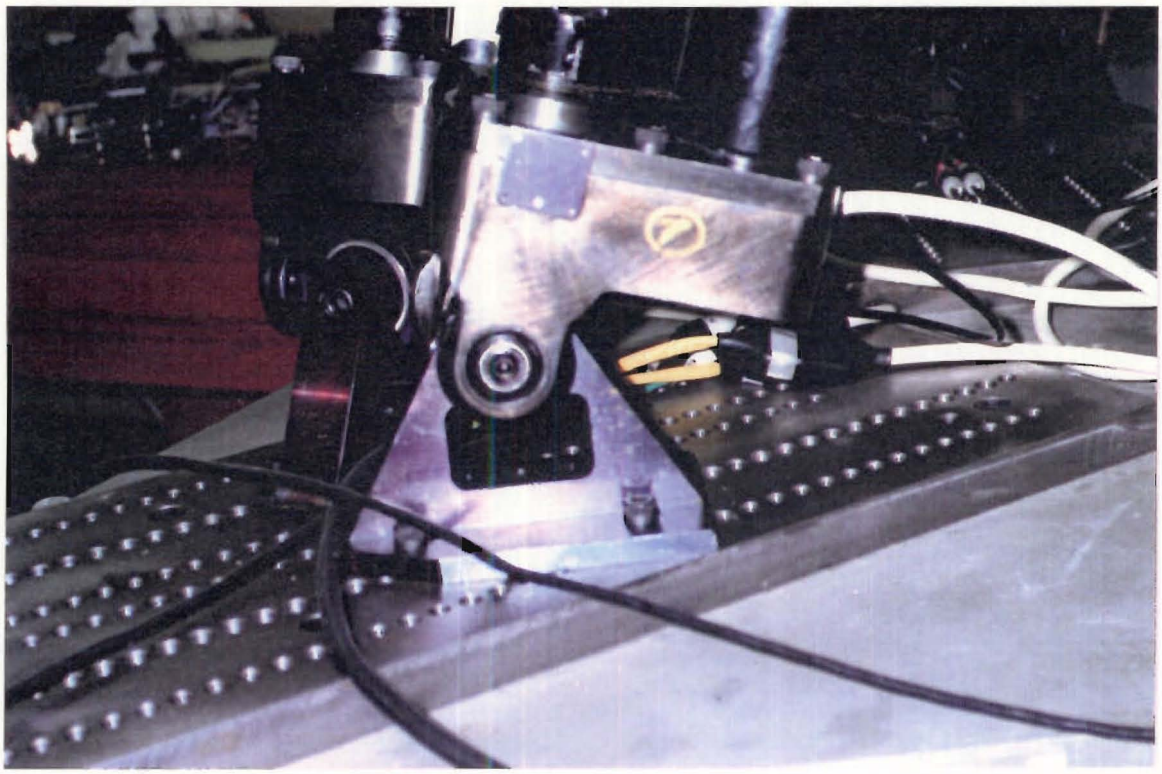

Fig. 5.3 Mounting bracket connecting the actuator-motor assembly to the baseplate

during the RSTP movement. The actuator gearbox and mounting bracket assembly is shown in Fig. 5.4.

The adjacent mounting brackets are displaced at an angle β along the base hexagon so as to avoid the interference between them during the robot movement (c.f. Fig. 5.5a and Fig. 5.5b). The RSTP configuration simulation programme 'CHECKANT.PAS' illustrates the effect of arranging the mounting brackets at different positions for a range of values of angle β. The simulation details are discussed under variable geometry simulation (c.f. section 5.3).

5.2.3 Actuators and Top Joint Subassembly

The top joint subassembly connects the two actuators together and to the platform as shown in Fig. 5.6 and Fig. 5.7. The subassembly consists of a cylindrical bearing housing [4] accommodating a pair of taper roller bearings [3 & 5] to carry the axial and radial thrust. The yoke [7] carries a rotating shaft [11] mounted on a pair of deep groove ball bearings [10] and positioned by end thurst bearings [8]. Specially designed connecting pieces [15] which are screwed to the actuator ends are clamped to the rotating shaft. The connecting pieces of the two actuators forming a triangle can slide into each other and overlap so as to reduce the minimum actuator length. This greatly reduces the minimum angle (Ψ_{ij}) that the two actuators can make with each other. This joint design allows a single point connection in the platform. Thus the two actuators and base line form a triangle which simplifies the kinematic analysis and reduces the number of computations required for the inverse kinematic transformations.

The top joint has been designed for the maximum range of rotation about the platform a, b and c axes. The angle Ψ_{ij} has a design range of 20° to 140° and γ_i has a range of 20° to 80° (c.f. Fig. 3.13). Fig. 5.8 shows the top joints in an extreme position when the antenna boresight axis is pointing at the horizon. The configuration simulation programme 'CHECKANT.PAS' calculates the angles Ψ_{ij} and γ_i for each position of the platform and checks the calculated values are within the allowable values.

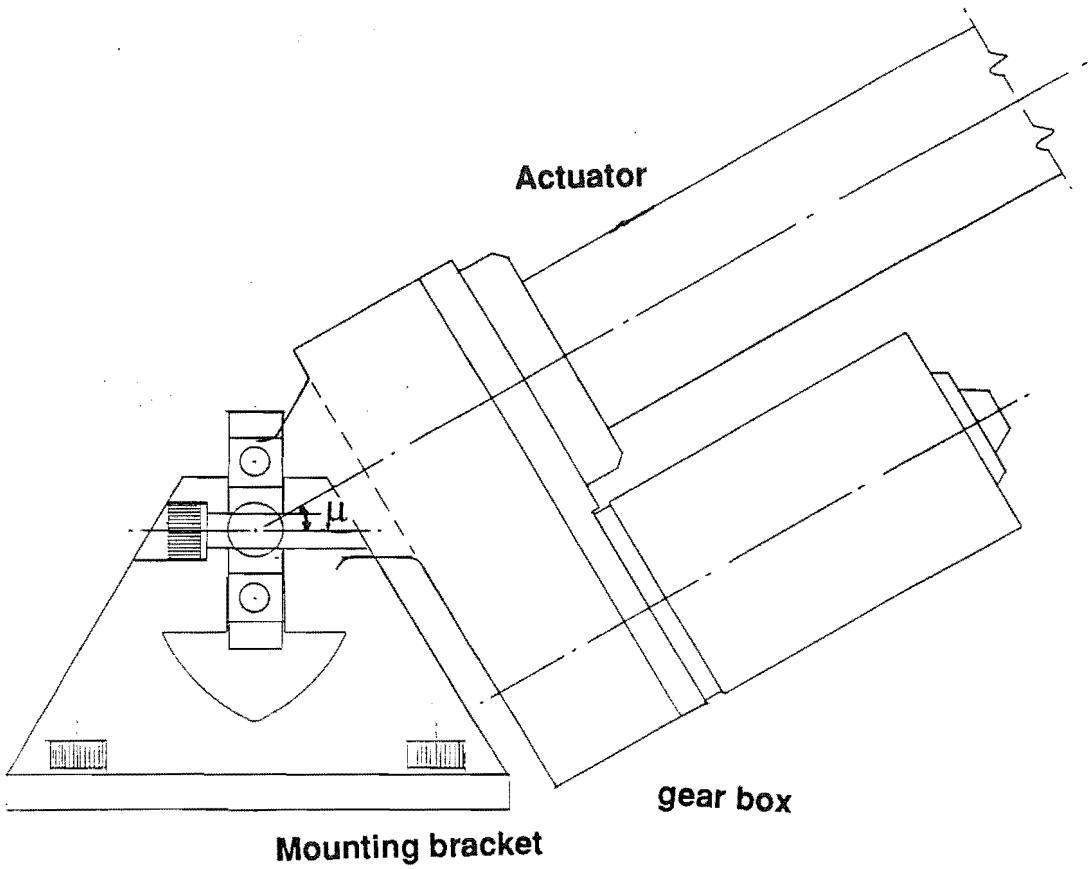

Fig. 5.4 The actuator-gearbox and the mounting bracket assembly
Drawing G R Johnson

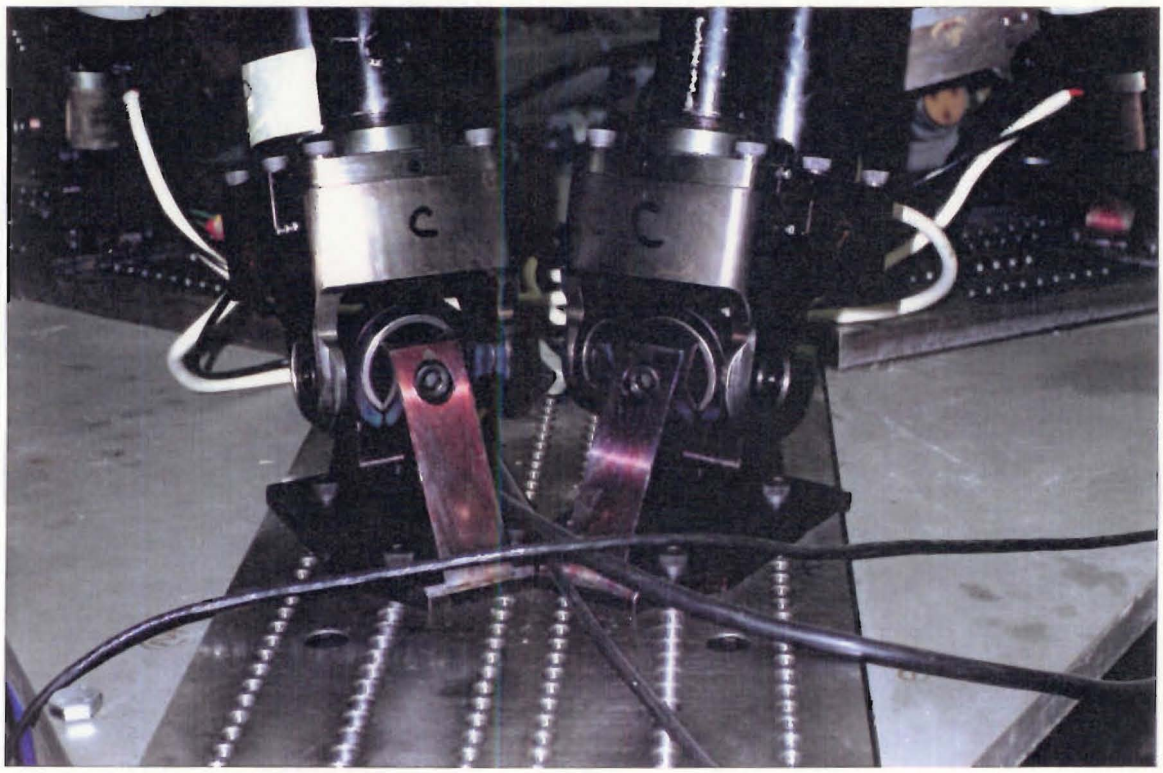

Fig. 5.5 (a) The mounting bracket arrangement to avoid interference between adjacent actuators

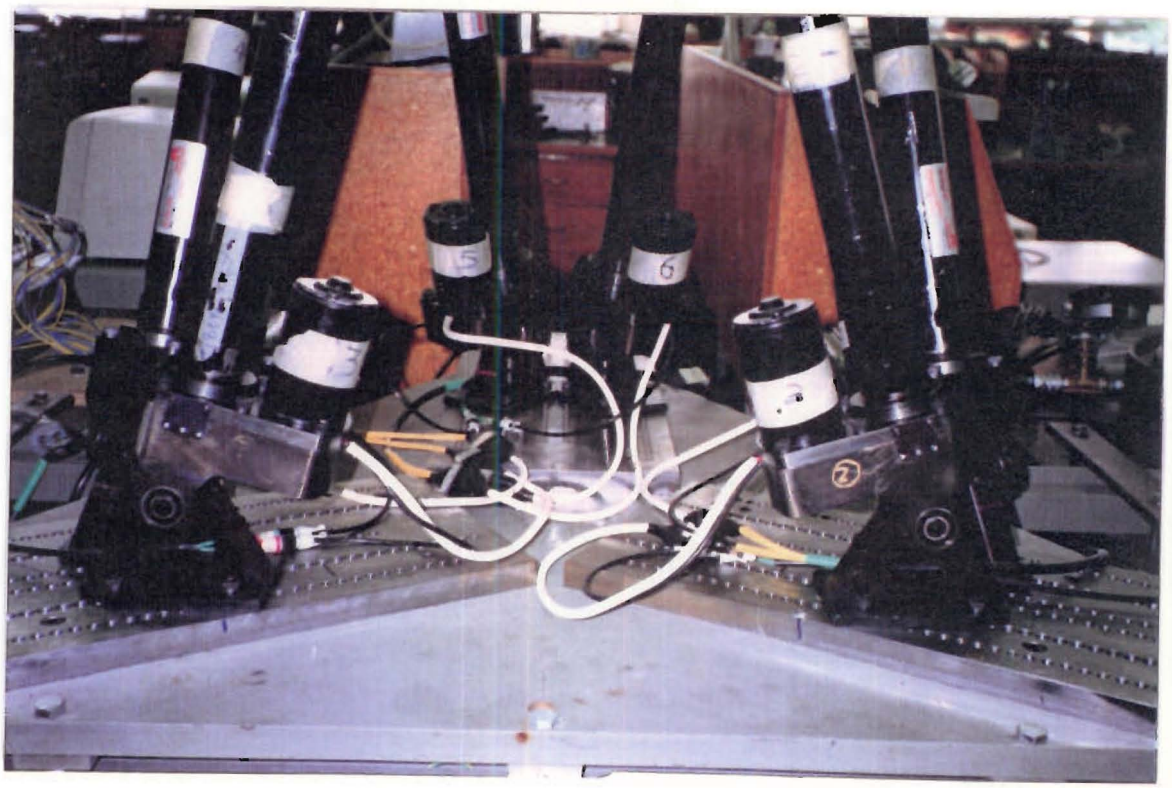

Fig. 5.5 (b) Six actuator-mounting bracket assembly arrangement

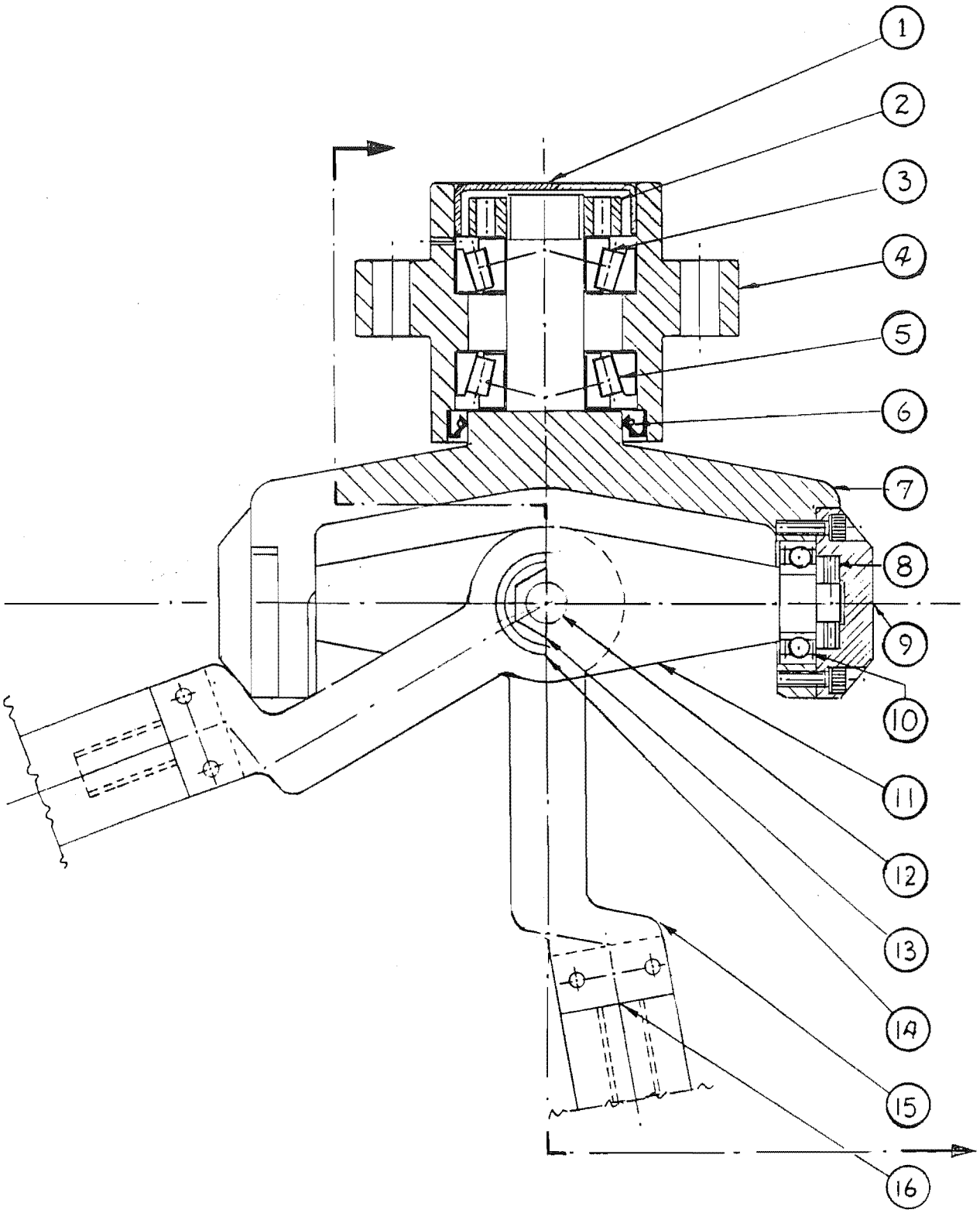

Fig. 5.6 Top joint assembly details

drawing G R Johnson

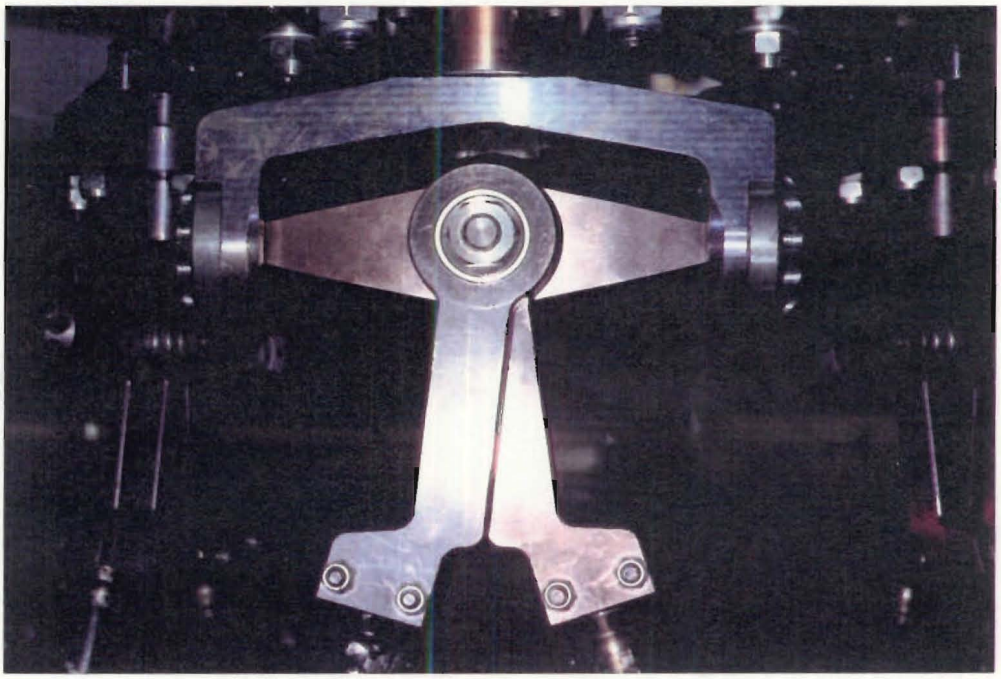

Fig. 5.7 A view showing the RSTP top joint assembly

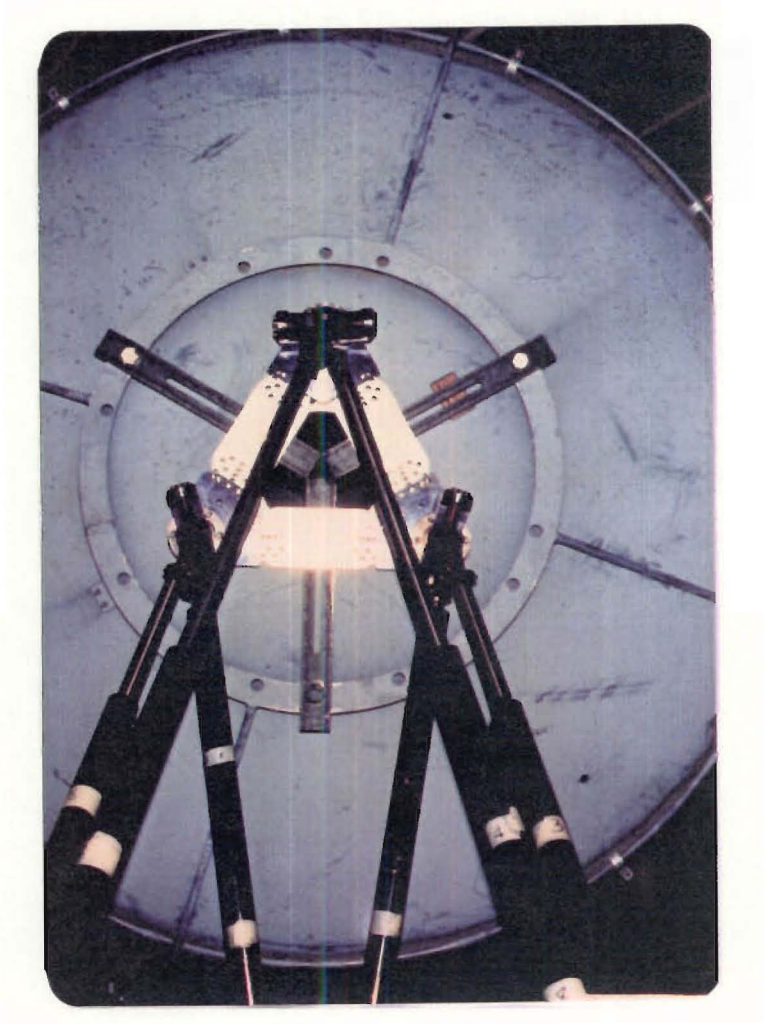

Fig. 5.8 A view of the top joints when the antenna boresight axis is pointing to the horizon

5.3 RSTP: VARIABLE GEOMETRY CONFIGURATION

In the prototype RSTP provision is made for changing the baseplate radius 'Rb' and the platform plate radius 'Rp'. This variable geometry arrangement allows the mechanism configuration to be changed. The simulation programme "CHECKANT.PAS" calculates the six actuator lengths for the specified motion of the platform. The simulation programme also calculates the mechanism constraints (discussed in detail in section 5.3.1). This simulation allows the motion limits of the mechanism for various combinations of baseplate and platform radii to be determined. The expansion ratio of the Electrac Series 100 actuators is fixed at 1.66 (1533.398/923.798). The procedure for optimizing the RSTP configuration using the simulation programme is discussed in detail in section 5.3.2.2. The total workspace of the mechanism is determined by the mechanical constraints as follows.

5.3.1 RSTP: Mechanical Constraints

1. Minimum length of the actuator, $L_{i\ min}$ is 923.798 mm (36370 Counts, Nominal).

2. Maximum length of the actuator, $L_{i\ max}$ is 1533.398 mm (60370 Counts, Nominal).

3. Top joint angles Ψ_{ij} and γ_i (c.f. Fig. 3.13).

4. Angle 2β between the adjacent mounting brackets .

5. All the eight singularity positions with this set-up should be avoided.

From the simulation programme results it was observed that the best utilization of the available actuator extensions is obtained for the following configuration of the RSTP:

$$Rb = Rp \tag{5.3}$$

But, it was also noted that, this configuration results in smaller values of the angle Ψ_{ij} in the extreme positions of the mechanism, thus reducing the

range of the movement (c.f. Table 5.2). To achieve the maximum angular movement, a smaller platform radius than the base radius needs to be used. This concept is further elaborated in the section 5.3.2.2.

5.3.2 Variable Geometry Simulation

A variable geometry simulation programme 'CHECKANT.PAS' was written to evaluate the effects of several different geometrical parameters on the mechanical constraints of the RSTP. The simulation programme was used to collect sets of data for different RSTP parameters Rb, Rp and L. Figures 5.9, 5.10 and 5.11 contain graphs showing variations in the six actuator lengths for three different RSTP configurations. It is interesting to note the almost sinusoidal nature of the actuator length curves for the particular RSTP configurations. In Appendix B, the actuator lengths for three RSTP configurations are listed in tables B-1, B-2 and B-3 respectively. Table B-4 shows the values of the angle Ψ_{ij} for the RSTP movement through $\theta \in (0^o,90^o)$ and $\phi = 0^o$ and 180^o. Table B-5 shows the values of the angle γ_i for the RSTP movement through $\theta \in (0^o,90^o)$ and $\phi = 0^o$ and 180^o. Table B-6 shows the values of the angle μ_i for the RSTP movement through $\theta \in (0^o,90^o)$ and $\phi = 0^o$ and 180^o.

5.3.2.1 Simulation validation

A string model was constructed using elastic strings and two drawing boards to act as the platform and base (c.f. Fig. 5.12). This model was used to validate the actuator lengths given by the simulation programme 'CHECKANT.PAS'. Different configuration parameters 'Rb', 'Rp' and 'L' were used at various elevation angles and length measurements were made. The measured lengths were in agreement with the results given by 'CHECKANT.PAS'. This model was also used to visualize the parallel mechanism manipulator and to formulate the basis for the design of the link joints.

5.3.2.2 Optimizing the RSTP configuration

It is necessary to select the optimum values of 'Rb', 'Rp' and 'L' for the RSTP so that a full 360^o azimuth rotation and lowest possible elevation angles are achieved for the satellite tracking application. The simulation programme

Rb (metres)	Rp (metres)	L (metres)	$\Psi^{o}_{16\ min}$
0.39654	0.2395	1.20	22.04
0.39654	0.2395	1.22	21.72
0.39654	0.2395	1.23	21.56
0.39654	0.2395	1.26	21.10
0.39654	0.2395	1.30	20.52
0.39654	0.2395	1.40	19.20
0.39654	0.2395	1.50	18.03
0.39654	0.2395	1.60	17.00
0.24654	0.2395	1.20	12.87
0.29654	0.2395	1.20	15.96
0.34654	0.2395	1.20	19.02
0.37154	0.2395	1.20	20.53
0.39654	0.2395	1.20	22.04
0.3715	0.2200	1.22	20.16
0.3715	0.2395	1.22	20.23
0.3715	0.2600	1.22	20.09
0.3715	0.2800	1.22	19.96
0.3715	0.3000	1.22	19.82

Table 5.2 Simulation results: Effect of changing Rb, Rp and L on angle Ψ_{16} at $\theta = 80^{o}$ and $\Phi = 0^{o}$

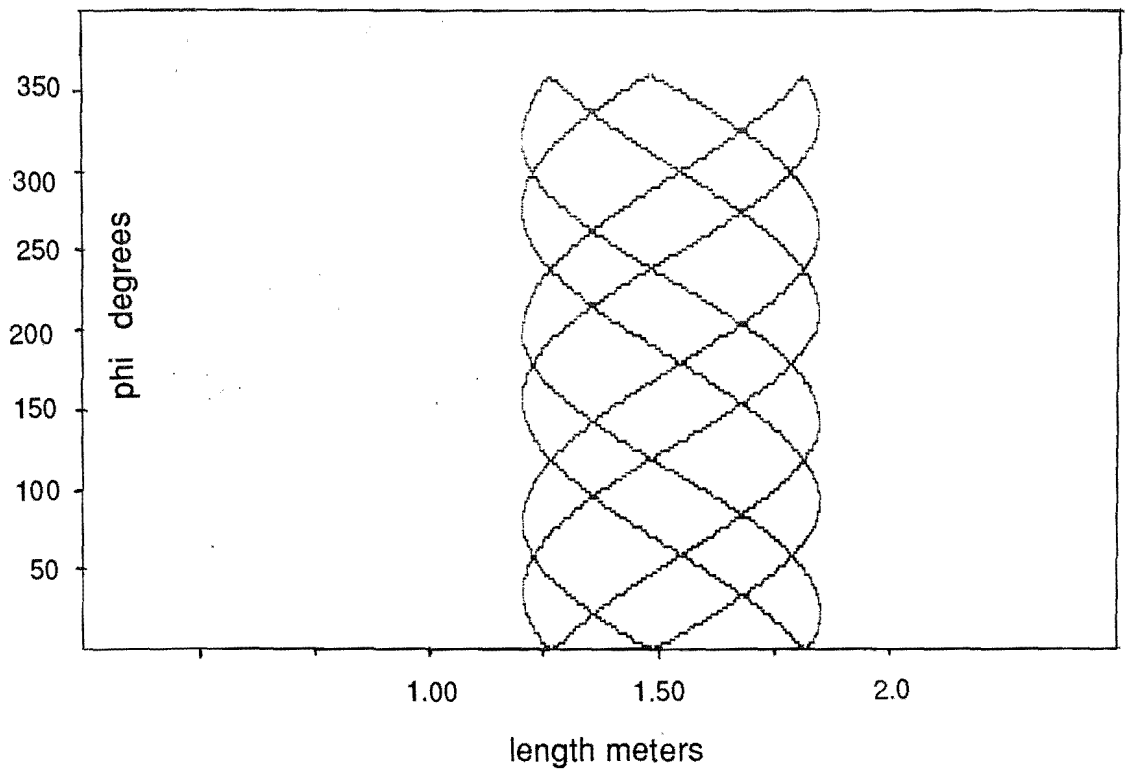

Fig. 5.9 **Graph showing the variation in the six actuator lengths for the mechanism with configuration Rb = 0.35904 m Rp = 0.23950 m L= 1.250m** $\theta = 75^{\circ}$, $\phi \in (0^{\circ}, 360^{\circ})$

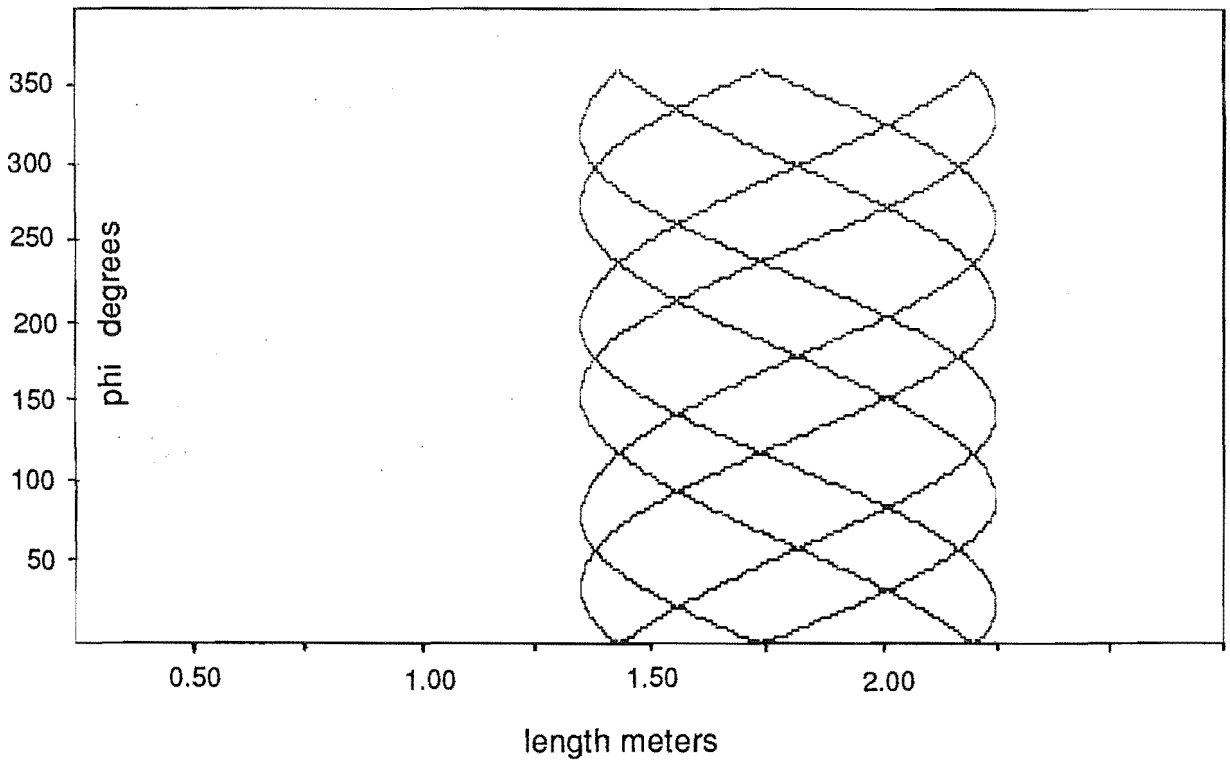

Fig. 5.10 **Graph showing the variation in the six actuator lengths for the mechanism with configuration Rb = 0.5 m Rp = 0.35 m L= 1.50 m**
$\theta = 75^{\circ}$, $\phi \ \varepsilon \ (0,360^{\circ})$

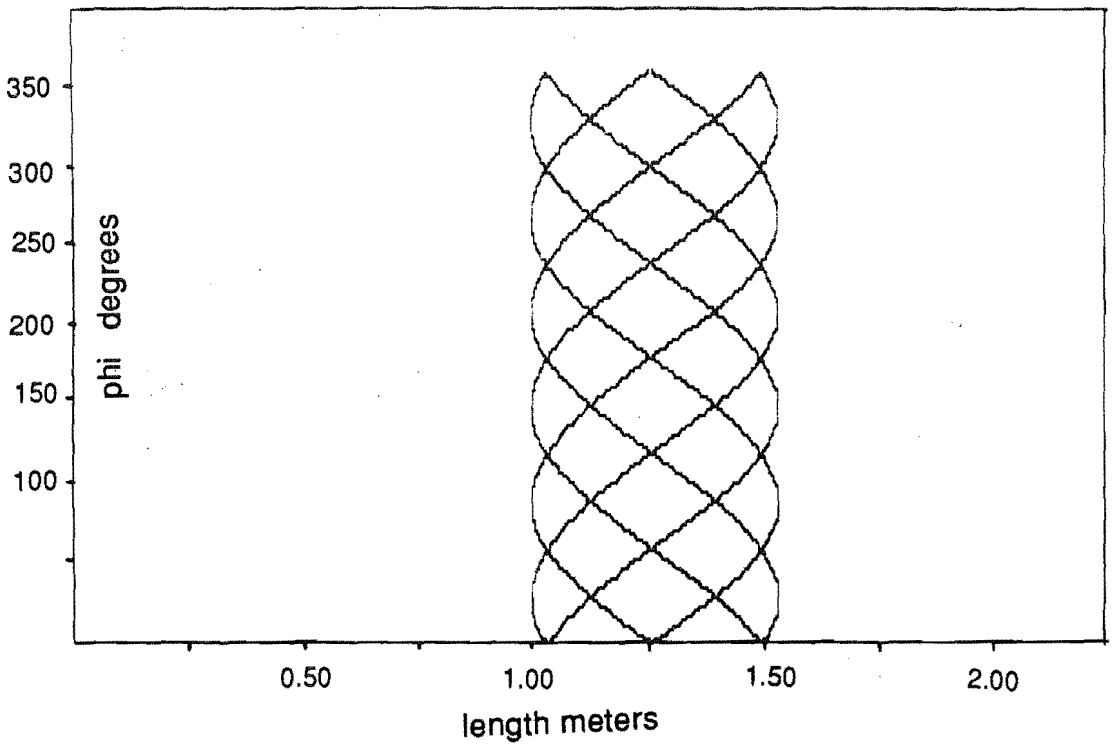

Fig. 5.11 **Graph showing the variation in the six actuator lengths for the mechanism with configuration Rb = 0.25 m Rp = 0.25 m L= 1.250m**
$\theta = 75^{\circ}$, $\phi \in (0,360^{\circ})$

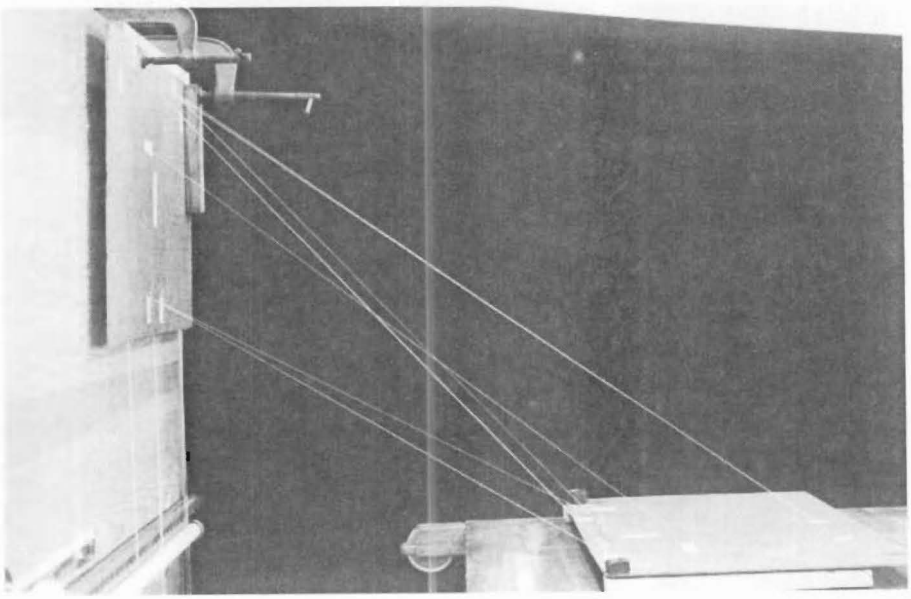

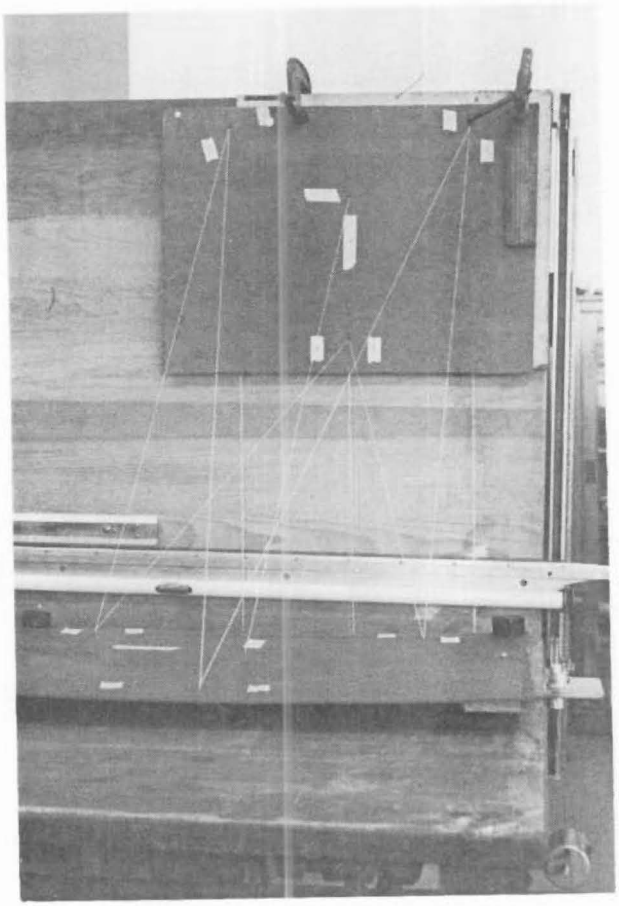

Fig. 5.12 The side and front view of the RSTP 'string model'

'CHECKANT.PAS' was run using different values of the controllable mechanical parameters of the RSTP.

To study the effects of using different values of 'Rb', 'Rp' and 'L', on the angle Ψ_{ij}, the expansion ratio Re and the maximum achievable angle θ, two of the three parameters were held constant and the third parameter was varied. The following tables summarize the relationships between these parameters. Table 5.2 lists the minimum values of the angle Ψ_{16} for different values of 'L', 'Rb' and 'Rp' for mechanism configuration with $\theta = 80^o$ and $\phi = 0^o$. In Figures 5.13a, 5.13b and 5.13c, graphs of angle Ψ_{16} vs L, Rb, and Rp are plotted. Using these graphs, the mechanical parameters of the RSTP can be selected so that the angle Ψ_{ij} stays within the design limit (20^o–140^o) throughout the platform movement.

From the graphs 5.13a, 5.13b and 5.13c the following is inferred:

1. As 'L' increases angle Ψ_{ij} decreases.
2. As 'Rb' increases angle 'Ψ_{ij}' increases.
3. As 'Rp' increases there is very little increase in angle Ψ_{ij}.

Thus the graphs 5.13a, 5.13b and 5.13c show that an optimum combination of the parameters is necessary so that the angle Ψ_{ij} stays within the design limit and maximum angular range of the movement is obtained.

Table 5.3 lists the values of the actuator expansion ratio 'Re' for different values of 'L' for the mechanism configuration with $\theta = 80^o$ and $\phi = 0^o$.

Rb (metres)	Rp (metres)	L (metres)	Max. actuator length, counts	Min. Actuator length, counts	Re
0.3715	0.2395	1.220	62270	36755	1.694
0.3715	0.2395	1.230	62660	37129	1.688
0.3715	0.2395	1.240	63049	37504	1.681
0.3715	0.2395	1.245	63244	37691	1.678
0.3715	0.2395	1.250	63439	37879	1.675

1 count = 0.0254 mm.

Table 5.3 Simulation results:Effect of changing L on expansion ratio Re.

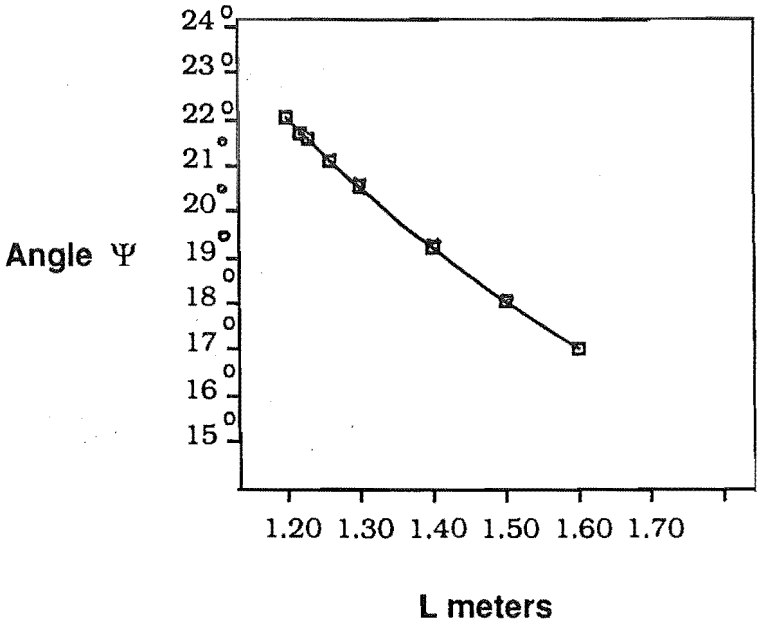

Fig. 5.13 (a) Graph of Length 'L' Vs Angle Ψ

For the mechanism configuration with

Rb = 0.3965 m Rp = 0.2395 m

$\theta = 80^{\circ}$ $\Phi = 0^{\circ}$

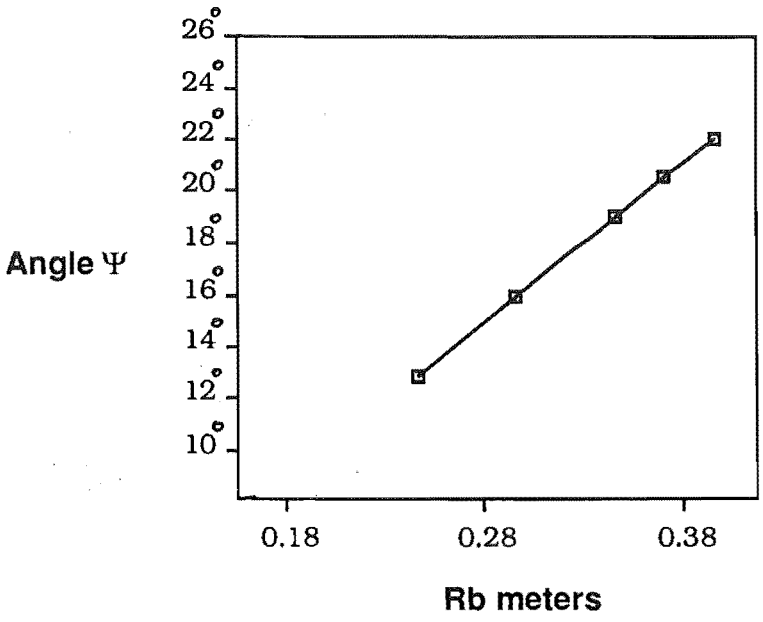

Fig. 5.13 (b) Graph of base radius Rb Vs Angle Ψ

For the mechanism configuration with

L = 1.20 m Rp = 0.2395 m

$\theta = 80^{\circ}$ $\Phi = 0^{\circ}$

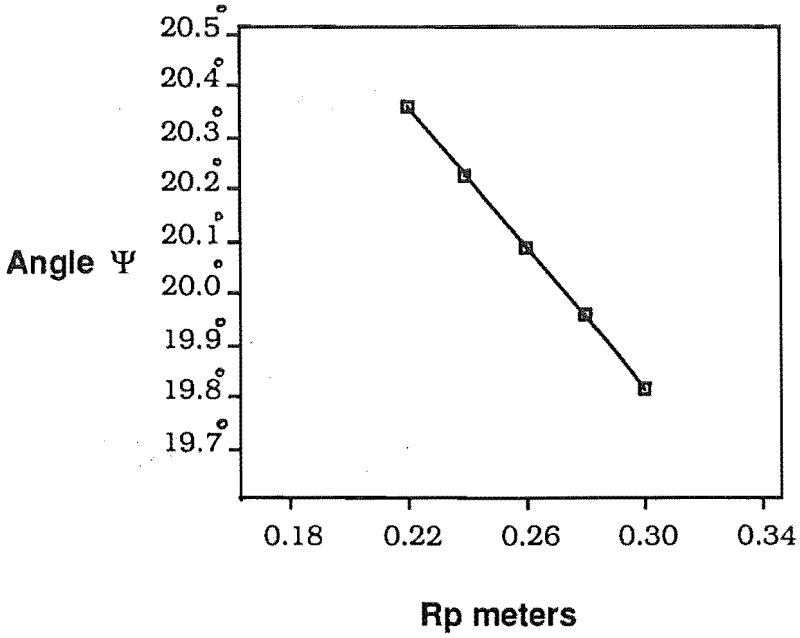

Fig. 5.13 (c) Graph of platform radius Rp Vs Angle Ψ

For the mechanism configuration with

L = 1.22 m Rb = 0.37154 m

$\theta = 80^{\circ}$ $\Phi = 0^{\circ}$

In Fig. 5.14 a graph of Re vs L is plotted. From the graph shown in Fig. 5.14 it can be concluded that as 'L' is increased, the expansion ratio 'Re' is reduced.

Table 5.4 lists the values of Rb and Rp, for the mechanism configuration with $\phi = 0^o$ and L =1.25, for the maximum angle θ reached by the mechanism before the actuator expansion limits are reached .

Rb (metres)	Rp (metres)	L (metres)	max. achievable angle θ
0.35904	0.2395	1.25	80°
0.32154	0.2395	1.25	85°
0.24654	0.2395	1.25	90°
0.38404	0.2395	1.25	75°
0.40904	0.2395	1.25	75°
0.35904	0.2395	1.25	80°
0.35904	0.2200	1.25	85°
0.35904	0.2000	1.25	90°
0.35904	0.1700	1.25	95°
0.35904	0.2600	1.25	75°

Table 5.4 Simulations Results: Effect of changing Rb and Rp on the maximum achievable angle θ

Graph of Rb and Rp vs maximum achievable angle θ is plotted in Fig. 5.15.

This graph indicates that by increasing 'Rb' and 'Rp', the minimum elevation angles which the RSTP can reach, before the actuator limits are reached, decrease. This relationship shows that use of a platform radius smaller than the base radius will result in a larger angular range of the RSTP.

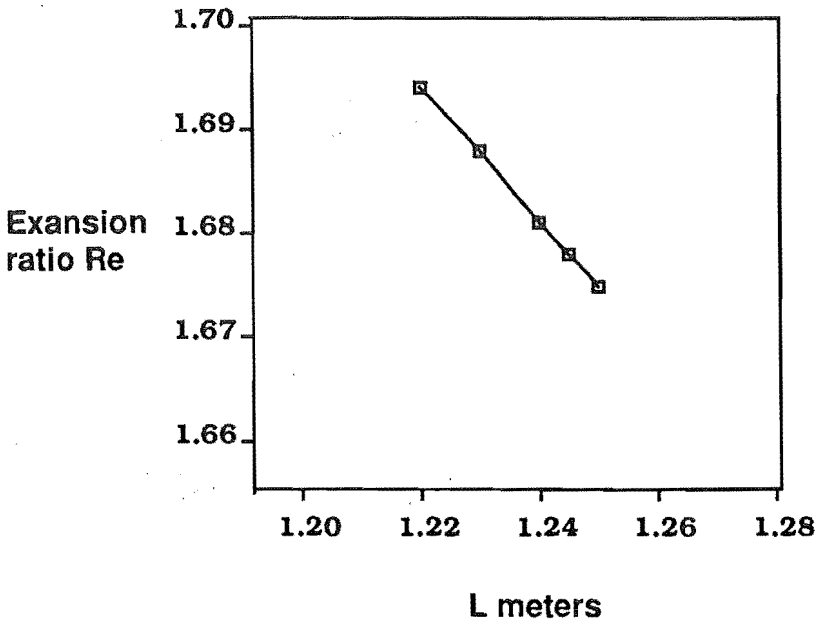

Fig. 5.14 Graph of Length 'L' Vs Expansion ratio Re

For the mechanism configuration with

Rb = 0.3715 m Rp = 0.2395 m

$\theta = 80^{\circ}$ $\Phi = 0^{\circ}$

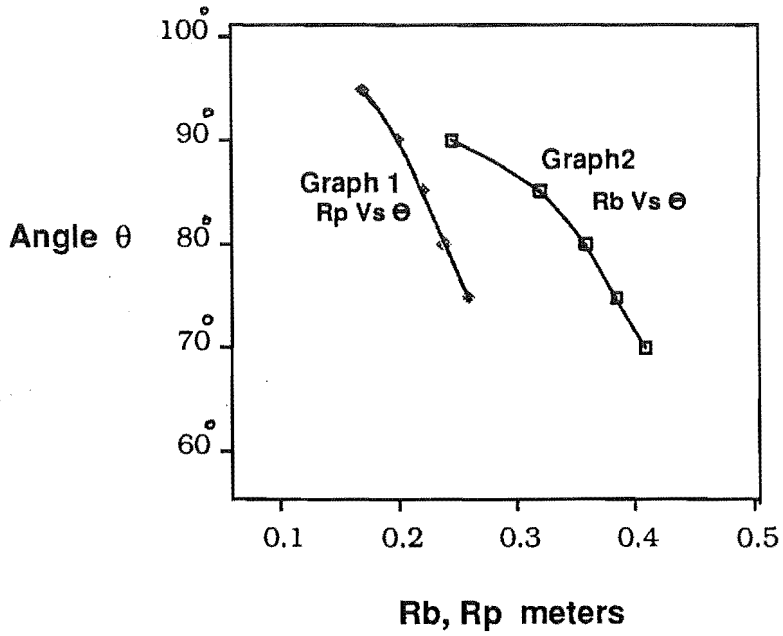

Fig. 5.15 Graph of Rb, Rp Vs maximum achievable angle Θ

For the mechanism configuration with

L = 1.25 m Rp = 0.2395 m $\Phi = 0^{\circ}$
for graph 2

L = 1.25 m Rb = 0.35904 m $\Phi = 0^{\circ}$
for Graph 1

Thus an optimum combination of 'Rb', 'Rp' and 'L' must be used to maximize the RSTP work envelope and keep the mechanism within the mechanical constraints discussed in the section 5.2.1.

The simulation programme has simplified the task of examining various mechanism configurations and selecting the optimum values of 'Rb', 'Rp' and 'L'. It has helped to test these configurations for the mechanical constraints of the mechanism. Thus the mathematical model of RSTP can be used as a tool for selecting the optimum geometrical configuration of the RSTP for the desired application.

5.4 SOFTWARE IMPLEMENTATION

Every aspect of the RSTP is computer controlled. A software programme is used to generate the position, velocity and acceleration profiles, and to drive the six axes of the RSTP synchronously. The RSTP control software can be split into three parts:

1. Orbital Satellite Bearing Calculations
2. Main Control Programme
3. Library Routines

The following section discusses the principles behind each part.

5.4.1 Orbital Satellite Bearing Calculations

Satellite position in space is defined in terms of its 'look angles' (section 2.4). The look angles for a particular orbiting satellite are predicted by running an orbit prediction programme 'TRACKSAT' (supplied by DSIR, New Zealand). The output of the programme consists of a series of values for a subsatellite latitude and longitude, azimuth, elevation and range values from an observer point. After supplying the necessary emphemeris data, the satellite orbit details are drawn from a global database.

The programme 'TRACKSAT' is run on a MICROVAX II and the data is downloaded to the Zenith Z-286 control computer via an RS232C communications port. A second programme 'DATA-CONVERSION'

processes this data and stores the information in the format to be used by the main control programme.

The programme 'TRACKSAT' was used to predict the orbital path of an orbiting weather satellite NOAA-7. NOAA-7 has the following Keplarien elements:

Anomalistic period:	102 minutes
Inclination:	98.93° (Near polar orbit)
Eccentricity:	0.00127
Height above Earth:	1600 Km

The table 5.5 gives the NOAA-7 satellite bearings for a high pass and a low pass. In the actual tracking set-up the time interval between two subsequent readings is chosen as 2.2200 seconds (1000 time samples for the position control microprocessor HCTL-1000 with sample time 2.2222 msec.). The main control programme linearly interpolates between these data points and provides pointing information at every 2.2200 msec. A cubic spline interpolation between the successive readings will give greater accuracy. But the extra computations required in carrying out the cubic spline interpolation will increase the total computation time. The increased accuracy is not necessary in the tracking application.

5.4.2 Main Control Programme

The main control programme resides in the host processor and is responsible for the operation of the RSTP. The main control programme consists of software routines to perform following operations:

1. Configuration of the RSTP for user selected values of 'Rb', 'Rb' and 'L'.

2. Configuration of the motion control chips HCTL-1000.

3. Read the look angle data.

4. Convert look angle information into actuator lengths.

Time (HH:MM:SS.FF)	Sub-satellite Latitude(N) (degrees)	Longitude(E) (degrees)	Observer-Satellite Azimuth (degrees)	Elevation (degrees)	Range (km)
High Pass					
04:47:00.000	25.34	4.75	9.92	2.54	3147.9
04:48:00.000	22.55	3.98	9.48	5.85	2828.3
04:49:00.000	18.82	3.06	8.90	11.02	2407.4
04:50:00.000	15.09	2.17	7.99	17.56	1995.2
04:51:00.000	11.36	1.30	6.45	26.42	1601.2
04:52:00.000	8.56	0.60	3.98	35.68	1328.5
04:53:00.000	4.82	359.76	357.11	53.74	1029.4
04:54:00.000	1.09	358.92	315.15	77.23	874.7
04:55:00.000	-2.65	358.08	215.84	63.95	939.4
04:56:00.000	-5.45	357.39	205.48	46.97	1115.7
04:57:00.000	-9.19	356.55	200.42	31.34	1442.7
04:58:00.000	-12.92	355.69	198.14	21.00	1823.0
04:59:00.000	-16.65	354.82	196.81	13.64	2228.2
05:00:00.000	-19.44	354.08	196.28	9.24	2542.3
Low Pass					
15:24:00.000	-13.85	23.39	121.84	1.08	3279.3
15:25:00.000	-10.11	22.53	114.95	3.67	3012.0
15:26:00.000	-6.36	21.68	106.79	6.08	2786.4
15:27:00.000	-2.61	20.84	97.31	8.09	2614.6
15:28:00.000	0.19	20.15	89.43	9.25	2521.6
15:29:00.000	3.94	19.31	78.24	9.91	2471.8
15:30:00.000	7.68	18.47	66.93	9.54	2500.3
15:31:00.000	11.42	17.61	56.26	8.25	2604.6
15:32:00.000	14.23	16.90	48.91	6.86	2722.2
15:33:00.000	17.96	16.02	40.40	4.51	2936.6
15:34:00.000	21.70	15.11	33.22	1.91	3196.7

Table 5.5 Typical NOAA-7 predicted path using"TRACKSAT"

5. Go to one of the four control modes of HCTL-1000.

6. Drive the DC motors to the desired position.

7. Monitor the motion for emergency stop signal.

8. Repeat these steps till the desired motion is completed.

These operations are outlined in the flowchart of Fig. 5.16.

The flowchart for the configuration of the HCTL-1000 and the selection of one of the four control modes is given in Fig. 5.17.

The software is written in Turbo Pascal version 5.0 and the graphics routines use the Turbo Pascal Graphics Tool Box version 3.0.

The motion is executed by using one of the four control modes of the motion control microprocessor HCTL-1000. The details of the tracking operation using the control modes is discussed in the following section.

5.4.2.1 Trajectory generation using HCTL-1000 control modes

RSTP position movements through the desired data points are executed by choosing one of the four control modes of the HCTL-1000. The following section describes the algorithms for using the position control and trapezoidal control mode of the HCTL-1000.

5.4.2.2 position control mode

To achieve coordinated motion of a multi-axis machine like RSTP, the position sampling and calculations of all the motion control chips must start together. This is achieved by having all the sample time registers embedded in the HCTL-1000 start the counting cycle at the same instant. Writing zero to all the sample time registers (RØFH) and then writing the desired value to all the sample time registers quickly and consecutively will start the sampling at almost the same time. The sampling start time will only

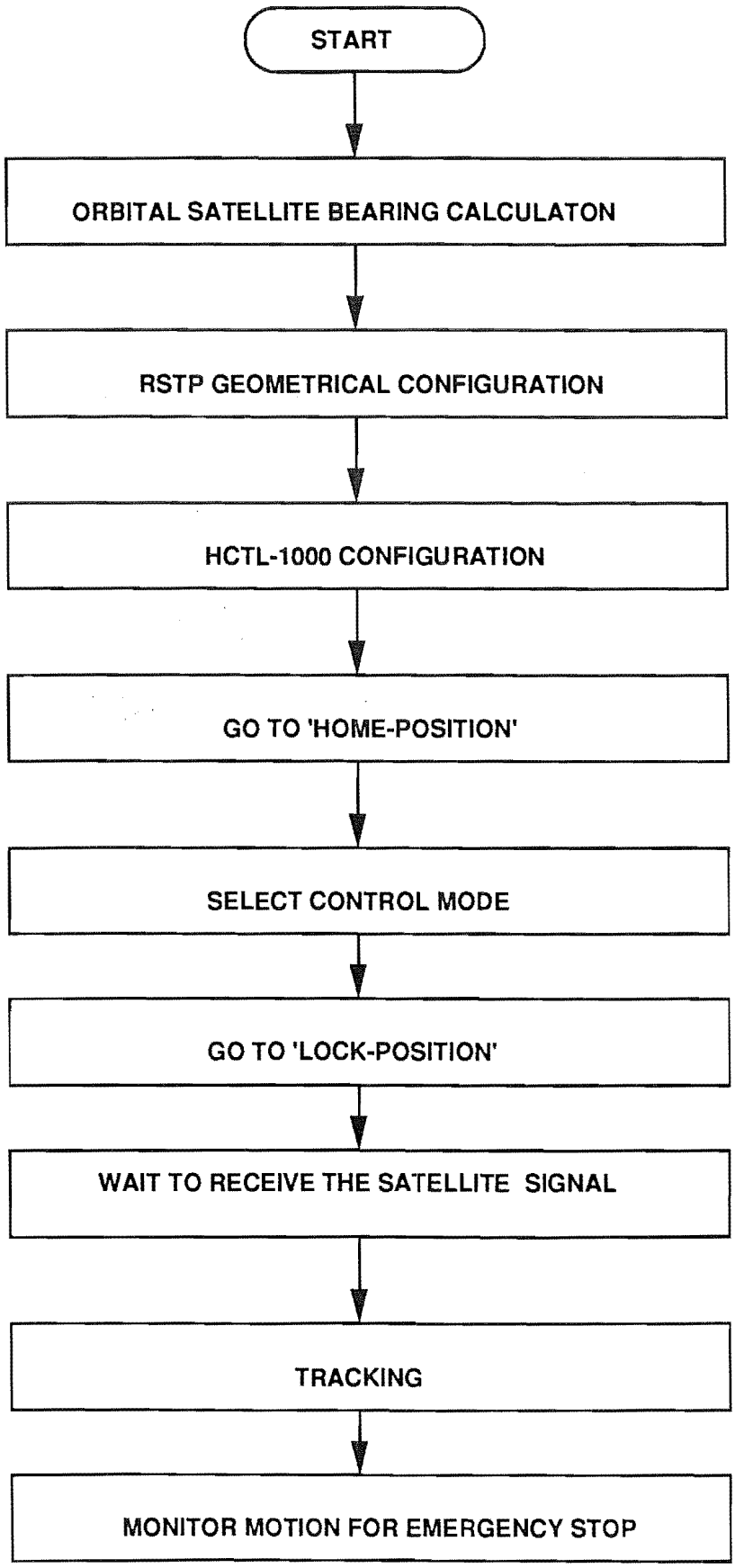

Fig. 5.16 Flowchart for overall satellite tracking operation using the RSTP

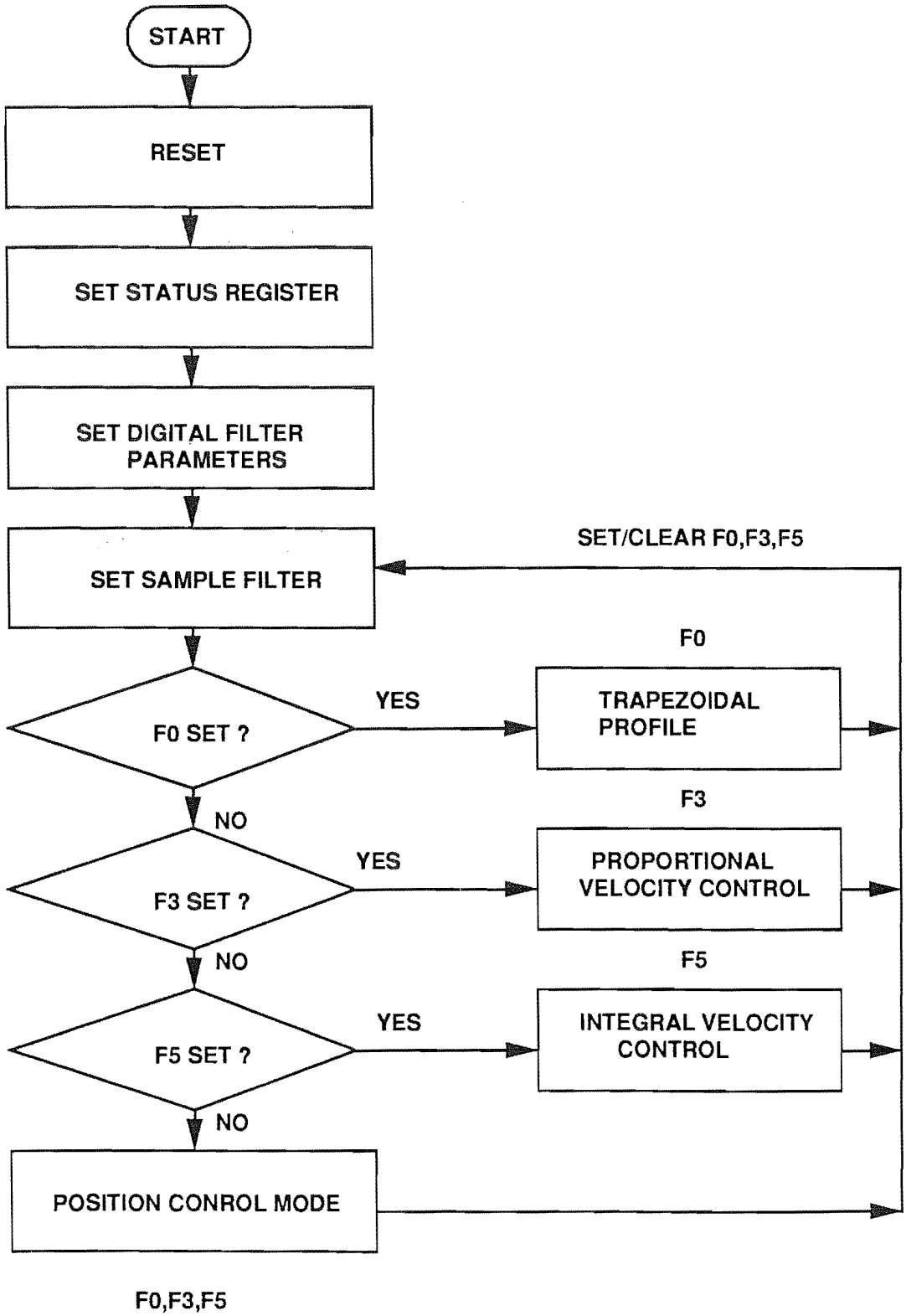

Fig. 5.17 Flowchart for HCTL- 1000 configuration and selection of a control mode

differ by a few microseconds, the time taken to write to the six sample time registers.

Fig. 5.18 contains the flowchart for execution of the RSTP motion in the position control mode. The synchronized motion of the actuators is achieved by calculating the number of steps to be executed by each motor during each sample time period. The step size is calculated for each actuator depending on the distance it has to travel in the sample time. The number of steps per sample time constitute the required increment in the current position per sample time. During one sample time the number of pulses will be output depending on the required number of steps. To illustrate the principle by an example, suppose for actuator 1 the step size is 0.8 steps per sample time, for actuator 2, 2.4 steps per sample time and for actuator 3, 3.6 steps per sample time. The number of pulses output for each actuator during consecutive sample time periods are as shown in Table 5.6.

Sample time period (msec)	Number of pulses output/sample time		
	Actuator 1	Actuator 2	Actuator 3
0.0000	0	0	0
1.1100	0	2	3
2.2200	1	2	4
3.3300	1	3	3
4.4400	1	2	4
5.5500	1	3	4
6.6600	0	2	3
7.7700	1	2	4

Table 5.6 Pulse Output Pattern

Thus all the movements are completed during the same time interval by driving the actuators at different speeds. Using this technique, coordinated point to point control of the RSTP is achieved in the position control mode. Fig. 5.19 shows a graph of the number of pulses output during a given period to achieve coordinated PTP control.

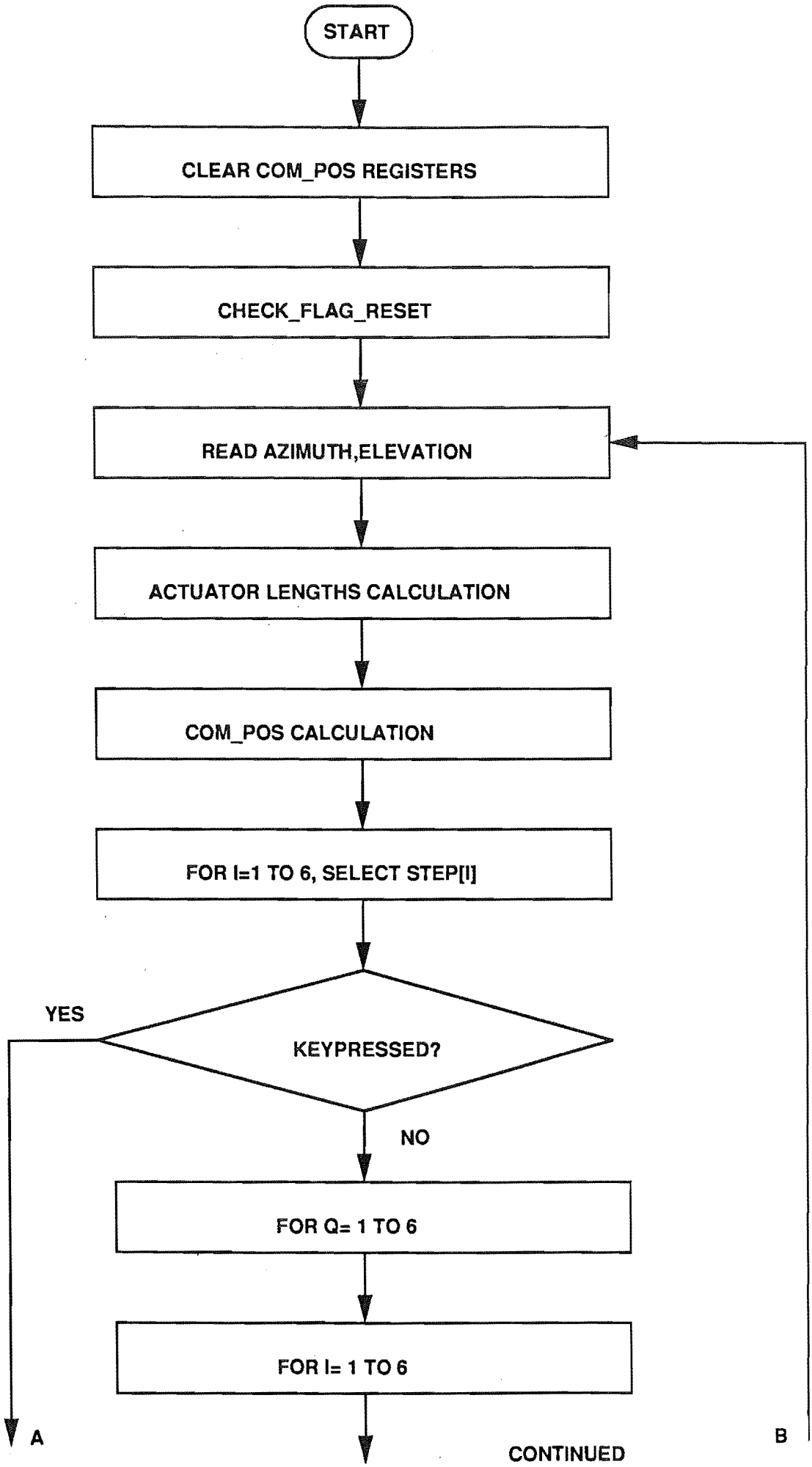
START
CLEAR COM_POS REGISTERS
CHECK_FLAG_RESET
READ AZIMUTH,ELEVATION
ACTUATOR LENGTHS CALCULATION
COM_POS CALCULATION
FOR I=1 TO 6, SELECT STEP[I]
YES
KEYPRESSED?
NO
FOR Q= 1 TO 6
FOR I= 1 TO 6
A
CONTINUED
B

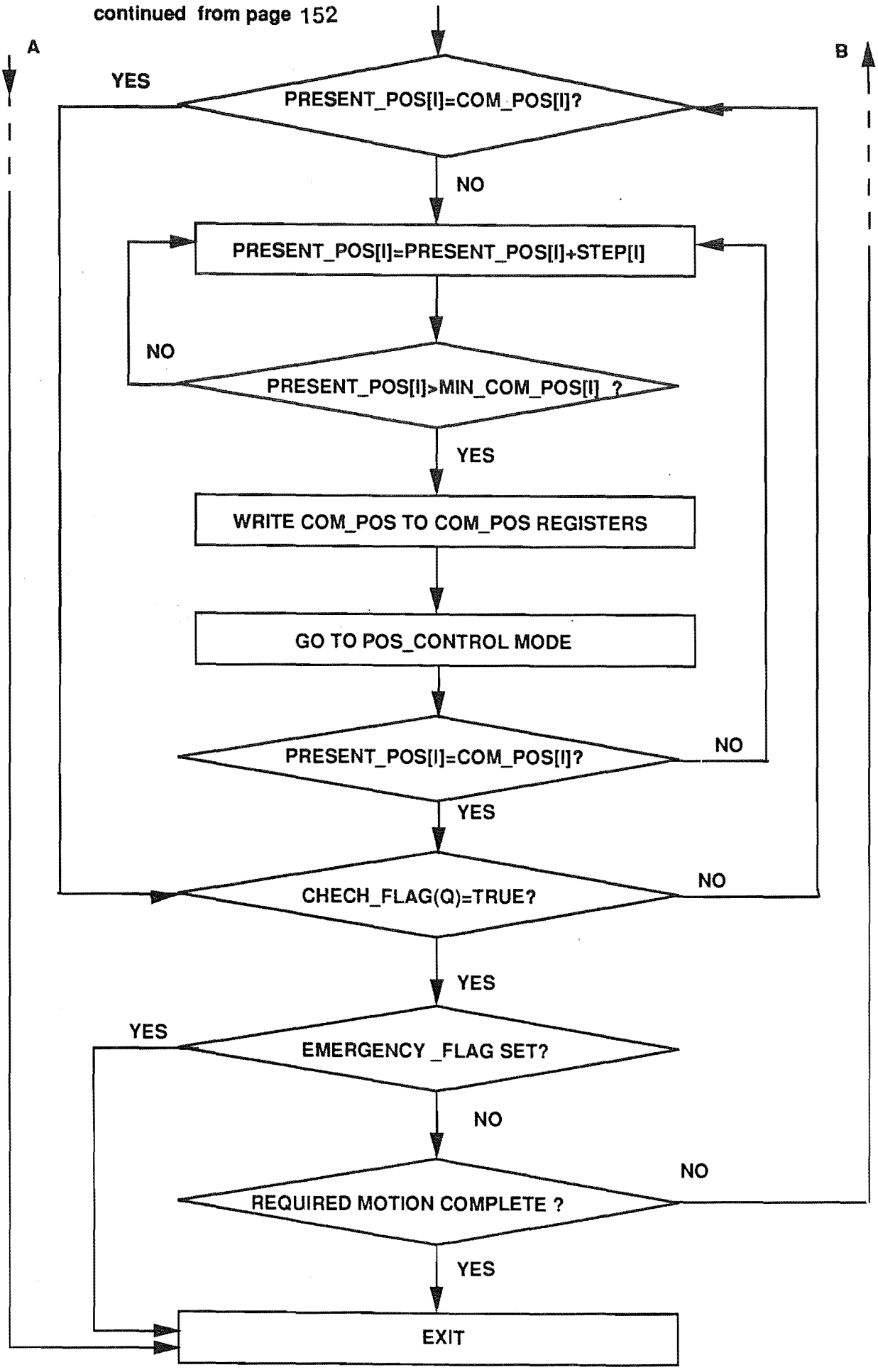

Fig. 5.18 Flowchart for executing motion in the position control mode of HCTL-1000

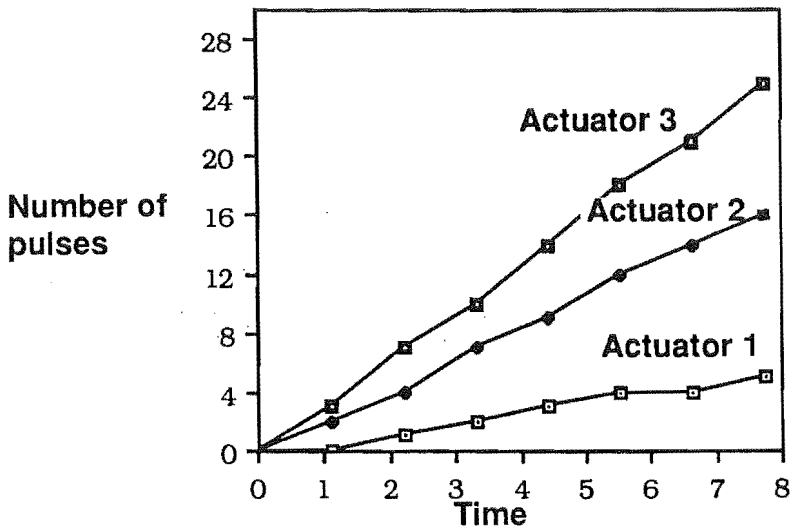

Fig. 5.19 Graph showing the pulse output pattern for the coordinated PTP control

5.4.2.3 Trapezoidal profile control mode

Trapezoidal profile control mode employs acceleration and deceleration ramps to control the RSTP movement. In this mode, the velocity trajectory is profiled to a trapezoid or triangle. The user specifies the desired final position, maximum velocity and acceleration values. The RSTP control programme computes the velocity and acceleration values from the distance to travel and time available information. The internal profile generator of HCTL-1000 produces a position profile using the present command position (RØCH-RØEH) as the starting point and the final position (R2AH-R2BH) as the end position.

In the trapezoidal profile control mode of the RSTP, if the sample time is set at 2.2220 msec [255 in RØFH] and the position is updated at every 2.2220 sec (1000 time samples), then the maximum velocity is calculated as: (c.f.Fig. 5.20).

$$\text{max. velocity} = \frac{\text{required position - current position}}{0.5 \times 2.2200}$$

The maximum acceleration is calculated as:

$$\text{Max. Acceleration} = \frac{\text{required position - current position}}{(0.5 \times 2.2200)^2}$$

Fig. 5.21 gives the flowchart for execution of the RSTP motion in the trapezoidal control mode.

From the simulation results of the programme 'CHECKANT.PAS' it was found that for a satellite tracking application, during 2.2200 second time interval the average actuator length change is less than 100 counts. These small positional increments result in velocity values which are less 1 count per sample time. In the trapezoidal control mode the maximum velocity values need to be greater than 1 count per sample time. Thus for a slow movement requiring relatively small velocities, the trapezoidal control mode cannot be used.

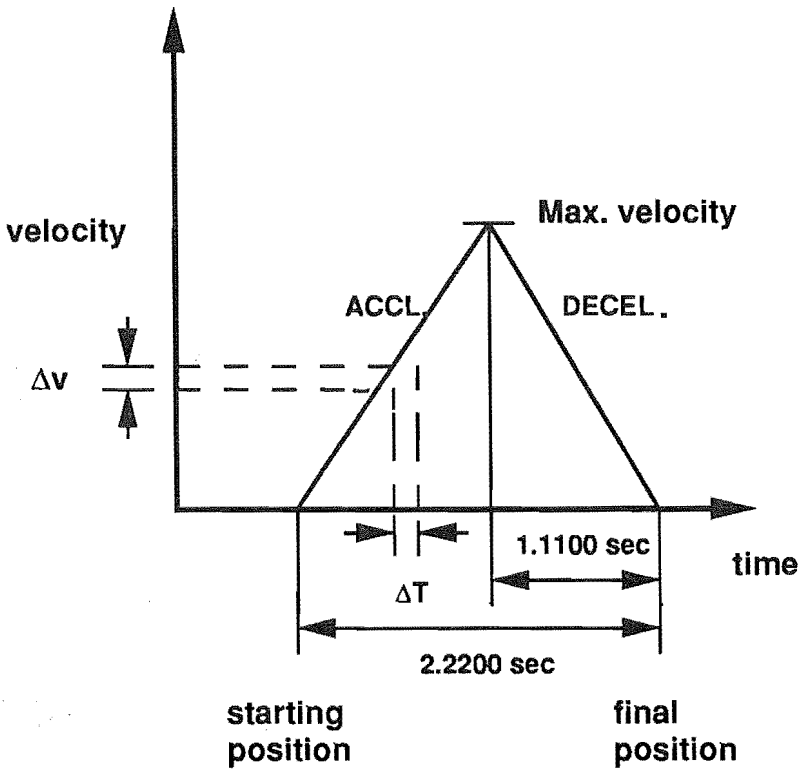

Fig. 5.20 Triangular velocity profile using the trapezoidal control mode

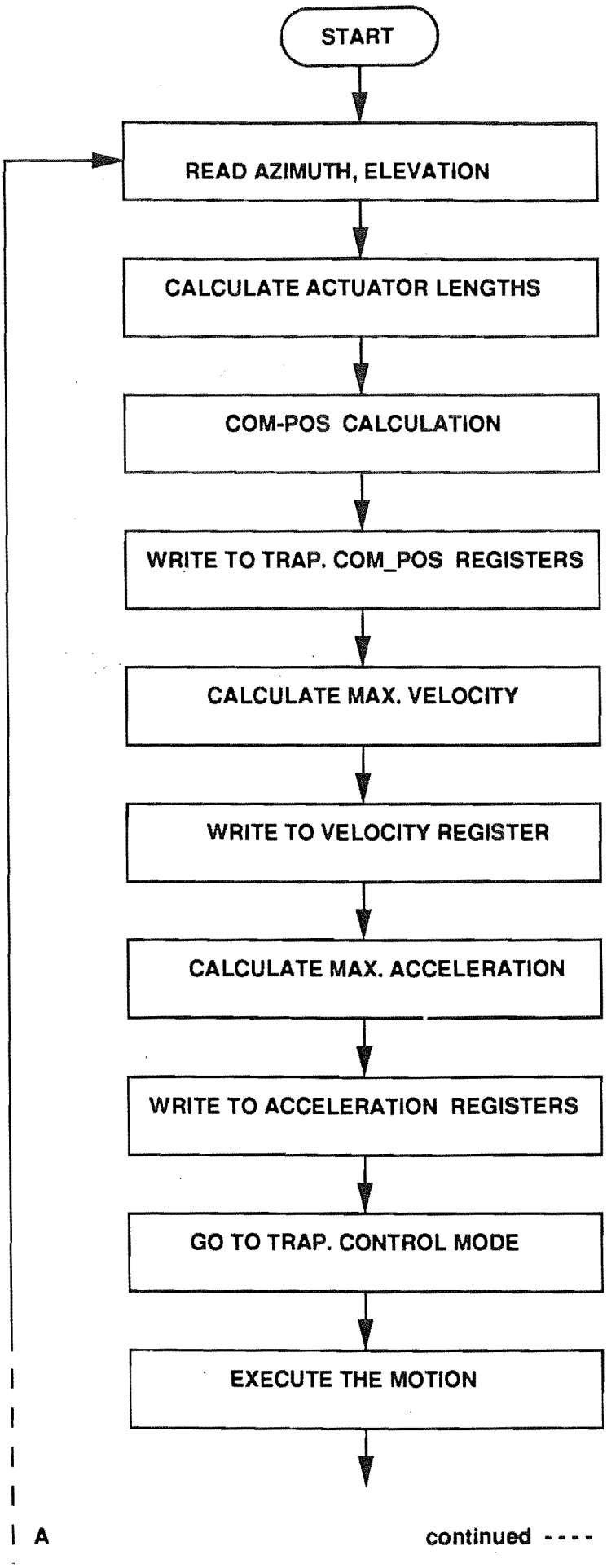
START
READ AZIMUTH, ELEVATION
CALCULATE ACTUATOR LENGTHS
COM-POS CALCULATION
WRITE TO TRAP. COM_POS REGISTERS
CALCULATE MAX. VELOCITY
WRITE TO VELOCITY REGISTER
CALCULATE MAX. ACCELERATION
WRITE TO ACCELERATION REGISTERS
GO TO TRAP. CONTROL MODE
EXECUTE THE MOTION
A
continued ----

continued from page 157

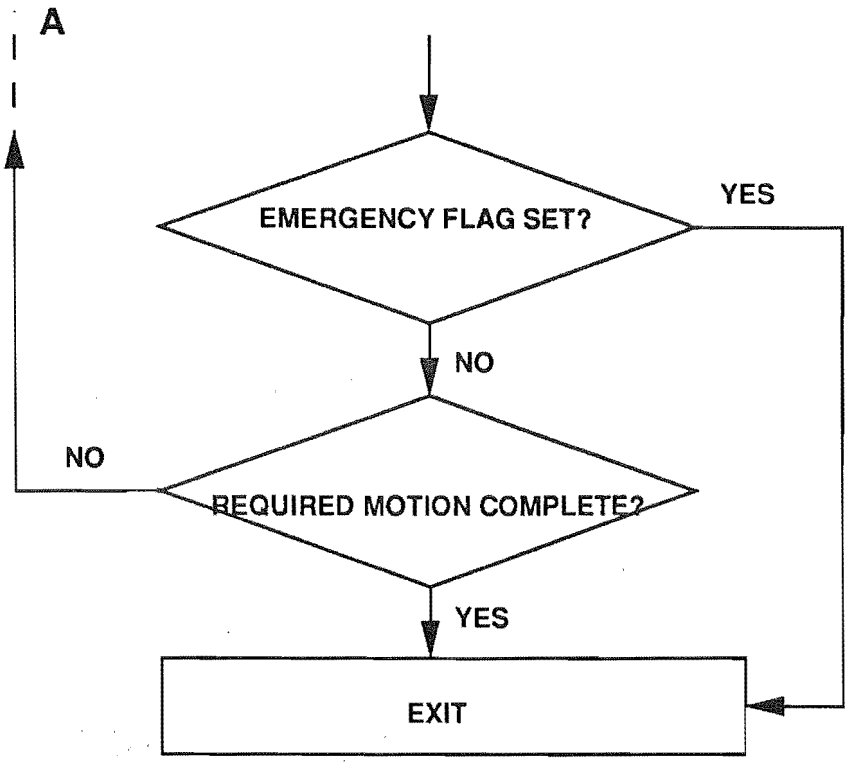

Fig. 5.21 Flowchart for executing motion in the trapezoidal control mode of the HCTL-1000

5.4.3 Library Routines

The main control programme and the simulation programme utilize various custom library routines to perform the vector arithmetic, vector transformations and various read and write operations to/from the HCTL-1000 registers. The related routines are grouped together and stored as library files.

5.5 PRETRACKING SETTING UP OF THE RSTP

After the RSTP mechanical parameters are selected and the HCTL-1000 motion control chips are configured, then the RSTP is ready for the pretracking setting up. In the pretracking setting up operation, the RSTP is driven to the 'HOME-POSITION'. In the 'HOME-POSITION' all the actuators will be set to identical lengths. This is achieved by driving all the actuators against stops to the minimum known positions. The position control mode is then used to drive each actuator up through a distance so that all actuators are of identical length. The actual position of each actuator is then set to zero mm at this position. The routine 'HOME-POSITION' in the main control programme performs this operation. From the 'HOME-POSITION' the RSTP is driven to the 'LOCK-POSITION'. This movement is performed by driving the actuators at high speeds to reduce the time taken to acquire the satellite. In the 'LOCK-POSITION' the satellite signal is received as it appears on the horizon. Once the satellite is acquired, the antenna follows the predicted path while avoiding all the singularity positions. Fig. 5.22 contains the flowchart describing the steps involved in the pretracking setting up of the RSTP.

5.6 SATELLITE TRACKING USING THE RSTP

A prototype RSTP based on the design described above was designed and built at the Department of Mechanical Engineering, University of Canterbury, Christchurch, New Zealand. A 1.8-m antenna dish was mounted on the platform. Fig. 5.23 shows the RSTP, the antenna dish and the control computer. The azimuth and elevation angle values given in Table 5.5 were used as satellite bearings and the tracking operation was performed. The RSTP was able to track both the low pass and high pass of the NOAA-7 satellite satisfactorily. Figures 5.24 and 5.25 show two extreme positions of

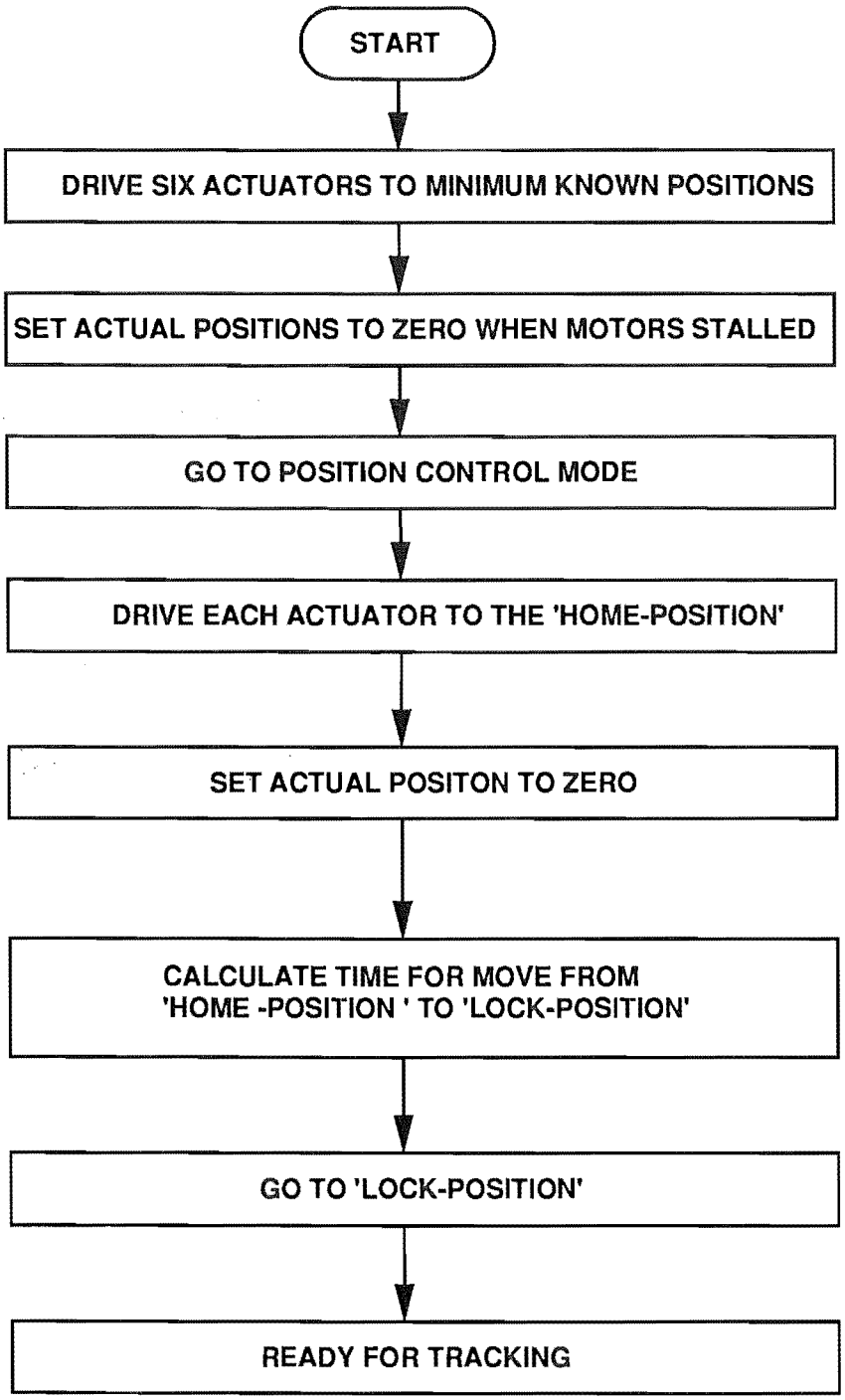

Fig. 5.22 Flowchart for pre-tracking setting up of the RSTP

Fig. 5.23 The RSTP antenna mount system designed and built at the University of Canterbury, New Zealand

the antenna mounted on the RSTP. Fig. 5.24 shows the antenna pointing to the horizon and Fig. 5.25 shows it moving through the zenith. The synchronized and smooth motion of the six actuators and the antenna proved the stability of the control system and verified the actuator length calculation algorithms. The low pass and high pass tracking ability established the correct design of the platform and base joints.

5.7 ADVANTAGES OF THE RSTP ANTENNA MOUNT

The advantages of using the RSTP for satellite tracking application are listed below.

1. The compact size, rigid structure and light weight construction makes this type of antenna mount ideal for marine application where there are severe restriction on available space and weight.

2. Manoeuvrability within the hemispherical range will allow large areas to be covered to maintain links with satellites at different latitudes and longitudes.

3. The pointing accuracy is extremely good, allowing the use of high gain, narrow beamwidth antenna.

4. The fast dynamic response means separate methods of platform stabilization are not required. This shows promise as a low cost terminal for small ships.

5. A microcomputer controlled mechanism makes the total operation fast. Electronic Beam Squinting can be incorporated for autotracking.

6. Closed linked structure will increase the wind pressure capabilities of the mount and help to maintain the pointing direction for a narrow beamwidth antenna.

5.8 PROGRAMME AND AUTOTRACKING MODES

In the prototype RSTP application a programme tracking method for pointing the antenna at the satellite has been used. The antenna is driven by the

Fig. 5.24 The antenna pointing to the horizon

Fig. 5.25 The antenna pointing to the Zenith

pointing information derived in advance from the predicted path of the satellite. Programme tracking is an open loop system and as such cannot detect a deviation of the actual orbit from the calculated one. Thus programme tracking has limitations when very high tracking accuracies are required for high gain, high frequency antennas.

In the autotracking systems, the transmission of the satellite is used to generate tracking error signals. The error signals control the antenna drive servo mechanism thus forming a closed loop system as described by the various autotracking methods discussed in chapter 2 (c.f. section 2.8). Electronic beam squirting (EBS) is the latest technique used for signal error detection. EBS can be employed to achieve the closed loop antenna drive system using the RSTP mount as discussed in the following section.

5.9 MARITIME APPLICATION OF THE RSTP

In the maritime satellite communication systems a stabilized platform is used to isolate the ship antenna from the dynamic motion of the ship. Various methods of passive and active stabilization have been discussed in Chapter 2. For smaller vessels requiring low cost terminal equipment, the cost of conventional stabilizing units may be too high. A combination of the microprocessor controlled RSTP and EBS would offer an ideal combination for a maritime tracking system (c.f. Afzulpurkar and Dunlop, 1989, Fig. 5.26). In the EBS system the error signal is sampled and the antenna position is updated at millisecond rates. The fast dynamic response of the RSTP system can compensate the ship motion and eliminate the requirement for a stabilized platform. Such a system offers good pointing accuracy enabling the use of a high gain antenna and full hemispherical coverage i.e. without any singularity positions. Thus the ship communication system will be able to maintain link with the satellites for elevation angles from 0^{o} to 90^{o} irrespective of the ship's position. Most present antenna mount systems exclude the polar regions from use and Alt-Azimuth systems experience difficulties in the equatorial regions.because of the keyhole problems (c.f. section 2.5.1).

In the maritime application of the RSTP, to update the antenna orientation at the required millisecond rates, use of faster computational platforms such as

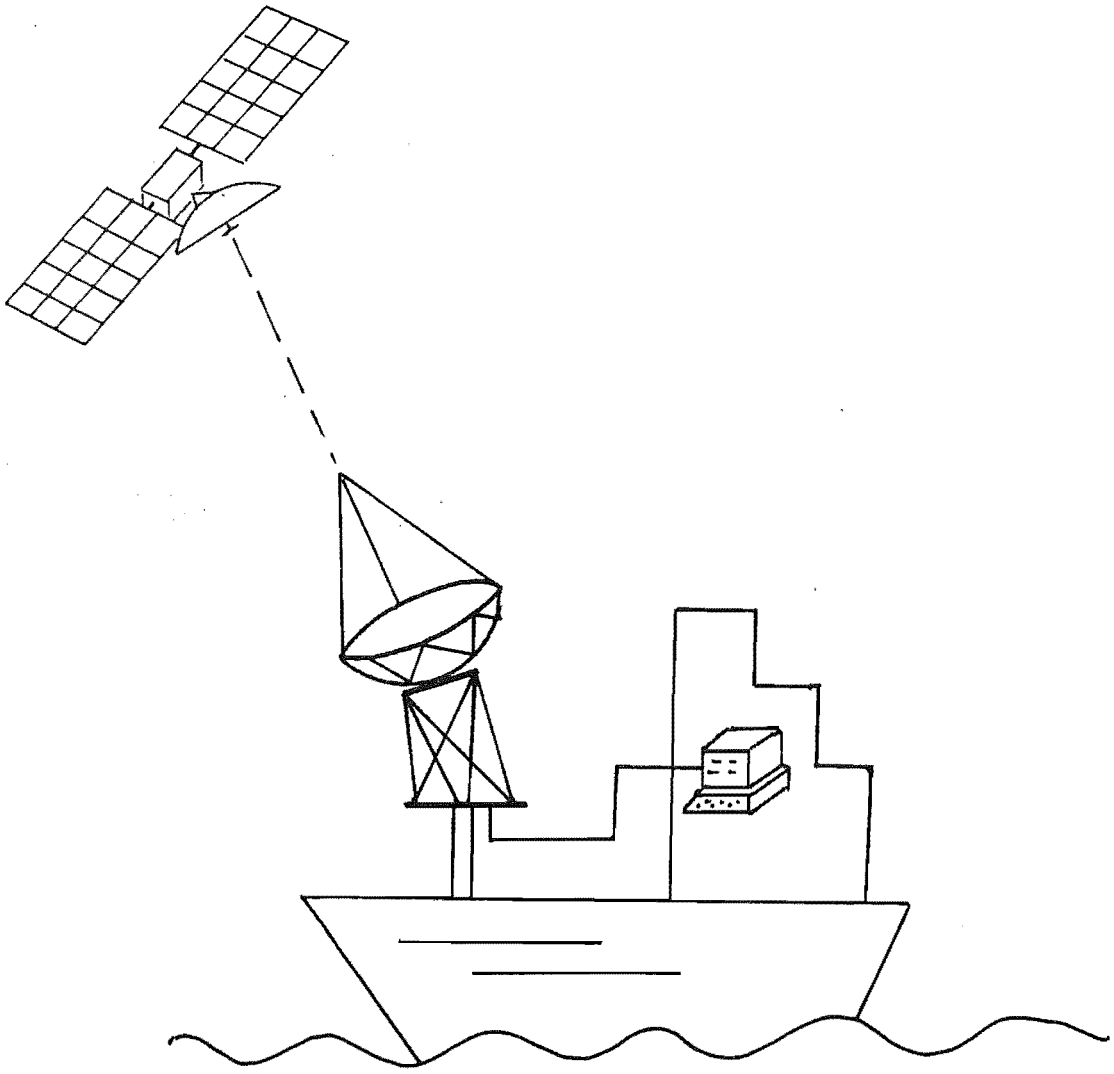

Fig. 5.26 Maritime application of the RSTP antenna mount

INTEL 80860 or special digital signal processing hardware such as TMS 320C30 is envisaged.

5.10 SUMMARY

The mechanical hardware required for building a prototype RSTP antenna mount was described in detail. The base joint and platform joint detailed construction was elaborated for achieving full hemispherical coverage. Various simulations done for achieving the optimum configuration of the RSTP were described. The logic behind the RSTP control software was explained with particular emphasis on the synchronized motion of all the six actuators. The pretracking setting up and actual satellite tracking procedures using RSTP were also explained. Successful tests have been conducted for tracking the motion of a weather satellite making a high pass or low pass. When combined with the EBS signal error detection technique, the RSTP shows potential as a low cost maritime satellite communication system. Other areas, where communication systems based on the RSTP principle can be effectively used, are suggested in the next chapter. A prototype RSTP antenna mount system was built at the Department of Mechanical Engineering, University of Canterbury, New Zealand to demonstrate the mount capabilities.

CHAPTER 6

CONCLUSIONS AND SUGGESTIONS FOR FURTHER RESEARCH

6.1 SUMMARY OF THE TECHNIQUES

A robotic manipulator with six degrees of freedom was designed, constructed and tested as a part of this thesis. The manipulator's closed kinematic link design was derived from the concept of the Stewart platform. The geometry and kinematics of such closed link manipulator offers many advantages over the conventional serial link open kinematic chain manipulators in many areas (c.f. section 3.3.1).

One such area of aplication was identified as an antenna mounting mechanism for satellite earth stations used to communicate with the fast moving orbiting satellites or space shuttles. Satellite communication using the present ground and ship based antenna mounting mechanisms suffer from various drawbacks (c.f. sections 2.5.1 and 2.5.2). The study of various design parameters affecting the performance of a satellite communication station suggested a need for an accurate, fast dynamic response, strong antenna mounting mechanism offering a contiuous tracking ability. Therefore the aformentioned robotic manipulator was developed for the satellite tracking application. The parallel link robotic manipulator consists of six linear actuators, connected in parallel, a moving platform and a fixed base. The six degrees of freedom result from in-parallel actuation of the six actuators. When an antenna dish is mounted on the platform, the antenna boresight axis can be aimed at the satellite by adjusting the actuator lengths.

The prototype manipulator design was selected after a detail study of the geometry and kinematics of various parallel link mechanisms. The kinematic analysis for the parallel manipulator consists of developing a set of kinematic equations for the six linear actuators in terms of the "world coordinates" (Φ , θ , α , x , y , z). These kinematic equations are then solved for the "machine coordinates" (L1,L2,L3,L4,L5,L6) which are the six actuator

lengths. The algorithin to achieve this inverse transformations from world to machine coordinates uses the rotational and translational transformations of a coordinate frame embedded in the platform with respect to the fixed frame embedded in the manipulator base (c.f. section 3.7). A computer programme generates a stream of machine coordinates in real time to drive the platform along the desired trajectory.

The control system designed for the simultaneous control of six axes involved addressing the problems of achieving maximum velocities and acceleration, sufficient speed resolution and high torques for the six drive motors. The synchronous multiple motor control was achieved by employing a separate 24-bit HCTL-1000 microprocessor for each axis running under the control of a host processor (Intel 80286) to provide central control over all axis processors and perform the real-time control task. The closed loop control system design required precise alignment of six optical incremental encoders on the six servomotor shafts and development of the interface circuitary with the processors. The development of operating software for the tracking application consisted of many routines written in Turbo Pascal. The software allows the user to configure the RSTP'S mechanical and control system parameters to suit the application. The software generation encompassed development of the complete software package, from calculating the 'look angle' data for a satellite to RSTP 'trajectory control'.

The mechanical design of the RSTP involved elaborate design of the base and platform joints. Various configurations of the base joint, platform joint and their relative positions were tried. The variable geometry configuration of the prototype RSTP set-up was used to establish relationships between the base and platform radii, various joint angles and the centre distance between the base and the platform (c.f. section 5.3.2.2). A simulation programme 'CHECKANT.PAS' has been developed to model the RSTP motion and select the optimum configuration for the required application.

6.2 SUMMARY OF THE RESULTS

A prototype antenna mounting system based on the theory described in the preceding section has been designed and constructed. A 1.8-m antenna dish was mounted on the platform and the orbital path of NOAA-7 weather

satellite was followed. Since the prototype was situated inside the laboratory and the antenna dish did not have any RF equipment, actual tracking and reception of signal from a satellite was not possible. Nevertheless, the path followed by the antenna dish has successfully demonstrated the use of RSTP as a novel antenna mount system. The design and interfacing of the multi-motor controller, based on the six Hewlett-Packard HCTL-1000 motion control chips, with the RSTP has been achieved. The operating software has successfully controlled the RSTP movement for the tracking operation. The six degrees of freedom of the mechanism has given the mount an ability to receive the satellite from horizon to horizon without any loss of the communication link because of keyhole problems. The use of incremental optical shaft encoders result in greater tracking precision to be achieved ($\simeq \pm 0.07^{o}$ for the prototype). The closed link antenna support structure results in a structurally stiff arrangement resulting in an improved ability to withstand wind.

In any robot work envelope, identification of the singular positions is important. The singular positions of the parallel mechanism used have been clearly identified (c.f.section 3.11.2.2). The combined rotational and translational transformation technique is used to circumvent the singular positions during the platform movement. A general method for the development of the stiffness matrix for the parallel mechanism is described.

The application of this antenna mount in a low cost marine satellite communication system is emphasized since the fast dynamic response of the system will eliminate the need for an expensive stabilized platform.

6.3 RSTP:OTHER APPLICATIONS

The use of satellite communication systems in remote areas is difficult because of the antenna alignment problems and power requirements. For remote land based site use, a portable communication system based on the RSTP can be employed (c.f. Dunlop, 1989). Such a portable system will consist of six identical actuators packed flat into a case, a folding antenna and a battery powered control computer. A self contained communication system can be developed by installing a small generator in a container. The

container top can serve as a base for mounting the actuators and the antenna.

Rapid deployment of the system would involve assembling the actuators and the antenna on the container top. Approximate alignment of the antenna is established by means of levelling and magnetic compass reading. The satellite emphemeris data, site longitude, latitude, elevations and magnetic deviation are entered in the control computer to generate the tracking data and to point the antenna at the satellite. Finally a local area search technique will lock on to the satellite and then follow the satellite path.

Such portable system can be effectively used at remote site developments or during civil defense emergencies to reestablish communications .

A stabilized platform on a ship, based on the RSTP principle can be employed as a landing platform for the helicopters and VTOL aircrafts. Such a platform offers a stable landing pad during rough weather conditions (c.f. Dunlop and Afzulpurkar, 1988).

RSTP can also be used as an airborne antenna mounting system on an aircraft provided sufficient space is available for the antenna to move outboard from the base as is required for avoiding the singular positions.

6.4 SUGGESTIONS FOR FURTHER RESEARCH

To overcome to limitations of programme tracking method, use of one of the autotracking methods has been suggested in combination with this novel mount design (section 5.8). A combination of the microprocessor controlled RSTP and satellite signal error detection using Electronic Beam Squinting has been suggested as an maritime satellite tracking system. To compensate the ship motion and eliminate the necessity of a stabilized platform, the error signal has to be sampled at millisecond rates, the machine coordinates (L1,L2,L3,L4,L5,L6) calculated within that time frame and the antenna position updated at millisecond rates. This will require the use of faster processors or special purpose digital signal processing hardware. Also the initial search and lock onto the satellite problem in the marine environment has to be addressed.

APPENDIX A

DEVELOPMENT OF THE STIFFNESS MATRIX

1 COMPATIBILITY MATRIX

McCallion (1973) has used a compatibility matrix to express the local displacements of the members of a structure in terms of the global displacements of the complete structure. The relationship is given as :

$$u_i = [C]\, U_i \qquad (1)$$

where u_i = local displacement matrix
U_i = global displacement matrix
[C] = compatibility matrix

For the development of the stiffnes matrix, the Stewart platform is treated as a structure. To simplify the analysis, three attachments points (A, B, C) are considered on the base and three (D, E, F) on the platform as shown in Fig. 1. As seen from Fig. 1, the base coordinate system XYZ and the platform coordinate system xyz coincide in the starting position.

The local displacements of the actuators from the position shown in Fig. 2 are represented by the vector:

$$u = [\delta L_1, \delta L_2, \delta L_3, \delta L_4, \delta L_5, \delta L_6]^T$$

or $u_i = [\delta L_i]^T \qquad i = 1..6$

The corrosponding global displacements of the platform are expressed as the vector:

$$U = [\delta x, \delta y, \delta z, \delta\Phi, \delta\theta, \delta\alpha]^T$$

where δx, δy, δz are the translations and $\delta\Phi$, $\delta\theta$, $\delta\alpha$ are the rotations about the X, Y and Z axes respectively.

If the rotational and translational displacements are small then equation (1) can be applied and the relationship between u_i and U can be expressed as:

$$[\delta L_1, \delta L_2, \delta L_3, \delta L_4, \delta L_5, \delta L6]^T = [C]\,[\delta x, \delta y, \delta z, \delta\Phi, \delta\theta, \delta\alpha]^T \quad (2)$$

Referring to Fig. 3, the change in the actuator length vector $\bar{L}_o$ is the vector $(\bar{L}_o - \bar{L}_n)$. This change has a component δL_o in the direction of $\bar{L}_o$. δL_o represents the magnitude of the change in the actuator length and can be expressed as:

$$\delta L_o = \frac{\bar{L}_o}{|\bar{L}_o|} \bullet (\bar{L}_o - \bar{L}_n) \quad (3)$$

where, $\frac{\bar{L}_o}{|\bar{L}_o|}$ is the unit vector in direction of $\bar{L}_o$.

Referring to Fig. 2.9 and Fig. 1, the coordinatres of the points A, B, C, D, E, F are written as follows:

A : (Rb/2, Rb/1.15, 0)
B : (Rb/2, - Rb/1.15, 0)
C : (- Rb, 0, 0)
D : (- Rb/2, Rb/1.15, 0)
E : (Rb, 0, 0)
F : (- Rb/2, - Rb/1.15, 0)

The platform coordinate system xyz is translated by a vector $\bar{T} = [0\ 0\ L]^T$ to arrive at the configuration shown in Fig.2. The rotation matrix R is an identity matrix.

Applying the transformation to $\bar{D}$, we get

$$\bar{D}' = \bar{T} + R\,\bar{D}$$

$$= \begin{bmatrix} 0 \\ 0 \\ L \end{bmatrix} + \begin{bmatrix} 1 & 0 & 0 \\ 0 & 1 & 0 \\ 0 & 0 & 1 \end{bmatrix} \begin{bmatrix} -Rb/2 \\ Rb/1.15 \\ 0 \end{bmatrix}$$

$$= \begin{bmatrix} Rb/2 \\ Rb/1.15 \\ L \end{bmatrix}$$

The rotations about the X, Y, Z axes are equivalent to a rotation about an arbitrary vector $\bar{a}$. When the rotations are sufficiently small, the differential rotation transform Rs is given by : (c.f. Paul, 1981)

$$Rs = \begin{bmatrix} 1 & -\delta\alpha & \delta\theta \\ \delta\alpha & 1 & -\delta\Phi \\ -\delta\theta & \delta\Phi & 1 \end{bmatrix}$$

where, $\delta\Phi$, $\delta\theta$ and $\delta\alpha$ are small rotations about an arbitrary vector $\bar{a}$.

Referring to Fig. 2,

$$\bar{L}_1 = \bar{D}' - \bar{A}$$
$$= [-Rb, 0, L]^T$$

Next, the platform coordinate system xyz is rotated through angles $\delta\Phi$, $\delta\theta$ and $\delta\alpha$ about the X, Y, Z axes respectively and translated by vector $\bar{T}s = [\delta x, \delta y, L + \delta z]^T$ as shown by dashed lines in Fig. 2.

Applying the transformation to $\bar{D}$, we get

$$\bar{D}'' = \bar{T}s + Rs\,\bar{D}$$

$$= \begin{bmatrix} \delta x \\ \delta y \\ L+\delta z \end{bmatrix} + \begin{bmatrix} 1 & -\delta\alpha & \delta\theta \\ \delta\alpha & 1 & -\delta\Phi \\ -\delta\theta & \delta\Phi & 1 \end{bmatrix} \begin{bmatrix} -Rb/2 \\ Rb/1.15 \\ 0 \end{bmatrix}$$

From Fig. 2,

$$\bar{L}_1' = \bar{D}'' - \bar{A}$$

$$\bar{L}_1' - \bar{L}_1 = \bar{D}'' - \bar{A} - \bar{D}' + \bar{A}$$
$$= \bar{D}'' - \bar{D}'$$

$$= \begin{bmatrix} -Rb\delta\alpha/1.15 + \delta x \\ -Rb\delta\alpha/2 + \delta y \\ Rb\delta\theta/2 + Rb\delta\Phi/1.15 + \delta z \end{bmatrix}$$

$$\bar{L}_1 \bullet (\bar{L}_1' - \bar{L}_1) = \begin{bmatrix} -Rb \\ 0 \\ L \end{bmatrix} \bullet \begin{bmatrix} -Rb\delta\alpha/1.15 + \delta x \\ -Rb\delta\alpha/2 + \delta y \\ Rb\delta\theta/2 + Rb\delta\Phi/1.15 + \delta z \end{bmatrix}$$

$$= \begin{bmatrix} Rb^2\delta\alpha/1.15 - Rb\,\delta x \\ 0 \\ RbL\delta\theta/2 + RbL\delta\Phi/1.15 + L\,\delta z \end{bmatrix}$$

Therefore $\delta L_1 = \frac{1}{L_o}$ [-Rb 0 L Rb L/1.15 RbL/2 Rb^2/1.15]

Where L_o is the length of the actuators in the position shown in the Fig. 2.

By repeating the procedure for actuators 2 to 6, the entire compatibility matrix [C] is obtained.

$$C = \begin{bmatrix} Rb & 0 & L & RbL/1.15 & RbL/2 & Rb^2/1.15 \\ Rb/2 & -Rb/1.15 & L & 0 & -RbL & -Rb^2/1.15 \\ Rb/2 & Rb/1.15 & L & 0 & -RbL & Rb^2/1.15 \\ -Rb & 0 & L & -RbL/1.15 & RbL/2 & -Rb^2/1.15 \\ Rb/2 & -Rb/1.15 & L & -RbL/1.15 & -RbL/2 & Rb^2/1.15 \\ Rb/2 & Rb/1.15 & L & RbL/1.15 & RbL/2 & -Rb^2/1.15 \end{bmatrix} \quad (4)$$

2 STIFFNESS MATRIX

2.1 Local Stiffness Matrix

If the six local coordinate axes are chosen along the six actuator axes, then the local stiffness matrix relating the actuator length changes to the actuator forces is given by :

$$[s] = K\,[I] \quad (5)$$

The above relation is true provided the forces in the actuators are purely axial and all the six actuators have equal stiffness K.

2.2 Global Stiffness Matrix

The global stiffness matrix [S] can be computed from the local stiffness matrix [s] by using the following relationship: (c.f. McCallion, 1973).

$$[S] = C^T [s] C \qquad (6)$$

Where C^T is the tranpose of the compatibility matrix C given by the equation (4).

Therefore from equations (4), (5) and (6), we get

$$S = \frac{K}{Lo^2} \begin{bmatrix} 3Rb^2 & 0 & 0 & 0 & 0 & 0 \\ 0 & 3Rb^2 & 0 & 0 & 0 & 0 \\ 0 & 0 & 6L^2 & 0 & 0 & 0 \\ 0 & 0 & 0 & 3Rb^2L^2 & 0 & 0 \\ 0 & 0 & 0 & 0 & 3Rb^2L^2 & 0 \\ 0 & 0 & 0 & 0 & 0 & 9Rb^4/2 \end{bmatrix} \qquad (7)$$

2.3 Stiffness Matrix for a general postion of the Stewart Platform

The procedure discussed in the sections 2.1 and 2.2 can be applied to develope the stiffness matrix for the Stewart platform in any position. In the following section, the stiffness matrix is developed for the platform configuration with:

$\Phi = 0^o, \theta = 60^o, \alpha = 0^o$

$x = L/2, y = 0, z = L/1.15$

The platform coordinate system xyz is transformed by a rotation matrix R and translated by a vector $\bar{T}$ to arrive at the position shown in Fig. 4. R is given by:

$$R = \begin{bmatrix} c60 & 0 & s60 \\ 0 & 1 & 0 \\ -s60 & 0 & c60 \end{bmatrix}$$

and $\quad \overline{T} = [L/2 \;\; 0 \;\; L/1.15]^T$

To simplify the expressions, L is expressed in terms of Rb, the relationship being L = 4 Rb.

Therefore $\overline{T}$ can be written as:

$$\overline{T} = [2Rb \;\; 0 \;\; 4Rb/1.15]^T$$

Referring to Fig. 4,

$$\overline{D}' = \overline{T} + R\,\overline{D}$$

$$= \begin{bmatrix} 2Rb \\ 0 \\ 4Rb/1.15 \end{bmatrix} + \begin{bmatrix} c60 & 0 & s60 \\ 0 & 1 & 0 \\ -s60 & 0 & c60 \end{bmatrix} \begin{bmatrix} -Rb/2 \\ Rb/1.15 \\ 0 \end{bmatrix}$$

$$= \begin{bmatrix} 7Rb/4 \\ Rb/1.15 \\ 9Rb/2.30 \end{bmatrix}$$

$$\overline{L_1}' = \overline{D}' - \overline{A}$$

$$= \begin{bmatrix} 5Rb/4 \\ 0 \\ 9Rb/2.30 \end{bmatrix}$$

Next the platform coordinate system is transformed by a rotation [Rs] [R] and translation $\overline{T}s = [\delta x, \delta y, L + \delta z]^T$ to arrive at the position shown by dashed lines in Fig. 4.

Therefore, $\bar{D}'' = \bar{T}s + [Rs][R]\bar{D}$

$$= \begin{bmatrix} -Rb\delta\alpha/1.15 + \delta x + Rb\,\delta\theta/2.30 \\ -Rb\delta\alpha/4 + \delta y - Rb\delta\Phi/2.30 \\ Rb\delta\theta/4 + Rb\delta\Phi/1.15 + \delta z \end{bmatrix}$$

$$\bar{L}_1' - \bar{L}_1 = \bar{D}'' - \bar{D}'$$

$$\bar{L}_1 \bullet (\bar{L}_1' - \bar{L}_1) = \begin{bmatrix} 5Rb/4 \\ 0 \\ 9Rb/2.30 \end{bmatrix} \bullet \begin{bmatrix} -Rb\delta\alpha/1.15 + \delta x + Rb\,\delta\theta/2.30 \\ -Rb\delta\alpha/4 + \delta y - Rb\delta\Phi/2.30 \\ Rb\delta\theta/4 + Rb\delta\Phi/1.15 + \delta z \end{bmatrix}$$

$$= \begin{bmatrix} 5Rb\delta x/4 + -5Rb^2\delta\alpha/4.6 + 5Rb^2\delta\theta/9.2 \\ 0 \\ 9Rb^2\delta\theta/9.2 + 9Rb^2\delta\Phi/2.7 + 9Rb\delta z/2.3 \end{bmatrix}$$

Therefore $\delta L_1 = \frac{1}{L_1} [\, 5Rb/4 \;\; 0 \;\; 9Rb/2.3 \;\; 9Rb^2/2.7 \;\; 7Rb^2/4.6 \;\; -5Rb^2/4.6 \,]$

Where L_1 is the length of actuator 1 in the position shown in Fig. 4.

By repeating the procedure for actuators 2 to 6, the entire compatibility matrix [C] is obtained.

C =

$$\begin{bmatrix} 5Rb/4L_1 & 0 & 9Rb/2.3L_1 & 9Rb^2/2.7L_1 & 7Rb^2/4.6L_1 & -5Rb^2/4.6L_1 \\ 2Rb/L_2 & -Rb/1.2 & 3Rb/1.2L_2 & -Rb^2/1.5L_2 & -7Rb^2/2.3L_2 & -Rb^2/2.3L_2 \\ 2Rb/L_2 & Rb/1.2 & 3Rb/1.2L_2 & Rb^2/1.5L_2 & -7Rb^2/2.3L_2 & 5Rb^2/2.3L_2 \\ 5Rb/4L_1 & 0 & 9Rb/2.3L_1 & -9Rb^2/2.7L_1 & 7Rb^2/4.6L_1 & 5Rb^2/4.6L_1 \\ 3Rb/4L_5 & -Rb/1.2L_5 & 9Rb/2.3L_5 & -8Rb^2/2.7L_5 & 3Rb^2/2.3L_5 & Rb^2/1.2L_5 \\ 3Rb/4L_5 & Rb/1.2L_5 & 9Rb/2.3L_5 & 8Rb^2/2.7L_5 & 3Rb^2/2.3L_5 & -Rb^2/1.2L_5 \end{bmatrix} \quad (8)$$

From the equations (5), (6) and (8) we can write

$$S = \frac{K}{Rb^2}\begin{bmatrix} s_{11}Rb^2 & 0 & s_{13}Rb^2 & 0 & s_{15}Rb^3 & 0 \\ 0 & s_{22}Rb^2 & 0 & s_{24}Rb^3 & 0 & s_{26}Rb^3 \\ s_{31}Rb^2 & 0 & s_{33}Rb^2 & 0 & s_{35}Rb^3 & 0 \\ 0 & s_{42}Rb^3 & 0 & s_{44}Rb^4 & 0 & s_{46}Rb^4 \\ s_{51}Rb^3 & 0 & s_{53}Rb^3 & 0 & s_{55}Rb^4 & 0 \\ 0 & s_{62}Rb^3 & 0 & s_{64}Rb^4 & 0 & s_{66}Rb^4 \end{bmatrix}$$

Where the coefficients s_{ij} are obtained by multiplying the constants in [C] and $[C^T]$.

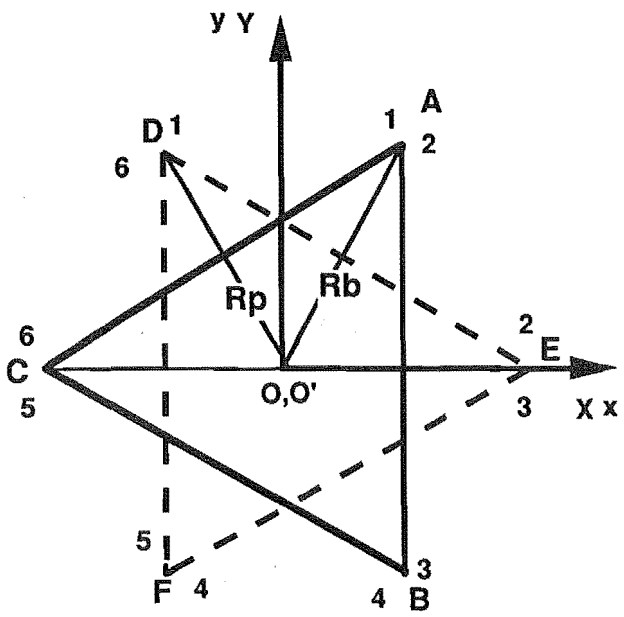

Fig. B The base and platform coordinate systems

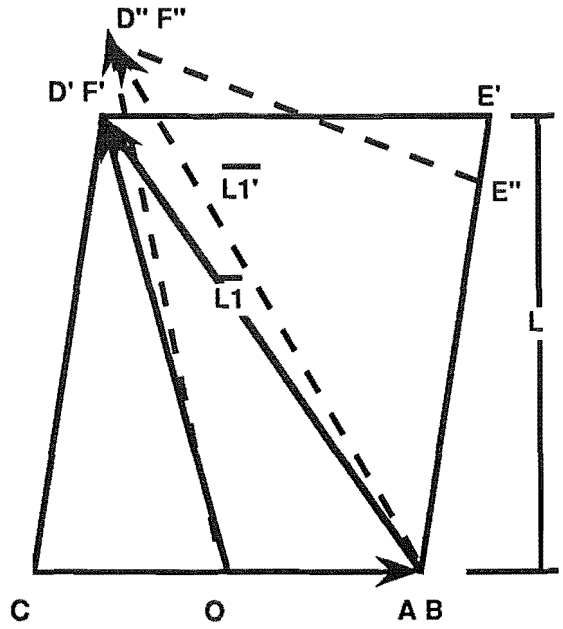

Fig. 2 Transformation of the platform coordinate system

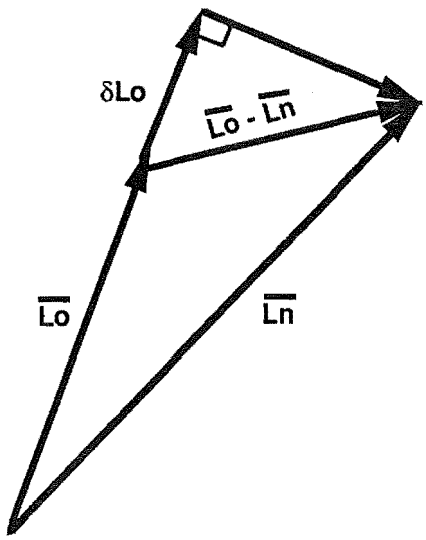

Fig. 3 Actuator length change

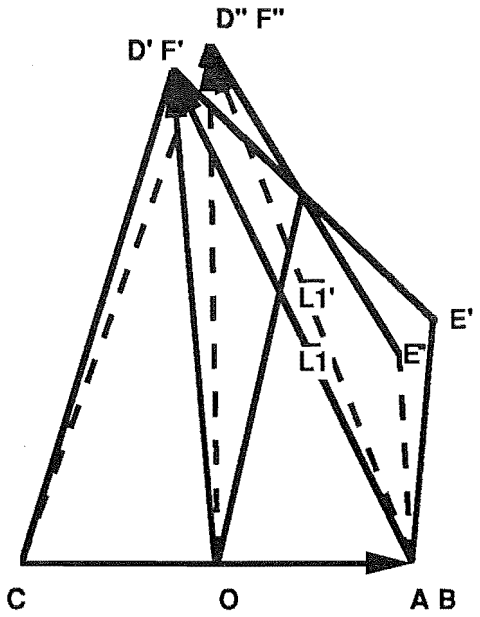

Fig. 4 Transformation of the platform coordinate system

APPENDIX B

Table B-1 Table showing the variation in the six actuator lengths for the mechanism with configuration Rb = 359.04 mm Rp = 239.50 mm L= 1250 mm $\theta \varepsilon (0^{\circ}, 90^{\circ})$, $\phi = 0^{\circ}$ and 180°

		Actuator length mm					
theta	phi	L1	L2	L3	L4	L5	L6
90.00	0.00	1261.73	963.22	963.22	1261.73	1601.55	1601.55
85.00	0.00	1263.12	977.24	977.24	1263.12	1587.50	1587.50
80.00	0.00	1264.51	991.85	991.85	1264.51	1572.86	1572.86
75.00	0.00	1265.90	1007.02	1007.02	1265.90	1557.65	1557.65
70.00	0.00	1267.28	1022.73	1022.73	1267.28	1541.90	1541.90
65.00	0.00	1268.63	1038.95	1038.95	1268.63	1525.64	1525.64
60.00	0.00	1269.95	1055.65	1055.65	1269.95	1508.89	1508.89
55.00	0.00	1271.23	1072.79	1072.79	1271.23	1491.68	1491.68
50.00	0.00	1272.47	1090.34	1090.34	1272.47	1474.04	1474.04
45.00	0.00	1273.66	1108.28	1108.28	1273.66	1456.01	1456.01
40.00	0.00	1274.78	1126.56	1126.56	1274.78	1437.60	1437.60
35.00	0.00	1275.84	1145.16	1145.16	1275.84	1418.86	1418.86
30.00	0.00	1276.83	1164.03	1164.03	1276.83	1399.82	1399.82
25.00	0.00	1277.74	1183.15	1183.15	1277.74	1380.50	1380.50
20.00	0.00	1278.57	1202.47	1202.47	1278.57	1360.95	1360.95
15.00	0.00	1279.32	1221.95	1221.95	1279.32	1341.19	1341.19
10.00	0.00	1279.98	1241.56	1241.56	1279.98	1321.26	1321.26
5.00	0.00	1280.55	1261.27	1261.27	1280.55	1301.20	1301.20
0.00	0.00	1281.03	1281.03	1281.03	1281.03	1281.03	1281.03
0.00	180.00	1281.03	1281.03	1281.03	1281.03	1281.03	1281.03
5.00	180.00	1281.42	1300.80	1300.80	1281.42	1260.80	1260.80
10.00	180.00	1281.71	1320.55	1320.55	1281.71	1240.53	1240.53
15.00	180.00	1281.91	1340.24	1340.24	1281.91	1220.27	1220.27
20.00	180.00	1282.02	1359.83	1359.83	1282.02	1200.06	1200.06
25.00	180.00	1282.04	1379.28	1379.28	1282.04	1179.92	1179.92
30.00	180.00	1281.97	1398.56	1398.56	1281.97	1159.89	1159.89
35.00	180.00	1281.81	1417.62	1417.62	1281.81	1140.02	1140.02
40.00	180.00	1281.58	1436.43	1436.43	1281.58	1120.33	1120.33
45.00	180.00	1281.27	1454.96	1454.96	1281.27	1100.86	1100.86
50.00	180.00	1280.88	1473.16	1473.16	1280.88	1081.66	1081.66
55.00	180.00	1280.43	1491.00	1491.00	1280.43	1062.75	1062.75
60.00	180.00	1279.92	1508.45	1508.45	1279.92	1044.18	1044.18
65.00	180.00	1279.34	1525.47	1525.47	1279.34	1025.98	1025.98
70.00	180.00	1278.72	1542.03	1542.03	1278.72	1008.19	1008.19
75.00	180.00	1278.06	1558.10	1558.10	1278.06	990.84	990.84
80.00	180.00	1277.36	1573.65	1573.65	1277.36	973.98	973.98
85.00	180.00	1276.64	1588.64	1588.64	1276.64	957.63	957.63
90.00	180.00	1275.89	1603.04	1603.04	1275.89	941.85	941.85

Lmax = 1603.04 mm Lmin = 941.85 mm Expansion ratio = 1.70

Table B-2 Table showing the variation in the six actuator lengths for the mechanism with configuration Rb = 296.54 mm Rp = 239.50 mm L= 1250 mm $\theta \varepsilon (0^{\circ}, 90^{\circ})$, $\phi = 0^{\circ}$ and 180°

		Actuator lenght mm					
theta	phi	L1	L2	L3	L4	L5	L6
90.00	0.00	1276.46	971.22	971.22	1276.46	1553.10	1553.10
85.00	0.00	1276.61	984.52	984.52	1276.61	1540.66	1540.66
80.00	0.00	1276.72	998.38	998.38	1276.72	1527.70	1527.70
75.00	0.00	1276.80	1012.76	1012.76	1276.80	1514.25	1514.25
70.00	0.00	1276.84	1027.63	1027.63	1276.84	1500.32	1500.32
65.00	0.00	1276.83	1042.97	1042.97	1276.83	1485.95	1485.95
60.00	0.00	1276.77	1058.76	1058.76	1276.77	1471.16	1471.16
55.00	0.00	1276.65	1074.96	1074.96	1276.65	1455.97	1455.97
50.00	0.00	1276.47	1091.53	1091.53	1276.47	1440.41	1440.41
45.00	0.00	1276.24	1108.45	1108.45	1276.24	1424.51	1424.51
40.00	0.00	1275.94	1125.69	1125.69	1275.94	1408.30	1408.30
35.00	0.00	1275.57	1143.22	1143.22	1275.57	1391.81	1391.81
30.00	0.00	1275.13	1160.99	1160.99	1275.13	1375.06	1375.06
25.00	0.00	1274.62	1178.98	1178.98	1274.62	1358.09	1358.09
20.00	0.00	1274.03	1197.16	1197.16	1274.03	1340.93	1340.93
15.00	0.00	1273.38	1215.48	1215.48	1273.38	1323.60	1323.60
10.00	0.00	1272.65	1233.91	1233.91	1272.65	1306.15	1306.15
5.00	0.00	1271.84	1252.42	1252.42	1271.84	1288.59	1288.59
0.00	0.00	1270.97	1270.97	1270.97	1270.97	1270.97	1270.97
0.00	180.00	1270.97	1270.97	1270.97	1270.97	1270.97	1270.97
5.00	180.00	1270.02	1289.52	1289.52	1270.02	1253.31	1253.31
10.00	180.00	1269.00	1308.05	1308.05	1269.00	1235.64	1235.64
15.00	180.00	1267.92	1326.51	1326.51	1267.92	1218.01	1218.01
20.00	180.00	1266.77	1344.87	1344.87	1266.77	1200.44	1200.44
25.00	180.00	1265.56	1363.10	1363.10	1265.56	1182.95	1182.95
30.00	180.00	1264.30	1381.15	1381.15	1264.30	1165.60	1165.60
35.00	180.00	1262.98	1399.00	1399.00	1262.98	1148.41	1148.41
40.00	180.00	1261.61	1416.61	1416.61	1261.61	1131.40	1131.40
45.00	180.00	1260.20	1433.94	1433.94	1260.20	1114.62	1114.62
50.00	180.00	1258.76	1450.97	1450.97	1258.76	1098.09	1098.09
55.00	180.00	1257.28	1467.66	1467.66	1257.28	1081.86	1081.86
60.00	180.00	1255.78	1483.97	1483.97	1255.78	1065.94	1065.94
65.00	180.00	1254.27	1499.89	1499.89	1254.27	1050.37	1050.37
70.00	180.00	1252.74	1515.37	1515.37	1252.74	1035.19	1035.19
75.00	180.00	1251.21	1530.38	1530.38	1251.21	1020.42	1020.42
80.00	180.00	1249.68	1544.91	1544.91	1249.68	1006.09	1006.09
85.00	180.00	1248.17	1558.91	1558.91	1248.17	992.23	992.23
90.00	180.00	1246.67	1572.36	1572.36	1246.67	978.88	978.88

Lmax = 1572.36 mm Lmin = 978.88 mm Expansion ratio = 1.60

Table B-3 Table showing the variation in the six actuator lengths for the mechanism with configuration Rb = 359.04 mm Rp = 239.50 mm L= 1500 mm
$\theta = 75^{\circ}$, $\phi \in (0^{\circ}, 360^{\circ})$

		Actuator length mm					
theta	phi	L1	L2	L3	L4	L5	L6
75.00	0.00	1512.26	1249.09	1249.09	1512.26	1805.06	1805.06
75.00	3.00	1494.81	1240.82	1258.07	1529.75	1813.34	1796.01
75.00	6.00	1477.46	1233.25	1267.72	1547.23	1820.82	1786.21
75.00	9.00	1460.25	1226.43	1278.02	1564.65	1827.49	1775.71
75.00	12.00	1443.25	1220.35	1288.94	1581.95	1833.32	1764.53
75.00	15.00	1426.49	1215.05	1300.47	1599.10	1838.28	1752.69
75.00	18.00	1410.03	1210.53	1312.58	1616.02	1842.37	1740.25
75.00	21.00	1393.92	1206.81	1325.23	1632.68	1845.57	1727.24
75.00	24.00	1378.20	1203.90	1338.40	1649.03	1847.87	1713.68
75.00	27.00	1362.92	1201.82	1352.06	1665.01	1849.26	1699.63
75.00	30.00	1348.12	1200.57	1366.18	1680.58	1849.74	1685.13
75.00	33.00	1333.85	1200.16	1380.71	1695.70	1849.29	1670.20
75.00	36.00	1320.14	1200.61	1395.64	1710.32	1847.92	1654.91
75.00	39.00	1307.04	1201.90	1410.92	1724.40	1845.63	1639.29
75.00	42.00	1294.57	1204.05	1426.51	1737.89	1842.43	1623.39
75.00	45.00	1282.78	1207.06	1442.38	1750.76	1838.32	1607.24
75.00	48.00	1271.68	1210.93	1458.49	1762.97	1833.31	1590.90
75.00	51.00	1261.32	1215.64	1474.79	1774.50	1827.42	1574.41
75.00	54.00	1251.71	1221.21	1491.26	1785.29	1820.65	1557.81
75.00	57.00	1242.87	1227.61	1507.83	1795.33	1813.04	1541.15
75.00	60.00	1234.83	1234.83	1524.48	1804.59	1804.59	1524.48
75.00	63.00	1227.61	1242.87	1541.15	1813.04	1795.33	1507.83
75.00	66.00	1221.21	1251.71	1557.81	1820.65	1785.29	1491.26
75.00	69.00	1215.64	1261.32	1574.41	1827.42	1774.50	1474.79
75.00	72.00	1210.93	1271.68	1590.90	1833.31	1762.97	1458.49
75.00	75.00	1207.06	1282.78	1607.24	1838.32	1750.76	1442.38
75.00	78.00	1204.05	1294.57	1623.39	1842.43	1737.89	1426.51
75.00	81.00	1201.90	1307.04	1639.29	1845.63	1724.40	1410.92
75.00	84.00	1200.61	1320.14	1654.91	1847.92	1710.32	1395.64
75.00	87.00	1200.16	1333.85	1670.20	1849.29	1695.70	1380.71
75.00	90.00	1200.57	1348.12	1685.13	1849.74	1680.58	1366.18
75.00	93.00	1201.82	1362.92	1699.63	1849.26	1665.01	1352.06
75.00	96.00	1203.90	1378.20	1713.68	1847.87	1649.03	1338.40
75.00	99.00	1206.81	1393.92	1727.24	1845.57	1632.68	1325.23
75.00	102.00	1210.53	1410.03	1740.25	1842.37	1616.02	1312.58
75.00	105.00	1215.05	1426.49	1752.69	1838.28	1599.10	1300.47
75.00	108.00	1220.35	1443.25	1764.53	1833.32	1581.95	1288.94
75.00	111.00	1226.43	1460.25	1775.71	1827.49	1564.65	1278.02
75.00	114.00	1233.25	1477.46	1786.21	1820.82	1547.23	1267.72
75.00	117.00	1240.82	1494.81	1796.01	1813.34	1529.75	1258.07
75.00	120.00	1249.09	1512.26	1805.06	1805.06	1512.26	1249.09
75.00	123.00	1258.07	1529.75	1813.34	1796.01	1494.81	1240.82
75.00	126.00	1267.72	1547.23	1820.82	1786.21	1477.46	1233.25
75.00	129.00	1278.02	1564.65	1827.49	1775.71	1460.25	1226.43
75.00	132.00	1288.94	1581.95	1833.32	1764.53	1443.25	1220.35
75.00	135.00	1300.47	1599.10	1838.28	1752.69	1426.49	1215.05
75.00	138.00	1312.58	1616.02	1842.37	1740.25	1410.03	1210.53
75.00	141.00	1325.23	1632.68	1845.57	1727.24	1393.92	1206.81
75.00	144.00	1338.40	1649.03	1847.87	1713.68	1378.20	1203.90

continued

continued from page 184

75.00	147.00	1352.06	1665.01	1849.26	1699.63	1362.92	1201.82
75.00	150.00	1366.18	1680.58	1849.74	1685.13	1348.12	1200.57
75.00	153.00	1380.71	1695.70	1849.29	1670.20	1333.85	1200.16
75.00	156.00	1395.64	1710.32	1847.92	1654.91	1320.14	1200.61
75.00	159.00	1410.92	1724.40	1845.63	1639.29	1307.04	1201.90
75.00	162.00	1426.51	1737.89	1842.43	1623.39	1294.57	1204.05
75.00	165.00	1442.38	1750.76	1838.32	1607.24	1282.78	1207.06
75.00	168.00	1458.49	1762.97	1833.31	1590.90	1271.68	1210.93
75.00	171.00	1474.79	1774.50	1827.42	1574.41	1261.32	1215.64
75.00	174.00	1491.26	1785.29	1820.65	1557.81	1251.71	1221.21
75.00	177.00	1507.83	1795.33	1813.04	1541.15	1242.87	1227.61
75.00	180.00	1524.48	1804.59	1804.59	1524.48	1234.83	1234.83
75.00	183.00	1541.15	1813.04	1795.33	1507.83	1227.61	1242.87
75.00	186.00	1557.81	1820.65	1785.29	1491.26	1221.21	1251.71
75.00	189.00	1574.41	1827.42	1774.50	1474.79	1215.64	1261.32
75.00	192.00	1590.90	1833.31	1762.97	1458.49	1210.93	1271.68
75.00	195.00	1607.24	1838.32	1750.76	1442.38	1207.06	1282.78
75.00	198.00	1623.39	1842.43	1737.89	1426.51	1204.05	1294.57
75.00	201.00	1639.29	1845.63	1724.40	1410.92	1201.90	1307.04
75.00	204.00	1654.91	1847.92	1710.32	1395.64	1200.61	1320.14
75.00	207.00	1670.20	1849.29	1695.70	1380.71	1200.16	1333.85
75.00	210.00	1685.13	1849.74	1680.58	1366.18	1200.57	1348.12
75.00	213.00	1699.63	1849.26	1665.01	1352.06	1201.82	1362.92
75.00	216.00	1713.68	1847.87	1649.03	1338.40	1203.90	1378.20
75.00	219.00	1727.24	1845.57	1632.68	1325.23	1206.81	1393.92
75.00	222.00	1740.25	1842.37	1616.02	1312.58	1210.53	1410.03
75.00	225.00	1752.69	1838.28	1599.10	1300.47	1215.05	1426.49
75.00	228.00	1764.53	1833.32	1581.95	1288.94	1220.35	1443.25
75.00	231.00	1775.71	1827.49	1564.65	1278.02	1226.43	1460.25
75.00	234.00	1786.21	1820.82	1547.23	1267.72	1233.25	1477.46
75.00	237.00	1796.01	1813.34	1529.75	1258.07	1240.82	1494.81
75.00	240.00	1805.06	1805.06	1512.26	1249.09	1249.09	1512.26
75.00	243.00	1813.34	1796.01	1494.81	1240.82	1258.07	1529.75
75.00	246.00	1820.82	1786.21	1477.46	1233.25	1267.72	1547.23
75.00	249.00	1827.49	1775.71	1460.25	1226.43	1278.02	1564.65
75.00	252.00	1833.32	1764.53	1443.25	1220.35	1288.94	1581.95
75.00	255.00	1838.28	1752.69	1426.49	1215.05	1300.47	1599.10
75.00	258.00	1842.37	1740.25	1410.03	1210.53	1312.58	1616.02
75.00	261.00	1845.57	1727.24	1393.92	1206.81	1325.23	1632.68
75.00	264.00	1847.87	1713.68	1378.20	1203.90	1338.40	1649.03
75.00	267.00	1849.26	1699.63	1362.92	1201.82	1352.06	1665.01
75.00	270.00	1849.74	1685.13	1348.12	1200.57	1366.18	1680.58
75.00	273.00	1849.29	1670.20	1333.85	1200.16	1380.71	1695.70
75.00	276.00	1847.92	1654.91	1320.14	1200.61	1395.64	1710.32
75.00	279.00	1845.63	1639.29	1307.04	1201.90	1410.92	1724.40
75.00	282.00	1842.43	1623.39	1294.57	1204.05	1426.51	1737.89
75.00	285.00	1838.32	1607.24	1282.78	1207.06	1442.38	1750.76
75.00	288.00	1833.31	1590.90	1271.68	1210.93	1458.49	1762.97
75.00	291.00	1827.42	1574.41	1261.32	1215.64	1474.79	1774.50
75.00	294.00	1820.65	1557.81	1251.71	1221.21	1491.26	1785.29
75.00	297.00	1813.04	1541.15	1242.87	1227.61	1507.83	1795.33
75.00	300.00	1804.59	1524.48	1234.83	1234.83	1524.48	1804.59

continued

continued from page 185

75.00	303.00	1795.33	1507.83	1227.61	1242.87	1541.15	1813.04
75.00	306.00	1785.29	1491.26	1221.21	1251.71	1557.81	1820.65
75.00	309.00	1774.50	1474.79	1215.64	1261.32	1574.41	1827.42
75.00	312.00	1762.97	1458.49	1210.93	1271.68	1590.90	1833.31
75.00	315.00	1750.76	1442.38	1207.06	1282.78	1607.24	1838.32
75.00	318.00	1737.89	1426.51	1204.05	1294.57	1623.39	1842.43
75.00	321.00	1724.40	1410.92	1201.90	1307.04	1639.29	1845.63
75.00	324.00	1710.32	1395.64	1200.61	1320.14	1654.91	1847.92
75.00	327.00	1695.70	1380.71	1200.16	1333.85	1670.20	1849.29
75.00	330.00	1680.58	1366.18	1200.57	1348.12	1685.13	1849.74
75.00	333.00	1665.01	1352.06	1201.82	1362.92	1699.63	1849.26
75.00	336.00	1649.03	1338.40	1203.90	1378.20	1713.68	1847.87
75.00	339.00	1632.68	1325.23	1206.81	1393.92	1727.24	1845.57
75.00	342.00	1616.02	1312.58	1210.53	1410.03	1740.25	1842.37
75.00	345.00	1599.10	1300.47	1215.05	1426.49	1752.69	1838.28
75.00	348.00	1581.95	1288.94	1220.35	1443.25	1764.53	1833.32
75.00	351.00	1564.65	1278.02	1226.43	1460.25	1775.71	1827.49
75.00	354.00	1547.23	1267.72	1233.25	1477.46	1786.21	1820.82
75.00	357.00	1529.75	1258.07	1240.82	1494.81	1796.01	1813.34
75.00	359.99	1512.31	1249.12	1249.07	1512.20	1805.03	1805.09

Lmax = 1849.74 Lmin = 1200.16 mm Expansion ratio = 1.54

Table B-4 Table showing the variation in the angle Ψ_{ij} for the mechanism with configuration Rb = 359.04 mm Rp = 239.50 mm L= 1500mm $\theta \varepsilon (0^{\circ}, 90^{\circ})$, $\phi = 0^{\circ}$ and 180°

theta	phi	Ψ_{16}	Ψ_{23}	Ψ_{45}
90.00	0.00	15.28	26.87	15.28
85.00	0.00	15.73	26.55	15.73
80.00	0.00	16.17	26.22	16.17
75.00	0.00	16.60	25.89	16.60
70.00	0.00	17.02	25.56	17.02
65.00	0.00	17.43	25.23	17.43
60.00	0.00	17.83	24.90	17.83
55.00	0.00	18.21	24.56	18.21
50.00	0.00	18.58	24.23	18.58
45.00	0.00	18.93	23.90	18.93
40.00	0.00	19.26	23.57	19.26
35.00	0.00	19.57	23.25	19.57
30.00	0.00	19.86	22.93	19.86
25.00	0.00	20.13	22.62	20.13
20.00	0.00	20.38	22.31	20.38
15.00	0.00	20.60	22.00	20.60
10.00	0.00	20.81	21.71	20.81
5.00	0.00	20.98	21.42	20.98
0.00	0.00	21.14	21.14	21.14
0.00	180.00	21.14	21.14	21.14
5.00	180.00	21.26	20.86	21.26
10.00	180.00	21.36	20.59	21.36
15.00	180.00	21.44	20.33	21.44
20.00	180.00	21.48	20.08	21.48
25.00	180.00	21.50	19.84	21.50
30.00	180.00	21.49	19.60	21.49
35.00	180.00	21.45	19.37	21.45
40.00	180.00	21.38	19.15	21.38
45.00	180.00	21.29	18.94	21.29
50.00	180.00	21.16	18.74	21.16
55.00	180.00	21.01	18.54	21.01
60.00	180.00	20.82	18.35	20.82
65.00	180.00	20.61	18.18	20.61
70.00	180.00	20.37	18.01	20.37
75.00	180.00	20.10	17.84	20.10
80.00	180.00	19.81	17.69	19.81
85.00	180.00	19.49	17.54	19.49
90.00	180.00	19.15	17.40	19.15

Table B-5 Table showing the variation in the angle γ_i for the mechanism with configuration Rb = 359.04 mm Rp = 239.50 mm L= 1500mm $\theta \varepsilon (0^{\circ}, 90^{\circ})$, $\phi = 0^{\circ}$ and 180°

theta	phi	γ_1	γ_2	γ_3	γ_4	γ_5	γ_6
90.00	0.00	81.72	83.01	76.57	76.57	81.72	83.01
85.00	0.00	81.49	82.79	76.73	76.73	81.49	82.79
80.00	0.00	81.27	82.57	76.89	76.89	81.27	82.57
75.00	0.00	81.06	82.34	77.05	77.05	81.06	82.34
70.00	0.00	80.85	82.12	77.22	77.22	80.85	82.12
65.00	0.00	80.66	81.90	77.39	77.39	80.66	81.90
60.00	0.00	80.49	81.68	77.55	77.55	80.49	81.68
55.00	0.00	80.32	81.47	77.72	77.72	80.32	81.47
50.00	0.00	80.17	81.25	77.89	77.89	80.17	81.25
45.00	0.00	80.03	81.05	78.05	78.05	80.03	81.05
40.00	0.00	79.90	80.84	78.21	78.21	79.90	80.84
35.00	0.00	79.79	80.64	78.38	78.38	79.79	80.64
30.00	0.00	79.69	80.45	78.53	78.53	79.69	80.45
25.00	0.00	79.61	80.26	78.69	78.69	79.61	80.26
20.00	0.00	79.54	80.08	78.85	78.85	79.54	80.08
15.00	0.00	79.49	79.90	79.00	79.00	79.49	79.90
10.00	0.00	79.46	79.74	79.15	79.15	79.46	79.74
5.00	0.00	79.44	79.58	79.29	79.29	79.44	79.58
0.00	0.00	79.43	79.43	79.43	79.43	79.43	79.43
0.00	180.00	79.43	79.43	79.43	79.43	79.43	79.43
5.00	180.00	79.44	79.29	79.57	79.57	79.44	79.29
10.00	180.00	79.47	79.17	79.70	79.70	79.47	79.17
15.00	180.00	79.51	79.05	79.83	79.83	79.51	79.05
20.00	180.00	79.57	78.95	79.96	79.96	79.57	78.95
25.00	180.00	79.64	78.86	80.08	80.08	79.64	78.86
30.00	180.00	79.73	78.78	80.20	80.20	79.73	78.78
35.00	180.00	79.83	78.72	80.31	80.31	79.83	78.72
40.00	180.00	79.95	78.67	80.42	80.42	79.95	78.67
45.00	180.00	80.08	78.63	80.53	80.53	80.08	78.63
50.00	180.00	80.22	78.61	80.63	80.63	80.22	78.61
55.00	180.00	80.38	78.61	80.73	80.73	80.38	78.61
60.00	180.00	80.55	78.62	80.82	80.82	80.55	78.62
65.00	180.00	80.74	78.65	80.91	80.91	80.74	78.65
70.00	180.00	80.93	78.70	81.00	81.00	80.93	78.70
75.00	180.00	81.13	78.76	81.08	81.08	81.13	78.76
80.00	180.00	81.35	78.84	81.16	81.16	81.35	78.84
85.00	180.00	81.57	78.94	81.23	81.23	81.57	78.94
90.00	180.00	81.80	79.05	81.30	81.30	81.80	79.05

Table B-6 Table showing the variation in the angle μi for the mechanism with configuration Rb = 359.04 mm Rp = 239.50 mm L= 1500mm θ ε (0°, 90°) , ϕ = 0° and 180°

theta	phi	μ1	μ2	μ3	μ4	μ5	μ6
90.00	0.00	51.49	42.97	42.97	51.49	39.66	39.66
85.00	0.00	54.24	45.36	45.36	54.24	41.88	41.88
80.00	0.00	56.98	47.75	47.75	56.98	44.11	44.11
75.00	0.00	59.70	50.13	50.13	59.70	46.33	46.33
70.00	0.00	62.40	52.50	52.50	62.40	48.56	48.56
65.00	0.00	65.08	54.87	54.87	65.08	50.79	50.79
60.00	0.00	67.73	57.22	57.22	67.73	53.03	53.03
55.00	0.00	70.35	59.56	59.56	70.35	55.26	55.26
50.00	0.00	72.93	61.87	61.87	72.93	57.50	57.50
45.00	0.00	75.46	64.16	64.16	75.46	59.74	59.74
40.00	0.00	77.93	66.41	66.41	77.93	61.98	61.98
35.00	0.00	80.28	68.61	68.61	80.28	64.22	64.22
30.00	0.00	82.44	70.74	70.74	82.44	66.46	66.46
25.00	0.00	84.21	72.77	72.77	84.21	68.69	68.69
20.00	0.00	85.16	74.67	74.67	85.16	70.91	70.91
15.00	0.00	84.86	76.38	76.38	84.86	73.11	73.11
10.00	0.00	83.49	77.82	77.82	83.49	75.28	75.28
5.00	0.00	81.57	78.87	78.87	81.57	77.40	77.40
0.00	0.00	79.42	79.42	79.42	79.42	79.42	79.42
0.00	180.00	79.42	79.42	79.42	79.42	79.42	79.42
5.00	180.00	77.15	79.39	79.39	77.15	81.27	81.27
10.00	180.00	74.83	78.79	78.79	74.83	82.81	82.81
15.00	180.00	72.49	77.70	77.70	72.49	83.78	83.78
20.00	180.00	70.14	76.23	76.23	70.14	83.89	83.89
25.00	180.00	67.79	74.49	74.49	67.79	83.08	83.08
30.00	180.00	65.44	72.56	72.56	65.44	81.60	81.60
35.00	180.00	63.10	70.49	70.49	63.10	79.72	79.72
40.00	180.00	60.77	68.33	68.33	60.77	77.61	77.61
45.00	180.00	58.45	66.11	66.11	58.45	75.35	75.35
50.00	180.00	56.15	63.82	63.82	56.15	73.01	73.01
55.00	180.00	53.85	61.50	61.50	53.85	70.59	70.59
60.00	180.00	51.57	59.15	59.15	51.57	68.12	68.12
65.00	180.00	49.30	56.77	56.77	49.30	65.61	65.61
70.00	180.00	47.05	54.38	54.38	47.05	63.05	63.05
75.00	180.00	44.81	51.97	51.97	44.81	60.46	60.46
80.00	180.00	42.58	49.54	49.54	42.58	57.84	57.84
85.00	180.00	40.36	47.10	47.10	40.36	55.18	55.18
90.00	180.00	38.16	44.66	44.66	38.16	52.49	52.49

REFERENCES

Afzulpurkar, N.V., Dunlop, G.R., Ma Li, Johnson, G.R. (1988) "Design of parallel link robot", Proc. of NELCON Conf., Christchurch, August 1988, New Zealand, pp. 52-58.

Afzulpurkar, N.V., Dunlop, G.R. (1989) "Application of parallel link mechanism for satellite tracking system", Proc. NELCON Conf., Wellington, August 1989, New Zealand, pp. 192-197.

Afzulpurkar, N.V., Dunlop G.R. (1989) "A novel antenna mount for orbital satellite tracking and marine communications", Proc. Fifth National Space Engineering Symposium, Canberra, November 1989, Australia, pp 92-96.

Ardayfio, D.D. (1987) Fundamentals of Robotics. Marcel Dekker, Inc. Michigan, U.S.A.

Brooks, C.W. (1973) "Operational shipborne earth stations". Proc. IEE Conference on Satellite Systems for Mobile Communications and Surveillance, 1973, pp. 52-55.

Brown, K.R., Crawford, C.I. and Davie, D.A. (1970) "A three axis stabilized mounting for a naval satellite communication system", Proc. IEE conference on Earth station technology, 1970, pp. 221-226.

CCIR (1978) Mobile Services. "Recommendations and reports of the CCIR", 1978. XIVth plenary assembly, Kyoto, Volume VIII, Rep. 594-1, pp. 381-399.

Dunlop, G.R., Afzulpurkar, N.V. (1988) "Six degree of freedom parallel link robotic mechanism: geometrical design considerations" Proc. IMC Conf., Christchurch, April 1988, New Zealand, pp. 29/1-8.

Dunlop, G.R., Ma Li (1988) "Multi-Axis Numberical Control" Proc. IMC Conference, Christchurch, April 1988, New Zealand, pp. 25/1-10.

Dunlop, G.R. (1989) "Communications systems for remote construction sites", Proc. First IES Information Technology Conference, Singapore, May 1989, vol. 1 pp. 178-184.

Earl, C.F. and Rooney, J. (1982) "Some kinematic structures for robot manipulator designs". American Society of Mechanical Engineers, Paper 82-DET-89.

Eley, R.G. (1970) "Auto-tracking receivers", Proc. IEE Conference on Earth Station Technology, 1970, pp. 302-308.

Fichter, E.F. and McDowell, E.D. (1980) "A novel design for a robot arm", Proc. Computer Technology Conf.,New York, ASME pp. 250-256.

Fichter, E.F. and McDowel, E.D. (1983) "Determining the motions of joints on a parallel connection manipulators". Proc. Sixth World Congress on Theory of Machines and Mechanisms, New Delhi, India. Dec. 1983, pp. 1003-1006.

Fitcher, E.F. (1984) "Kinematics of a parallel connection manipulator", American Society of Mechanical Engineers, paper 84-DET-45.

Fichter, E.F. (1987) "A Stewart platform based manipulator: General theory and practical construction". Kinematics of robot manipulators. McCarthy, J.M. (Ed.) MIT Press, London, pp. 165-190.

Fitzgerald, A.E. et al. (1975) Basic Electrical Engineering. McGraw-Hill Book Company, New York.

Fthenakis, E. (1984) Manual of satellite communications. McGraw-Hill Book Company, U.S.A.

Harries, G. (1970) "Design problems in shipborne terminals", Proc. IEE Conference on Earth station technology, 1970, pp. 70-75.

Harries, G. and Heaviside, J.W. (1973) "Naval satellite communications terminal", Proc. IEE Conference on Satellite Systems for Mobile Communications and Surveillance, 1973, pp. 48-51.

Hawkins, G.J. Edwards, D.J., and McGeen, J.P. (1988) "Tracking systems for satellite communications". Proc. IEE, Vol. 135, Pt. F, No. 5, pp. 393-407.

Hewlett Packard Optoelectronics Designer's Catalog 1986.

Huele, H.T. (1981) "An earth station for weather satellites". Philiphs Telecommunication Review, Vol. 39, No. 3, pp. 118-129.

Hunt, K.H. (1978) Kinematic Geometry of Mechanisms. Oxford University Press, London.

Hunt, K.H. (1982) "Geometry of Robotic Devices". The Institute of Engineers, Australia Transactions, 1982 pp. 213-220.

Hunt, K.H. (1983) "Structural kinematics of in-parallel-actuated robot-arms", Transactions of the ASME Journal of Mechanisms, Transmissions and Automation in Design, Vol. 105, pp. 705-712.

Inou, F. and Kaitsuka, T. (1981) "K-Band tracking system for domestic satellite communication system", IEEE Transactions on Aerospace and Electronic Systems, Vol. AES-17, No. 4, pp. 561-570.

Inoue, H., Tousaka, Y. and Fukuizumi (1985) "Parallel Manipulator" Proc. Third International Symposium Robotic Research, Gouvieux, France, 1985, pp. 321-327.

James, M.R. and Maney, J.J. (1985) "Adaptive alignment of a shipboard satellite terminal", Proc. IEEE Military Communications Conference, MILCOM'85, Boston, Vol. 1, pp. 300-305.

Johnson, M.B. (1978) "Antenna control system for a ship terminal for Marisat", Proc. Maritime and Aeronautical Satellite Communication and Navigation, IEE Conference Publication No. 160, pp. 123-126.

Kirby, R.J. (1973) "A simple stabilized antenna platform for maritime satellite communications" IEE Conference Publication No. 95, pp. 135-139.

Kuo, B.C. (1987) Automatic Control Systems. Prentice-Hall, Inc. New Jersey, U.S.A.

Lozier, J.C., Nostoh, J.A. and Iwama, M. (1963) "The servo system for antenna positioning", Bell System Technical Jounral, 1963, pp 1253-1281.

Ma Li, (1989) "Multi-axis numerical control", University of Canterbury M.E. Thesis, Christchurch, New Zealand.

Martin, M. (1978) Communications Satellite Systems, Prentice-Hall, Inc. New Jersey, U.S.A.

McCallion, H. (1973) Vibration of Linear Mechanical Systems. Longman Group Limited, London.

McCallion, and Truong, P.D. (1979) "The analysis of six DOF work station for mechanized assembly", Proceedings of fifth World Congress on theory of machines and mechanisms, 1979, pp. 611-616.

McCloy, D. and Harris, M. (1986) Robotics: An Introduction. Open University Press, Milton Keynes.

Miya, K. (Ed.) (1981) Satellite Communications technology. KDD Engineering and Consulting Ltd., English Ed.

Optoelectronics Data Book (1988) Pacesetter Electronics USA, Inc.

Paul, R.P. (1981) Robot Manipulators: Mathematics, programming, and control, MIT Press, Cambridge, Massachusetts.

Pham, D.T. (1979), "Techniques, hardware and software for robotic assembly", University of Canterbury Ph.D. thesis, Christchurch, New Zealand.

Potton, S.L. (1983) "GEC advanced device for the assembly", Proc. The CIRP conference on assembly automation, June, 1983, pp. 130-144.

Powell, I.L. (1981) "The kinematic analysis and simulation of the parallel topology manipulator:, MTR 81/30, G B Marconik Research Laboratories.

Pratt, T and Bostian, C.W. (1986) Satellite Communications. John Wiley and Sons, Inc. New York.

Rathbun, G.P. (1986), "A Stewart platform six-axis milling machine development", University of Canterbury, M.E. Thesis, Christchurch, New Zealand.

Ruocco, S.R. (1987) Robot Sensors and Transducers. Open University Press, Milton Keynes.

Snyder, W. (1985) Industrial Robots: Computer Interfacing and Control, Prentice-Hall Industrial Robots series, New Jersey, U.S.A.

Stewart, D. (1965) "A platform with six degrees of freedom". Proc. I.Mech.E., Vol. 180, No. 1, pp. 371-386.

Tocci, R.J. and Laskowski, L.P. (1979) Microprocessors and Microcomputers Hardware and Software. Prentice-Hall, Inc., New Jersey.

Turbo Pascal - Reference Manual (1989), Ver. 4.0, Borland International, CA, USA.

Vygodsky, M. (1978) Mathematical Handbook MIR Publishers, Moscow.

Warner Electric Catalogue (1986) Electrac Linear Actuator Systems. IL, U.S.A.

Yang, D.C.H. and Lee, T.W. (1984). "Feasibility study of a platform type of robotic manipulators from a kinematic viewpoint", Transactions of the ASME Journal of Mechanisms, Transmissions and Automation in Design, June 1984, Vol. 106, pp. 191-198.

Zenith Data Systems (1988) 80286 Technical Reference Manual. Michigan, U.S.A.